Grid Integration of Offshore Wind Farms via VSC-HVDC – Dynamic Stability Study

Liu, Hongzhi

Publication date:
2014

Document Version
Publisher's PDF, also known as Version of record

Grid Integration of Offshore Wind Farms via VSC-HVDC – Dynamic Stability Study

HONGZHI LIU

DEPARTMENT OF ENERGY TECHNOLOGY
AALBORG UNIVERSITY

Grid Integration of Offshore Wind Farms via VSC-HVDC - Dynamic Stability Study

by
Hongzhi Liu

Dissertation submitted to the Faculty of Engineering and Science at Aalborg University

in partial fulfillment of the requirements for the degree of

Doctor of Philosophy in Energy Technology

DEPARTMENT OF ENERGY TECHNOLOGY
AALBORG UNIVERSITY
AALBORG, DENMARK
JUNE 2014

Grid integration of offshore wind farms via VSC-HVDC – grid dynamic stability study

Printed in Denmark by Aalborg University

June 2014
ISBN: 978-87-92846-43-3

AALBORG UNIVERSITY
Department of Energy Technology
Pontoppidanstraede 101
DK-9220 Aalborg East
Denmark

Telephone: 0045 50114828
Fax: 0045 9815 1411
Web address: http://www.et.aau.dk

Grid Integration of Offshore Wind Farms via VSC-HVDC - Dynamic Stability Study

PhD Student: Hongzhi Liu

Supervisors: Prof. Zhe Chen

Publication List

[1] Hongzhi Liu, Zhe Chen, "Aggregated Modelling for Wind Farms for Power System Transient Stability Studies," in *Asia-Pacific Power and Energy Engineering Conference (APPEEC)*, Shanghai, China, March 2012.

[2] Hongzhi Liu, Zhe Chen, "Fault ride-through and grid support of permanent magnet synchronous generator-based wind farms with HVAC and VSC-HVDC transmission systems," in *IEEE International Energy Conference and Exhibition (ENERGYCON)*, Florence, Italy, September 2012.

[3] Hongzhi Liu, Zhe Chen, "Impacts of large-scale offshore wind farm integration on power systems through VSC-HVDC," in *IEEE Grenoble PowerTech (POWERTECH)*, Grenoble, France, June 2013.

[4] Hongzhi Liu, Zhe Chen, Chengxi Liu, "Enhanced Dynamic Voltage Stability Support by VSC-HVDC for Offshore Wind Applications using Trajectory Sensitivity Analysis", in *12th International Workshop on Large-scale Integration of Wind Power into Power Systems as well as on Transmission Networks for Offshore Wind Power Plants*, London, UK, October 2013.

[5] Hongzhi Liu, Zhe Chen, "Coordinated frequency regulation by offshore wind farms and VSC-HVDC transmission," *International journal of smart grid and clean energy*, vol. 3, no. 1, pp 1-7, January 2014.

[6] Hongzhi Liu, Zhe Chen, "Contribution of VSC-HVDC to Frequency Regulation of Power Systems with Offshore Wind Generation," *IEEE Trans. On Energy Conversion (Submitted).*

[7] Hongzhi Liu, Zhe Chen and Jiakun Fang, "Enhancement of Voltage Support Capability of VSC-HVDC for Offshore Wind Applications Using Trajectory Sensitivity Analysis," *Renewable Energy (Submitted)*.

This present report combined with the above listed scientific papers has been submitted for assessment in partial fulfilment of the PhD degree. The scientific papers are not included in this version due to copyright issues. Detailed publication information is provided above and the interested reader is referred to the original published papers. As part of the assessment, co-author statements have been made available to the assessment committee and are also available at the Faculty of Engineering and Science, Aalborg University.

Acknowledgement

The research work documented in this thesis was supported by Norwegian Centre for Offshore Wind Energy (NORCOWE) under grant 193821/S60 from Research Council of Norway (RCN) and Department of Energy Technology, Aalborg University, Denmark. NORCOWE is a consortium with partners from industry and science, hosted by Christian Michelsen Research.

First of all, I would like to express my deepest appreciation to my supervisor, Professor Zhe Chen for his consistent understanding, support and guidance throughout the entire period of this project. The enlightening discussions with him and encouraging comments from him contribute tremendously to the success of my PhD.

I sincerely thank to my colleagues Chunqi Wang, Dr. Chi Su, Dr. Yan Liu, Dr. Fujin Deng, Dr. Sanjay Chaudhary and Rongwu Zhu for their valuable technical assistance and useful discussions. Special thanks go to Dr. Chengxi Liu and Dr. Jiakun Fang for their inspiring suggestions and generous help.

Many thanks go to visiting guests Associate Professor PingPing Han from Hefei Institute of Technology, China, for her kind patience, professional knowledge-sharing and continuous support, Professor Haishun Sun from Huazhong University of Science and Technology, China, who helped me to understand and analyse the power system dynamics, and Associate Professor Jun Yao from Chongqing University, China, who gave me practical tips on wind turbine modelling. I am also thankful to many others who have followed and contributed to this project.

Last but not least, I would like to thank my parents and my family for their truly love, genuinely comprehension and endless support.

Hongzhi Liu
June, 2014
Aalborg

Abstract

Offshore wind farms tend towards larger capacity to make good use of the stronger winds and allow improved fixed cost allocation. An offshore wind farm could be sized at hundreds of MWs, which is competitive with conventional power plants. Consequently, grid integration of such size offshore wind farms could seriously impact the operation and stability of their interconnected power system. To assist in maintaining the power system stability when large disturbances occur in the grid, modern offshore wind farms consisting of variable-speed wind turbines are required to provide ancillary services such as voltage and frequency control.

The greater distance to shore makes commonly used high voltage AC (HVAC) connection unsuitable economically and technically for large offshore wind farms. Alternatively, voltage source converter (VSC)-based high voltage DC (HVDC) transmission becomes more attractive and practical to integrate large-scale offshore wind farms into the onshore power grid, owing to its high capacity, advanced controllability and stabilization potential for AC networks etc.

In this dissertation, some of the key technical issues with grid integration of large-scale offshore wind farms via VSC-HVDC transmission are addressed. The main objectives have been to study the dynamic interactions between offshore wind farms and interconnected power systems, pinpoint the impact on the electrical grid while integrating large-scale offshore wind farms via VSC-HVDC link and propose potential solutions to improve the dynamic stability of the network.

This research work starts with the modelling of full converter wind turbine and VSC-HVDC transmission system. Then, based on those models, the impact of integration of a large offshore wind farm into the power system through VSC-HVDC transmission is investigated. In addition to steady-state voltage profile analysis, dynamic voltage stability and transient angle stability simulations are also conducted at different wind penetration levels. The comprehensive analysis of the results helps to understand the stability concerns of the offshore wind power integration.

VSC-HVDC link is characterized by independent active and reactive power control and hence is able to provide reactive power / voltage support during grid voltage disturbances. However, for a given VSC capacity, the more the active power output, the less the available reactive power output. Therefore, the voltage support capability of VSC-HVDC is limited by both its VSC capacity and the control scheme. In reference to the control strategies of VSC-HVDC used in this research

project, a trajectory sensitivity analysis (TSA)-based approximation is proposed as a method to identify the minimum onshore VSC capacity with which the VSC-HVDC link is able to provide effective support for stabilizing the grid voltage following a grid disturbance. The developed TSA-based method implements a two-stage approximation strategy to improve the accuracy of the linear approximation. Both reactive power-based and voltage-based trajectory sensitivities are used to verify the effectiveness of the proposed method. This proposed method avoids running large amount of repeated time-domain simulations.

Due to the decoupling of VSC-HVDC and communication delay, offshore wind farms that run in a de-loading mode to provide frequency reserve, may not be able to respond to the onshore grid frequency excursion in time. Consequently, the stability and security of power system will be put at risk, especially for those with high wind penetration. A coordinated frequency control scheme is developed not only to reduce the responding latency of offshore wind farms effectively but also to allow VSC-HVDC to contribute to system frequency regulation by adjusting its DC-link voltage. The adaptive control of the DC-link voltage enables the DC capacitors of VSC-HVDC to release/absorb energy to regulate the frequency deviation. To further enhance the system frequency response, the frequency support from VSC-HVDC is also finely coordinated with that from offshore wind farm according to the latency of offshore wind turbines responding to onshore grid frequency disturbances.

Deploying energy storage systems is considered an effective way of dealing with the challenges brought by high wind power penetration. Therefore, a PWM converter-interfaced battery energy storage system (BESS) is applied to the power system integrated with a large offshore wind farm via VSC-HVDC link. The BESS is used to provide primary frequency control in cooperation with wind power fluctuation mitigation. A new converter rating evaluation approach as well as a new power management strategy is proposed to enable the BESS to enhance the system frequency response on the basis of wind power fluctuation mitigation.

Danske Resumé

Offshore vindmølleparker går imod større kapacitet for at udnytte den stærkere vind og tillade en bedre fast allokering af omkostningerne. En offshore vindmøllepark kan have en størrelse på hundrede af MW og være konkurrencedygtige med konventionelle kraftværker. Derfor kan netpåvirkningen af sådanne offshore vindmølleparker have stor indflydelse på driften og stabiliteten på nettet de tilsluttes. For at assistere i at opretholde netstabiliteten når der sker store forstyrrelser i nettet, skal moderne vindmøller med variabel hastighed være i stand til at yde ekstra netservice i form af spændings- og frekvenskontrol

Længere afstande til kysten gør at den normalt anvendte AC-tilslutning økonomiske og teknisk uanvendlig for store vindmølleparker. I stedet bliver spændingstyrede (VCS) jævnspændingsforbindelser attractive og praktiske til storskala integration af vindmølleparker og deres tilslutning på land på grund af deres store kapacitet, avancerede styrings- og stabilitetsmuligheder for AC-nettene.

I denne afhandling adresseres nogle af hovedproblemstillingerne ved stor skala integration af offshore vindmølleparker via VSC-HVDC transmission. Hovedformålet har været at studere den dynamiske interaktion mellem offshore vindmøllerne og el-nettet de tilsluttes, finde påvirkningen ved storskala offshore tilslutning via VSC-HVDC og foreslå løsninger til at forbedre den dynamiske stabilitet i nettet.

Forskningen starter med modellering af en fuld konverter vindmølle og et VSC-HVDC transmission system. Baseret på disse modeller undersøges dernæst påvirkningen på el-nettet ved storskala integrationen af offshore vindparken via VSC-HVDC transmissionen. Udover stationær anlyse af spændingsprofiler, er der i projektet også foretaget dynamisk spændingsstabilitets og transient vinkelstabilitets simuleringer ved forskellige vindintegrations andele. Den dybdegående analyse af resultaterne hjælper til at forstå stabilitetsforholdene ved vindmølle integration.

VSC-HVDC linjer er karakteriseret ved at kunne styre den aktive og reaktive effekt uafhængigt af hinanden og kan derfor yde reaktiv effekt/spændingsstabilisering ved spændingsforstyrrelser. For en given VSC kapacitet er det imidlertid sådan at jo mere aktiv effekt der udtages jo mindre reaktiv effekt vil der kunne udtages. Derfor et spændingsstabiliseringskapaciteten for en VSC-HVDC linje begrænset bade af VSC kapaciteten og styringen. Med hensyn til VSC-HVDC styringen, der er

anvendt i dette project, anvendes en trajektorie følsomhedsanalyse approximation (TSA) som metode til at identificere minimum kapaciteten af VSC systemet på land, med hvilken VSC-HVDC linjen er i stand til at yde effektiv support til at stabilisere netspændingen efter en forstyrrelse. Den udviklede TSA-metode anvender en to-steps approximerings strategi til at forbedre nøjagtigheden af den lineære approximation. Både reaktiv effektbaseret og spændingsbaseret trajectorie følsomhed anvendes til at verifice effektiviteten af den foreslåede metode. Den foreslåede metode betyder at at et stort antal gentagne tidsdomæne simuleringer kan undgås.

På grund af afkobling imellem VSC-HVDC systemet og kommunikationsforsinkelser, kan offshore vindparker, der ikke kører for fuld last fordi de skal yde frekvensreserve måske ikke være i stand til at reagere på frekvensforstyrrelser på land i tide. Som følge heraf løbes en risoko mht. stabiliteten og sikkerheden i elnettet især ved stor vindmølleintegration. Der er udviklet en koordineret frekvensstyringsmetode ikke kun for at reducere svartiden for offshore vindparken men også for at lade VSC-HVDC systemet bidrage til frekvensreguleringen ved at justere på DC spændingen. Den adaptive styring af DC spændingen tillader DC kapacitorerne i VSC-HVDC systemet til at afgive/absorbere energi for at styre frekvensafvigelsen. For yderligere at forbedre frekvensresponsen fra VSC-HVDC systemet er det koordineret med systemet for offshore vindparken med hensyn til forsinkelsen der sker når offshore vindmøllerne reagerer på frekvensforstyrrelserne fra land.

Anvendelse af energilagringssystemer anses for en effektiv måde at tage højde for de udfordringer der sker ved høj integration af vindmøller. Derfor er der anvendt et PWM konverterbaseret batteri lagringssystem (BESS) til elsystemet der er tilsluttet med offshore vindparken via VSC-HVDC linjen. BESS systemet er anvendt til at yde primær frekvenskontrol samtidig med at det skal modvirke vind fluktuationer. Der er foreslået en ny konvertereffekt bestemmelsesmetode såvel som en ny effektstyringsstrategi der skal gøre BESS systemet i stand til at forbedre system frekvensresponsen som følge af vindfluktuationerne.

Table of Contents

Chapter 1

Introduction

To fight with the global warmth and foreseeable energy crisis, renewable energy has been introduced and played an increasing import role in our energy supply chain. As one of the most significant renewable sources of electrical power, wind energy has the most mature technology in operation and been given great attention. Particularly, offshore wind has been actively developed in many countries as the sustainable and secure energy supply. Since offshore wind farms normally have large-scale capacities and tend to replace conventional power plants, the grid connection of offshore wind farms raises challenges for the stability and security of interconnected power grids.

1.1 Background

Globalization and modernization have facilitated economies and bettered lives of millions of population. However, these benefits are shadowed by disastrous climate changing, soaring fuel prices and fast depletion of fossil energy reserves. To pursue the diversity and security of energy supply and ensure environmental sustainability, significant research and implementation has been directed towards harnessing renewable energy sources world-wide for decades.

Among various renewable energy sources, wind energy is being viewed as a mainstream power generation technology and achieving increasingly fast growth globally since 1980s. The very low lifetime carbon emissions, significant exploitable resource potential and relatively mature technology have attracted many countries to set ambitious targets for using wind power at utility scale [1], [2]. To maintain technological leadership and boost low-carbon economy, EU has continuously invested a vast sum of funds in wind energy technology. It aims to make wind the most competitive energy source in Europe and enable wind energy to supply 14% of Europe's total electricity demand in 2020 and 33% in 2030, up from 5.3% in 2010 [3]. The focuses are not only on the development of onshore wind energy, but also on the exploitation of offshore wind.

Onshore wind energy is one of the most cost-effective renewable technologies and has been well understood and implemented. However, its growth potential is seriously limited by sitting spaces and human activities. In contrast, offshore wind farms are normally far from shore and have lower effects on human activities. Owing to good wind conditions, offshore wind is able to provide higher

and steadier energy yields. Although offshore wind is expensive mainly due to construction and connection costs, the huge energy potential of offshore wind and the imperative of carbon emission reductions still give countries and stakeholders strong incentives to invest in offshore wind technology. It is expected that the annual net increase in offshore wind capacity will grow steadily from 1.1 GW in 2011 to 6.5 GW in 2020 and Europe will have had more than 40 GW installed capacity of offshore wind power by 2020 and 150 GW in 2030 [3] – [5]. Offshore wind energy becomes more significant in the North Sea neighbouring countries. Figure 1.1 shows the future development of offshore wind capacity in the North Sea.

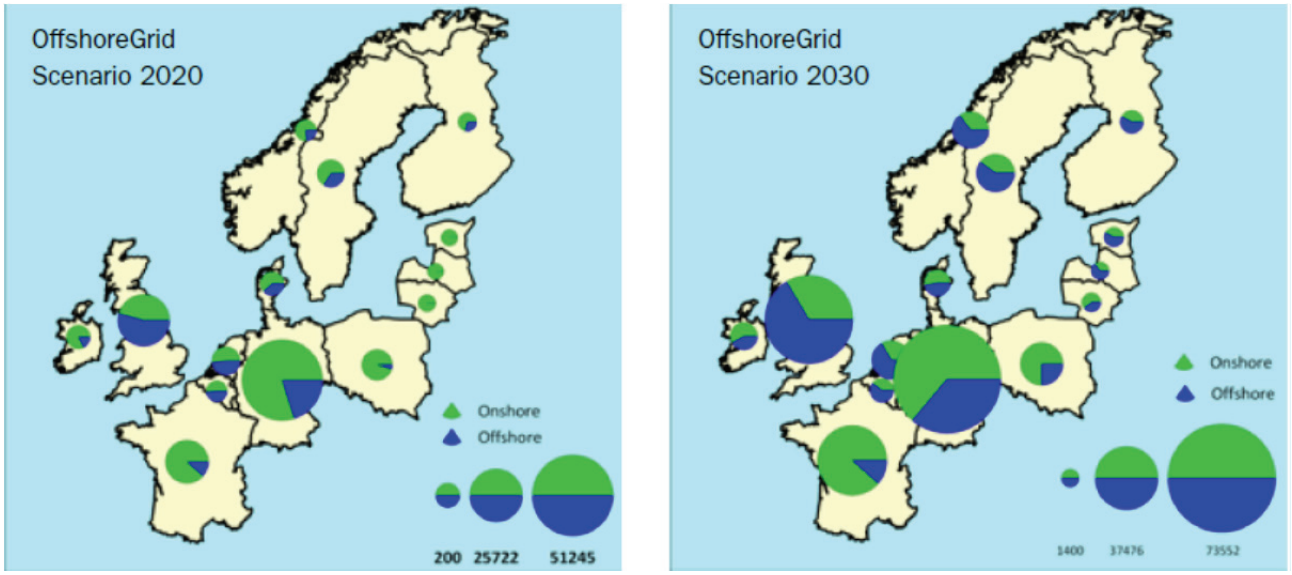

Figure 1.1 Offshore and onshore wind farm installations in Northern Europe in 2020 and 2030 [4].

For low wind power penetration levels, the performance of the wind generation will not affect the grid operation to any significant extent. For higher penetration levels of wind power and in view of the fact that offshore wind farms are large enough to replace conventional power plants, the grid integration of large offshore wind farms will inevitably influence the power system stability and control, and introduce a series of challenges and issues on [1], [2], [4] :

- System operation,
- Grid connection of wind power and system transient stability,
- Grid infrastructure issues,
- Contribution of wind power to system adequacy,
- Market redesign issues to facilitate wind power integration.

1.2 Power system requirements for high wind penetration

1.2.1 Wind power effects on the power system

The impact of wind power on the power system is not only related to the wind power penetration level, but also determined by the size and capacity of the power system, the electricity generation mix and load variations in the system etc. As an important generation source to replace conventional power plants, the wind power brings the power system both short-term and long-term impacts and these impacts matter locally and system-widely [1], [6], [7].

TABLE 1.1

Power system impacts of wind power, causing integration costs [1], [6], [7].

	Effects	Time-scale	Affecting area	Wind power contribution
Short-term impacts	Voltage management	Minutes	Local	Dynamic voltage support
	Production efficiency of thermal / hydro	1-24 hours	System	Depending on how the system is operated and on the use of short-term forecast
	Transmission / distribution benefits	1-24 hours	Local or system	Depending on penetration level, wind farms may create additional investment costs or benefits. Wind energy can reduce network losses.
	Regulating reserves	Minutes to 1 hour	System	Wind power can partially contribute to primary and secondary control.
	Discarded energy	Hours	System	Wind power may exceed the amount of the system can absorb.
Long-term impacts	System reliability (power adequacy)	Years	System	Wind power can contribute to power system adequacy.

The short-term impacts are caused by the variable output of wind power generation that results in additional requirements of balancing the system on the operational time scale (from several minutes to several hours). In the long-term, large-scale integration of wind power may risk the power supply at times of peak demand, namely the adequacy of power capacity, due to the intermittent nature of wind power. As modern wind farms are able to control its active and reactive

power output, wind power can provide local voltage management. From the system point of view, wind power affects the system power flow, spinning reserves, production efficiency of other power generation systems and the adequacy of the system. Large wind farms are also required to provide ancillary services like conventional power plants. With high penetration levels, wind power essentially participates in maintaining the system stability and supply security. Table 1.1 summarizes the impacts that wind power has on the power system.

1.2.2 Grid code requirements

Modern power system is a complex interconnected network of multiple generating sources, transmission networks and consumers. A properly designed and operated power system must be able to provide minimum-cost and qualified electricity to meet the continuously changing demand at all times and at the same time maintain adequate power reserves.

Wind power generation is characterized by its variation, intermittency and uncertainty. With the increasing penetration levels, the integration of large-scale wind power brings the power system profound influences as above mentioned. Thus, to maintain the system stability and reliability with large-scale wind power integration, transmission system operators (TSO) have updated their grid codes with specific interconnection requirement for the operation of wind farms including offshore wind farms.

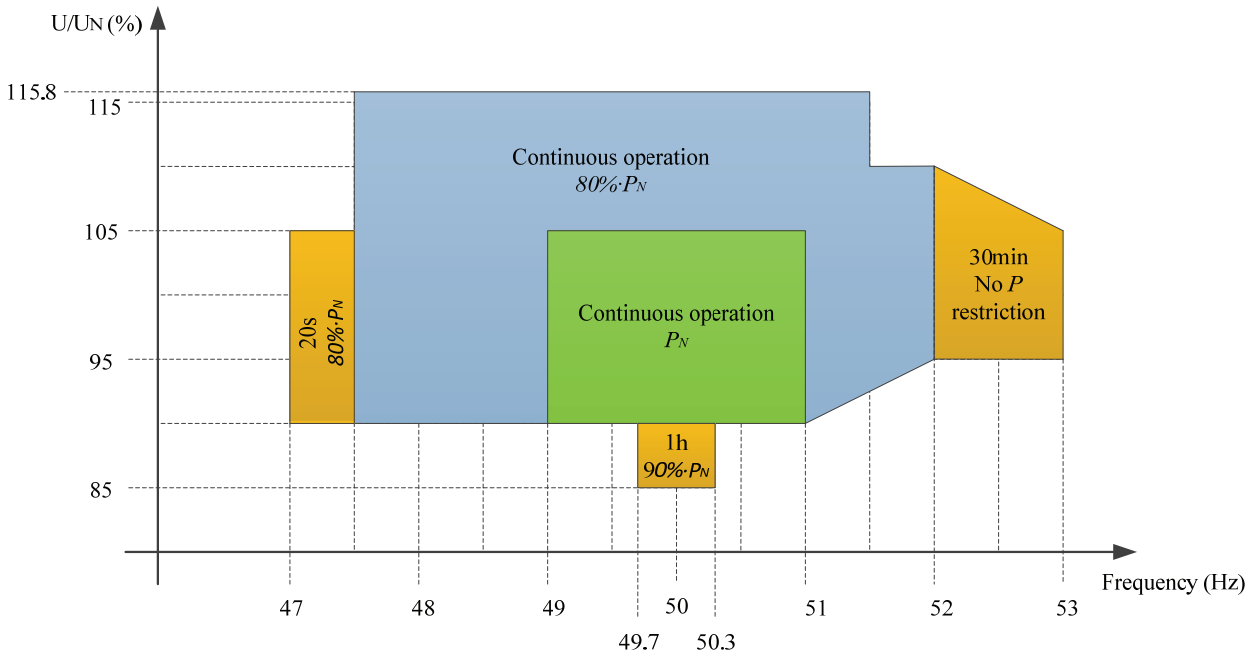

Figure 1.2 The frequency-voltage boundary for wind farm operation of various grid codes [9].

Due to the differences among power networks and assorted wind penetration levels, grid codes normally vary from country to country. However, there are some common technical requirements within most of the current grid codes as following [7]-[13]:

- Frequency and voltage operating range,
- Control of active power,
- Control of reactive power,
- Low voltage ride through,
- Reactive power injection during voltage dips.

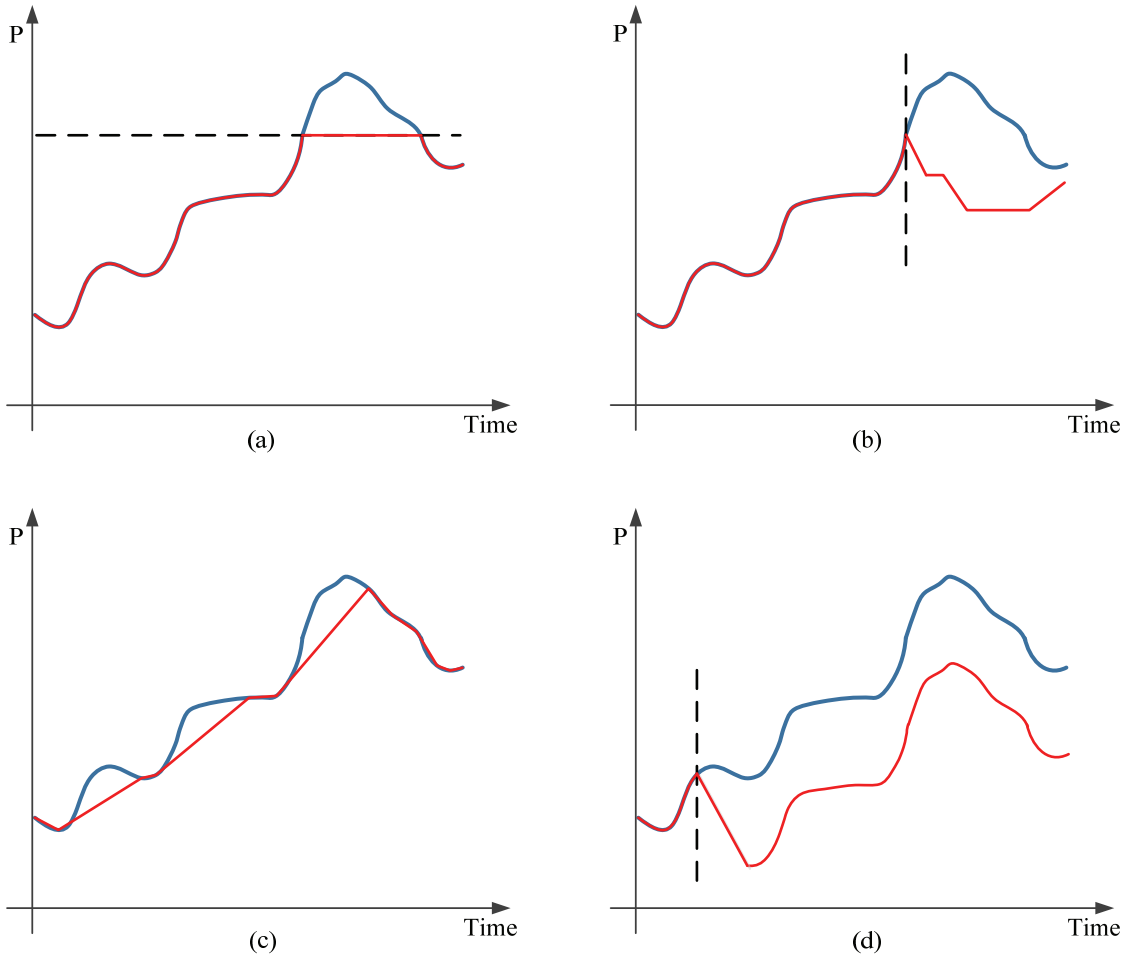

Figure 1.3 Active power control strategies for wind farms [7]: (a) Absolute power control; (b) Power balance control; (c) Power rate limitation control; (d) Delta control.

Grid codes specify that wind farms must operate continuously within the voltage and frequency variation limits in normal operation conditions and also be capable of remaining connected for a certain time under abnormal frequencies in order to support the system for a fast frequency

restoration. Figure 1.2 summarizes the most restricting frequency-voltage boundary for wind farm operation defined by several grid codes. For the purpose of frequency regulation and energy discarding, wind farms are required to adjust their active power output in accordance with the requests from the TSO or the deviations of the system frequency. For different purposes, various control strategies could be implemented, for example, absolute power limitation, power balance control, power rate limitation control and delta control as shown in Figure 1.3 [7]. The reactive power control requirement aims to maintain the voltage level at the point of common coupling (PCC) during voltage fluctuations by injecting / absorbing reactive power. The amount of the reactive power compensation and the effects mainly depends on power system configurations and the grid short-circuit capacity etc. The reactive power requirements of different grid codes are presented in Figure 1.4 by *P*-*Q* diagram.

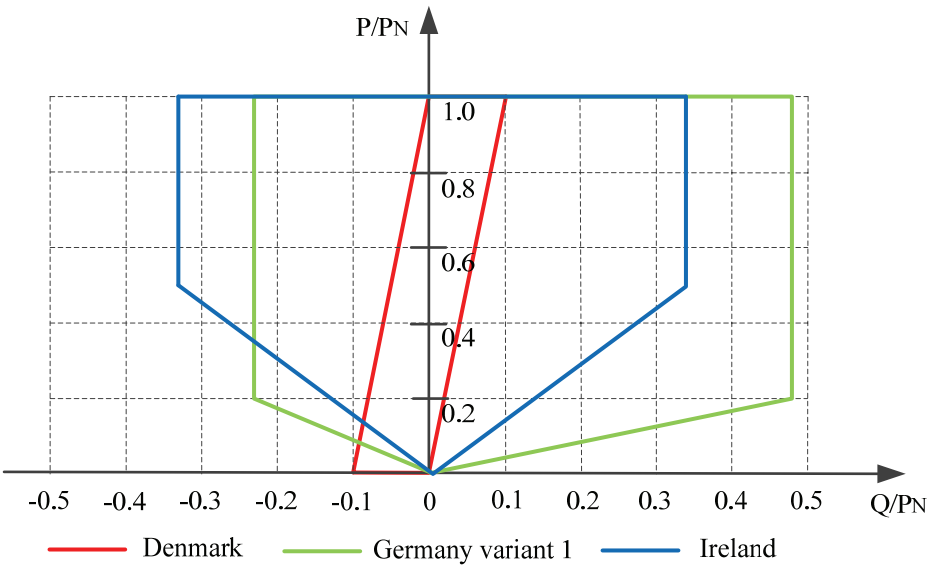

Figure 1.4 Reactive power requirements of different grid codes.

Low voltage ride through (LVRT) is a requirement for wind farms to remain connected during grid disturbances and low grid voltages. The disconnection of a large amount of wind generation can lead to larger voltage depression and eventually voltage collapse in the affected area, and can also aggravate the power supply-demand imbalance and thus the frequency deviation [8], [9]. Therefore, the LVRT capability is increasingly essential for networks with a high share of wind power generation to maintain stable operation while faults occurring. Figure 1.5 shows the LVRT requirements of Denmark, Germany and Ireland, in which the wind farm need to stay connected to

the grid at voltages above the borderline. To support the grid voltage, some grid codes further require wind farms to provide reactive current injection in line with the absolute deviation of the voltage during voltage dips. And if necessary, the active power even can be sacrificed to meet the reactive current output requirement. For instance, E.ON grid code specifies that the generating plants must provide reactive current injection of at least 2% of the rated current for each per cent of the voltage dip [14]. If necessary, 100% of the rated current must be available for reactive current output.

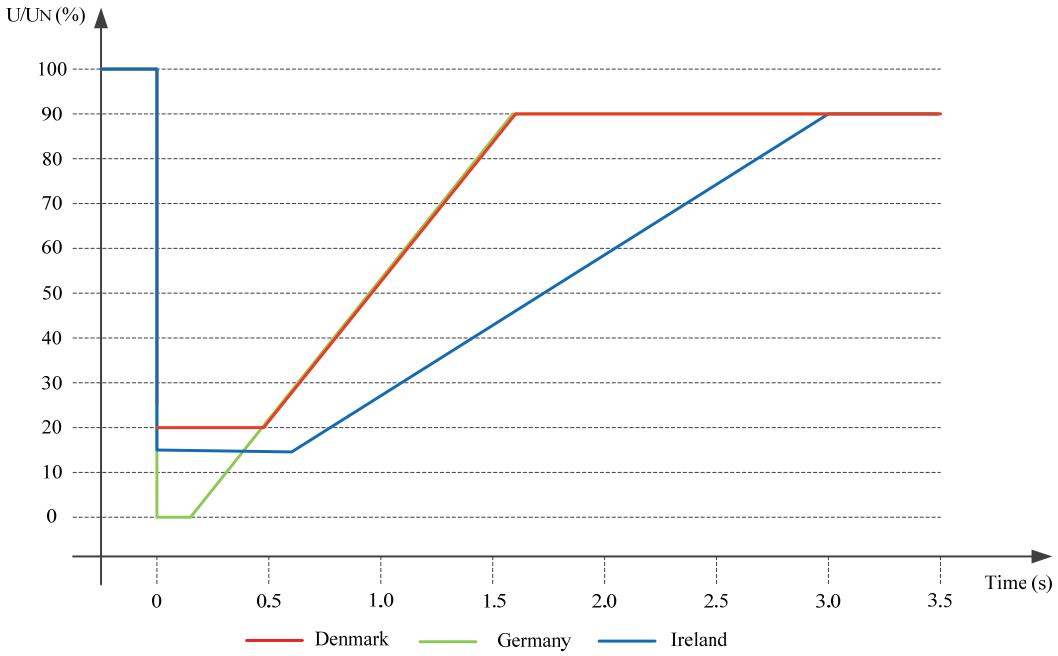

Figure 1.5 LVRT requirements of Denmark, Germany and Ireland.

1.2.3 Grid connection of offshore wind farms

To feed large-scale offshore wind generation into onshore grid, either high voltage alternating current (HVAC) or high voltage direct current (HVDC) transmission systems are applicable. However, for wind farms close to shore, HVAC connection is generally used owing to its simple, economic and mature technology. When it is related to remotely located large-size offshore wind farms, the excessive charging current and capacity limits of HVAC cables make this option off the table, whereas HVDC system becomes a better solution because of its full control of power flow, interconnection of asynchronous grids, no cable charging current, lower cable power loss and higher transmission capacity [7], [15]-[18].

The HVDC technology can be further categorized into conventional line-commuted converter based HVDC (LCC-HVDC) using thyristors and voltage source converter (VSC)-based HVDC (VSC-HVDC) using IGBTs. The LCC-HVDC has been in commercial applications for more than half century with respectful reliability and availability. It offers higher voltage level and transmission capacity compared to VSC-HVDC. However, the requirement for a strong offshore network for commutation as well as the need for comparatively large offshore substation converter stations limit the LCC-HVDC implementations in offshore wind industry [7]. Moreover, the foreseeable construction of a super grid system based on multi-terminal HVDC also reduces the likelihood of utilization of LCC-HVDC technology offshore [1].

In comparison, VSC-HVDC link is self-commutated which means it does not require a strong external network. The converter stations are relatively compact at it needs less number of filters. It also provides advantages such as independent reactive and active power control, black start capacity, fast and reversible power flow control, and contribution to power system stability [7], [17], [18]. The above beneficial characteristics make VSC-HVDC more attractive and feasible for integration of remote-located large-scale offshore wind farms.

1.3 Research objectives

With the increasing penetration of wind energy, grid integration of offshore wind farms exerts significant impact on the system operation and stability, and raises a series of technical challenges as mentioned in the previous sections. Therefore, the overall objective of this research project is to analyse the impact and technical issues that are related to the expected increased offshore wind integration on power systems, and probe out potential solutions for improving the system dynamic stability.

To fulfil the research objectives, four different tasks are conducted as follows:

1) To study the impact on the system stability of integrating a large offshore wind farm via VSC-HVDC connection with regard to steady-state voltage stability, dynamic voltage stability and transient angle stability;

2) To develop a method to design the capacity of onshore VSC to enable VSC-HVDC with given control strategy to provide enough support for the improvement of system voltage stability after a grid disturbance;

3) To develop a coordinated frequency regulation strategy to enable VSC-HVDC to provide frequency regulation together with frequency support from offshore wind farms to enhance the system frequency response;

4) To develop a new power management strategy to enable the battery energy storage system (BESS) to provide reliable and essential frequency reserve on the basis of wind power fluctuation mitigation.

1.4 Scopes and limitations

The scopes and limitations of this research are as follows:

1) The system modelling and simulations are implemented in DIgSILENT/PowerFactory platform. Time domain simulations are based on Root Mean Square (RMS) values (Electromechanical Transients). EMT (Electromagnetic Transients) is not considered in the simulations. The network representation uses balanced components and only balanced contingencies are studied in this project.

2) The voltage-sources converter model used in this research is represented by the built-in PWM Converter model of DIgSILENT based on controlled voltage source instead of detailed model.

3) Only symmetrical faults occurred in the onshore power grid have been implemented and analysed in this research project. Disturbances in the offshore wind farm internal interconnection grid and faults on the HVDC DC link are not considered.

4) The offshore wind farm with a large number of the wind turbines is represented by one re-scaled wind turbine model. During the simulations within 30s, the wind speed is assumed to be invariant.

1.5 Dissertation organization

This dissertation is divided into seven chapters and the summary of each chapter is presented as follows:

Chapter 1: Introduction

This chapter provides an overview of the development of wind energy and the challenges and issues that are related to the integration of large-scale wind power into power systems, especially the offshore wind. The power system requirements for wind power are then summarized and motivate the conduction of this research. The research objectives and limitations are also pinpointed in this chapter.

Chapter 2: Modelling and control of full converter wind turbine and VSC-HVDC

This chapter provides a brief description of wind turbine concepts at first. Next, the detailed modelling of the full-converter wind turbine and VSC-HVDC transmission system are presented and their basic control and operation are also introduced.

Chapter 3: Impact of VSC-HVDC-based integration of offshore wind farms on power system stability

This chapter investigates the impacts of integrating a large-scale offshore wind farm into the transmission system of a power grid through VSC-HVDC connection. The concerns are focused on steady-state voltage stability, dynamic voltage stability and transient angle stability with different penetration levels of wind power.

Chapter 4: Enhancement of voltage support capability of VSC-HVDC for offshore wind applications using trajectory sensitivity analysis

In this chapter, for the studied voltage support strategies of VSC-HVDC, a trajectory sensitivity analysis (TSA)-based approach is proposed to identify the minimum onshore VSC capacity with which VSC-HVDC can provide enough support for stabilizing the grid voltage following a grid disturbance. The proposed TSA-based method implements a two-stage approximation strategy to improve the accuracy of the linear approximation. Both reactive power-based and voltage-based trajectory sensitivities are used to verify the effectiveness of the proposed method.

Chapter 5: Coordinated frequency regulation by offshore wind farm and VSC-HVDC

This chapter details a coordinated control scheme that not only reduces the responding latency of offshore wind farms effectively, but also allows VSC-HVDC to contribute to system frequency regulation by adjusting its DC-link voltage. By means of this approach, the DC capacitor banks of VSC-HVDC are controlled to absorb or release energy so as to provide frequency support. To further enhance the system frequency response, the frequency support from VSC-HVDC is also

finely coordinated with that from offshore wind farm according to the latency of offshore wind farm responding to onshore grid frequency excursion. Simulation studies for under- and over-frequency event are carried out to verify the proposed control scheme.

Chapter 6: Application of battery energy storage system to enhance frequency response of power system with high wind power penetration

In this chapter, a PWM converter-interfaced BESS is applied to the power system integrated with a large offshore wind farm via VSC-HVDC link. The BESS is used to provide primary frequency control in cooperation with wind power fluctuation mitigation. A new converter rating evaluation approach as well as a new power management strategy is proposed to enable the BESS to enhance the system frequency response on the basis of wind power fluctuation mitigation. Case studies are conducted with respect to various charging and discharging state of the BESS to verify the effectiveness of the proposed approaches.

Chapter 7: Conclusions and future work

This chapter draws the main conclusions of this research project and discusses the topics of future work.

1.6 List of publications

[1] Hongzhi Liu, Zhe Chen, "Aggregated Modelling for Wind Farms for Power System Transient Stability Studies," in *Asia-Pacific Power and Energy Engineering Conference (APPEEC)*, Shanghai, China, March 2012.

[2] Hongzhi Liu, Zhe Chen, "Fault ride-through and grid support of permanent magnet synchronous generator-based wind farms with HVAC and VSC-HVDC transmission systems," in *IEEE International Energy Conference and Exhibition (ENERGYCON)*, Florence, Italy, September 2012.

[3] Hongzhi Liu, Zhe Chen, "Impacts of large-scale offshore wind farm integration on power systems through VSC-HVDC," in *IEEE Grenoble PowerTech (POWERTECH)*, Grenoble, France, June 2013.

[4] Hongzhi Liu, Zhe Chen, Chengxi Liu, "Enhanced Dynamic Voltage Stability Support by VSC-HVDC for Offshore Wind Applications using Trajectory Sensitivity Analysis", in *12th International Workshop on Large-scale Integration of Wind Power into Power Systems as well as on Transmission Networks for Offshore Wind Power Plants*, London, UK, October 2013.

[5] Hongzhi Liu, Zhe Chen, "Coordinated frequency regulation by offshore wind farms and VSC-HVDC transmission," *International journal of smart grid and clean energy*, vol. 3, no. 1, pp 1-7, January 2014.

[6] Hongzhi Liu, Zhe Chen, "Contribution of VSC-HVDC to Frequency Regulation of Power Systems with Offshore Wind Generation," *IEEE Trans. On Energy Conversion (Submitted)*.

[7] Hongzhi Liu, Zhe Chen and Jiakun Fang, "Enhancement of Voltage Support Capability of VSC-HVDC for Offshore Wind Applications Using Trajectory Sensitivity Analysis," *Renewable Energy (Submitted)*.

Bibliography

[1] European Wind Energy Association, “Large scale integration of wind energy in the European power supply: analysis, issues and recommendations,” December 2005. [online]. Available: http://www.ewea.org, accessed in November, 2010.

[2] D. Justus, “International energy technology collaboration and climate change mitigation – Case Study 5: wind power integration into electricity systems,” Organization for Economic Co-operation and Development, 2005. [online]. Available: http://www.oecd.org/env/cc/34878740.pdf, accessed in October, 2013.

[3] European Wind Energy Association, “EU energy policy to 2050,” March 2011. [online]. Available: http://www.ewea.org, accessed in October, 2013.

[4] European Wind Energy Association, “OffshoreGrid: offshore electricity infrastructure in Europe,” October 2011. [online]. Available: http://www.ewea.org, accessed in October, 2013.

[5] European Wind Energy Association, “Pure Power – wind energy targets for 2020 and 2030, 2009 update” November 2011. [online]. Available: http://www.ewea.org, accessed in October, 2013.

[6] H. Holttinen, “The impact of large scale wind power on the Nordic electricity system,” VTT Publications 554, 2004 (PhD thesis). [online]. Available : http://www.vtt.fi/inf/pdf/publications/2004/P554.pdf , accessed in October, 2013

[7] T. Ackermann (Editor), *Wind Power in Power Systems (First Edition)*. John Wiley & Sons, Ltd, 2005.

[8] Z. Chen, "Issues of Connecting Wind Farms into Power Systems," in *Transmission and Distribution Conference and Exhibition: Asia and Pacific*, pp. 1-6, 2005.

[9] C. Sourkounis and P. Tourou, "Grid Code Requirements for Wind Power Integration in Europe," *Conference Papers in Energy*, vol. 2013, Article ID 437674, 9 pages, 2013.

[10] Erlich, W. Winter, and A. Dittrich, "Advanced grid requirements for the integration of wind turbines into the German transmission system," in *IEEE Power Engineering Society General Meeting*, 2006.

[11] T. Ackermann, A. Ellis, J. Fortmann, J. Matevosyan, E. Muljadi, R. Piwko, et al., "Code Shift: Grid Specifications and Dynamic Wind Turbine Models," *IEEE Power and Energy Magazine*, vol. 11, pp. 72-82, 2013.

[12] Arulampalam, G. Ramtharan, N. Jenkins, V. K. Ramachandaramurthy, J. B. Ekanayake, and G. Strbac, "Trends in wind power technology and grid code requirements," in *International Conference on Industrial and Information Systems*, pp. 129-134, 2007.

[13] W. Jarzyna and P. Lipnicki, "The comparison of Polish grid codes to certain European standards and resultant differences for WPP requirements," in *2013 15th European Conference on Power Electronics and Applications (EPE)*, pp. 1-6, 2013.

[14] Grid code: High and Extra High Voltage, E.ON Netz GmbH Tehc, Rep., 2006, Status: 1.

[15] L. Xu, L. Z. Yao, and C. Sasse, "Grid Integration of Large DFIG-Based Wind Farms Using VSC Transmission," *IEEE Transactions on Power Systems*, vol. 22, no. 3, pp. 976-984, 2007.

[16] Reidy and R. Watson, "Comparison of VSC based HVDC and HVAC interconnections to a large offshore wind farm," in *IEEE Power Engineering Society General Meeting*, Vol. 1, pp. 1-8, 2005.

[17] L. Xu and B. R. Andersen, "Grid connection of large offshore wind farms using HVDC," *Wind Energy*, vol. 9, no. 4, pp. 371-382, 2006.

[18] S. K. Chaudhary, R. Teodorescu, and P. Rodriguez, "Wind Farm Grid Integration Using VSC Based HVDC Transmission - An Overview," in *IEEE Energy 2030 Conference*, pp. 1-7, 2008.

Chapter 2

Modelling and Control of Full Converter Wind Turbine and VSC-HVDC Transmission System

The booming of renewable energy industry has promoted the development of technologies significantly. Though wind energy technology is relatively mature, grid integration of large-scale offshore wind farms still raises new requirements and challenges. This chapter gives an overview of different wind turbine concepts first. Then, the model and control of the wind turbine with full converter and VSC-HVDC transmission system that are applied in this research project are described.

2.1 Wind turbine concepts

The continuous attempts and efforts to make wind power as mainstream power generation are driving the evolvement of wind turbines since the early 1990s. Though a variety of wind turbine concepts have been proposed and under test, there are mainly four types of wind turbine that predominate today's global market. These four wind turbine concepts are all based on horizontal axis, three blades and upwind turbine structures, but can be distinguished by their generator types and power control strategies. They are explained in the following.

2.1.1 Type A: Fixed speed wind turbine

Fixed speed wind turbine (FSWT), which is also recognized as Danish concept, has been introduced and widely used in the early 1990s. As can be seen from Figure 2.1, a fixed speed wind turbine is based on a squirrel cage induction generator (SCIG), its high-speed rotor is coupled with the low-speed turbine rotor via a gearbox and its stator is directly connected to the power grid through a step-up transformer. The electronic soft starter is used to provide a smoother grid connection. Since the induction generator is not capable of controlling reactive power, a shunt capacitor bank is used for reactive power compensation to reduce voltage fluctuation at the point of connection.

This type of wind turbines has simple structure and robust components, and is relatively low-cost.

However, due to the fixed rotation speed of SCIG, the wind fluctuations are directly converted into mechanical fluctuations and consequently into electrical power fluctuations [1]. Thus, the main drawbacks of the fixed speed wind turbine are that its output has significant fluctuations and its components have to tolerate excessive mechanical stress.

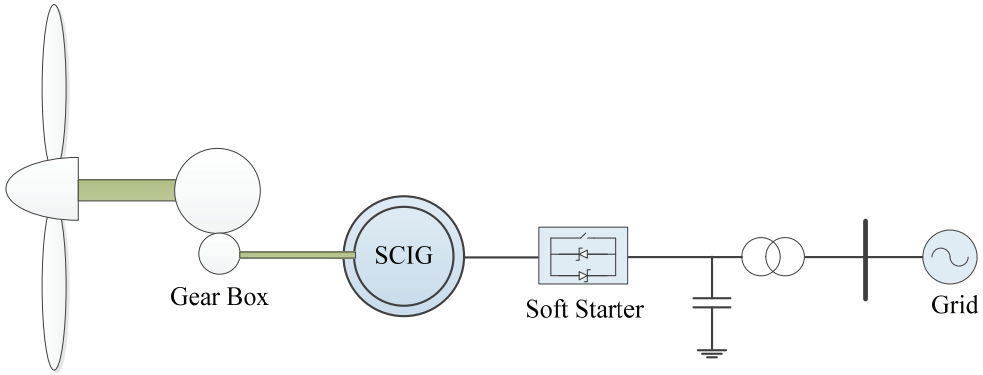

Figure 2.1 Fixed speed wind turbine configuration.

2.1.2 Type B: Limited variable speed wind turbine

This type of wind turbines is equipped with a wound rotor induction generator (WRIG) that is directly connected to the power grid. The gear box, soft starter and shunt capacitor banks in this type play the same roles as in a fixed speed wind turbine. The distinct characteristic is that it has a power electronics controlled variable rotor electrical resistor that enables slip control and allows both the rotor and the generator to vary their speed, typically up to 10%, during wind gusts. Moreover, an active blade pitch control system is also equipped to wind turbines of this type.

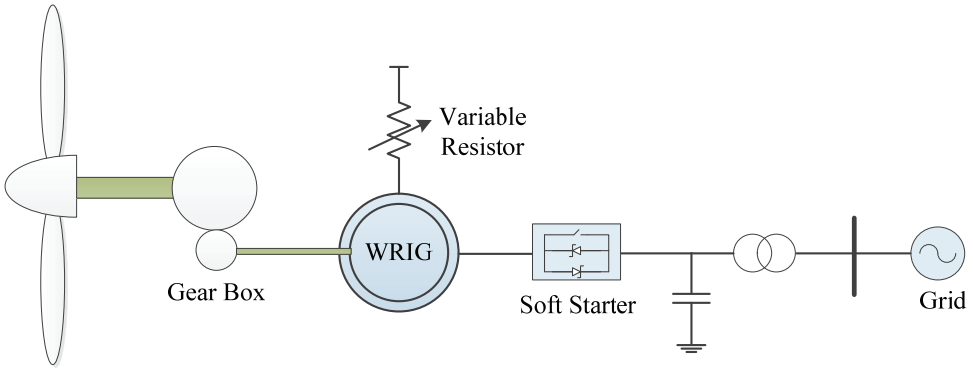

Figure 2.2 Limited variable speed wind turbine configuration.

Compared to Type A wind turbine, a limited variable speed wind turbine is slightly

aerodynamically more efficient and has better power quality and lower drive-train mechanical loading. However, it is still not the preferred choice for nowadays large-scale offshore wind farms.

2.1.3 Type C: Variable speed wind turbine with double-fed induction generator

The configuration of the variable speed pitch-controlled wind turbine with a double-fed induction generator (DFIG) is shown in Figure 2.3. The stator of the DFIG is directly connected to the power grid, whereas the DFIG's rotor circuit is connected to the grid through a partial-scale back-to-back voltage source converter system. The converter system is usually rated at 30% of the nominal generator rating. Besides providing reactive power compensation and smoothing grid connection, the partial-scale converter system enables a wide range of variable speed operation (normally ±30% of the synchronous speed) by varying the slip.

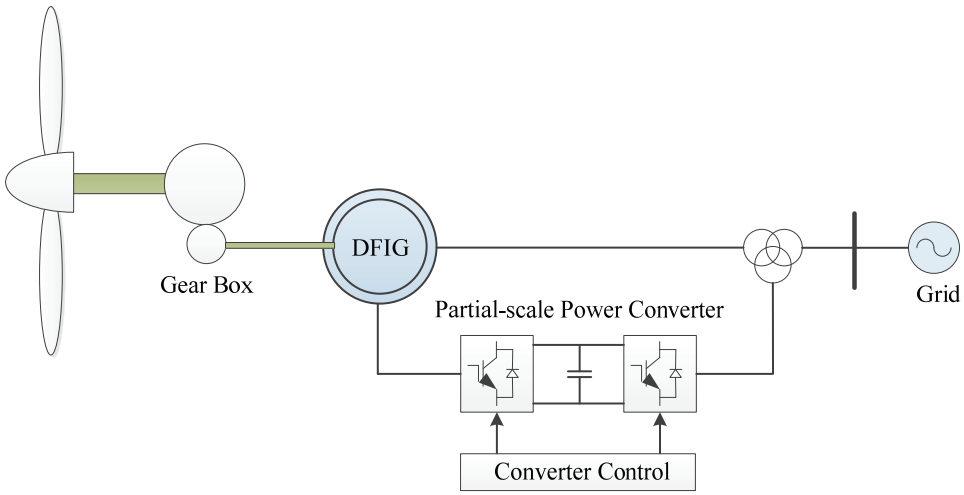

Figure 2.3 DFIG-based wind turbine configuration.

This concept is aerodynamically more efficient and has lower drive-train mechanical stress and power fluctuations. The smaller converter also makes it more cost-efficient. Thus, DFIG-based wind turbine is the most popular system in the current market. However, it needs special rotor current protection system and the use of slip rings reduces its reliability.

2.1.4 Type D: Variable speed wind turbine with full power converter

In this concept (see Figure 2.4), various types of generators can be used: wound rotor synchronous generator (WRSG), WRIG and permanent magnet synchronous generator (PMSG). When a low speed multipole SG is used, the turbine rotor can be interfaced to the SG directly

instead of via a gear box. It is clear from Figure 2.4 that the generator is connected to the power grid through a full-scale back-to-back power electronic converter system. The converter system decouples the generator from the power grid and thus enables a full range of variable speed operation.

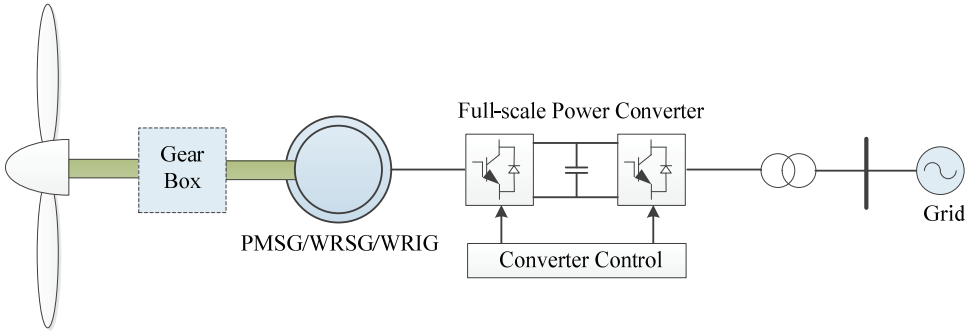

Figure 2.4 Full converter wind turbine configuration.

Compared to Type C wind turbine, full converter wind turbines (FCWT) have better controllability and grid support capability owing to its larger converter system.

2.2 Full converter wind turbine modeling

The spacious sea and higher winds allow offshore wind turbines to be bigger to capture more energy. However, the harsh environment out at the sea also requires that offshore wind turbines must be easy to be assembled and maintained and have higher reliability and performance compared with inland wind turbines. Thus, according to the above summary of wind turbine concepts, it is apparent that the direct-drive variable speed wind turbines with full converter (FCWT) are relatively the most suitable concept for offshore wind applications. Figure 2.5 presents a demonstrative diagram of the wind turbine model used in this research project.

Since the work in this dissertation focuses on the system stability studies concerning the impact of large offshore wind farm on the power system, the offshore wind farm is represented by one equivalent wind turbine with re-scaled power capacity based on aggregation technique [2] – [4]. Therefore, only the detailed modelling of single FCWT is presented here and the modelling of large offshore wind farm is not introduced in this work.

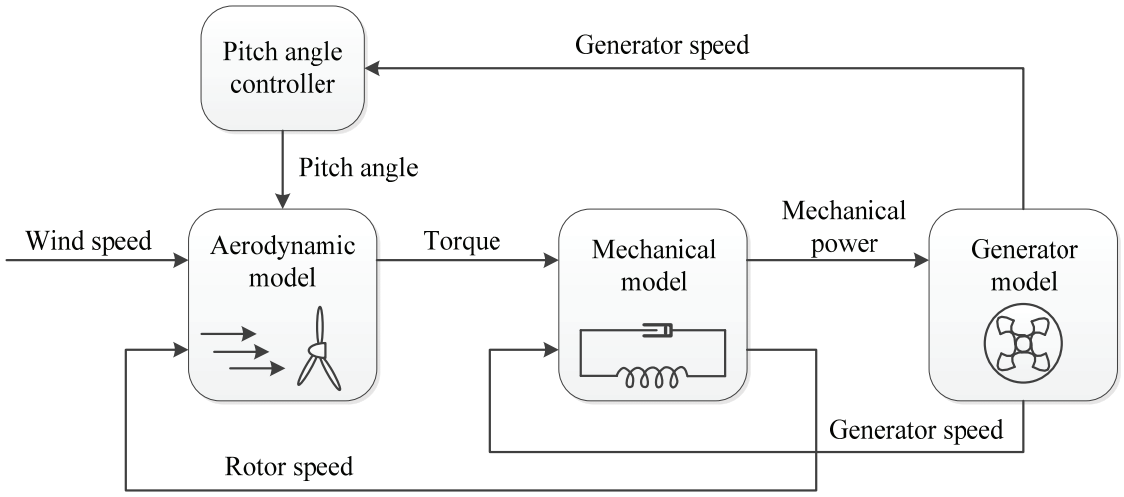

Figure 2.5 Block diagram of the wind turbine model.

2.2.1 Aerodynamic model

The wind turbine system extracts kinetic energy from the wind and converts it to mechanical power to drive the generator. The aerodynamic model of a wind turbine is based on the aerodynamic equation given by [5], [6]:

$$P_M = \frac{1}{2}\rho\pi R^2 v_w^3 c_p(\theta,\lambda) \tag{2.1}$$

where P_M is the mechanical power extracted from the wind; ρ is the air density; R is the rotor radius; v_w is the wind speed; c_p is the aerodynamic power coefficient which depend on the pitch angle θ and the tip speed ratio λ.

The tip speed ratio is the ratio between the rational speed of the tip of a blade and the actual velocity of the wind. It depends on R, v_w and the wind turbine rotational speed ω_t, as:

$$\lambda = \frac{\omega_t R}{v_w}. \tag{2.2}$$

For given values of θ, the relationship of c_p and λ can be illustrated by $c_p - \lambda$ curves as shown in Figure 2.6, which is based on measurement data and modelled as a look-up table as shown in Table 2.1 in this project. Since it is not realistic to list all the c_p corresponding to all $\theta - \lambda$ pairs, Table 2.1 lists part of the $\theta - \lambda - c_p$ relationship. The rest is calculated using the DIgSILENT built-in function '*sapprox2(xl, xc, matrix_i)*'. This function returns the spline approximation *y=f(xl, xc)* of a two-

dimensional array, where *f* is defined by the *matrix_i*, *xl* represents the line value of the matrix and *xc* represents the column value of the matrix. Therefore , we can get

$$c_p = sapprox2(\theta, \lambda, matrix\_i) \tag{2.3}$$

where *matrix_i* is defined by Table 2.1.

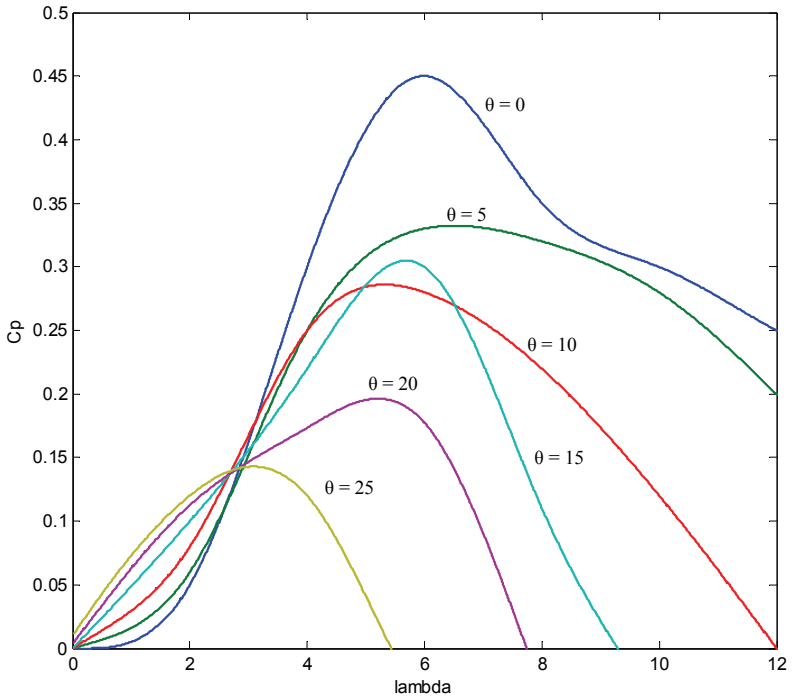

Figure 2.6 c_p-λ curves for given pitch angles

TABLE 2.1

$\theta - \lambda - c_p$ relationship

θ \ λ / c_p	**0**	**2**	**4**	**6**	**8**	**10**
0	0	0.05	0.3	0.45	0.35	0.3
5	0	0.06	0.25	0.33	0.32	0.28
10	0	0.08	0.25	0.28	0.22	0.12
15	0	0.1	0.22	0.3	0.11	-0.05
25	0.01	0.12	0.12	-0.05	-0.2	-0.5

Apparently, over a wide range of wind speeds, the wind turbine achieves the maximum aerodynamic efficiency if the c_p is the maximum for a given pitch angle according to Equation 2.1.

Thus, for a variable speed wind turbine, the maximum aerodynamic efficiency is obtained by controlling its turbine rotational speed to keep the tip speed ratio constant at a predefined value that corresponds to the maximum power coefficient over the range of operational wind speeds [1].

2.2.2 Mechanical model

A two-mass drive train model has been implemented in this project, in which a relative larger mass corresponds to the turbine rotor inertia and a relatively smaller mass corresponds to the generator inertia. The two-mass shaft model not only allows turbine and generator inertias to be represented separately, along with shaft stiffness and damping [7], but also provides enough accuracies of wind turbine's response during grid faults for power system stability studies [8].

The mechanical model of the two-mass shaft can be expressed by [5]-[7], [9]:

$$J_t \frac{d\omega_t}{dt} = T_t - T_{sh} \tag{2.4}$$

$$J_g \frac{d\omega_g}{dt} = T_{sh} - T_e \tag{2.5}$$

$$T_{sh} = D_{sh} \frac{d\theta}{dt} + K_{sh}\theta \tag{2.6}$$

$$\frac{d\theta}{dt} = \omega_t - \omega_g \tag{2.7}$$

where J_t is the wind turbine rotor inertia; J_g is the generator inertia; T_t is the wind turbine rotor torque; T_{sh} is the shaft toqure; T_e is the generator torque; ω_t is the wind turbine rotor speed; ω_g is the generator rotor speed; θ is the shaft twist angle; K_{sh} is the shaft stiffness; D_{sh} is the damping coefficient of the shaft.

2.2.3 Pitch angle control

In variable speed wind turbine generation systems, the pitch angle control is used to: a) optimize the power generation of wind turbines at low and medium wind; b) prevent the mechanical power from exceeding the rated power when the wind is above the rated speed; c) protect the turbine mechanical construction from overloading and risks of damages [6].

Generally, when the wind is below the rated speed, the variable speed wind turbine is required to operate at its maximum efficiency, namely to extract as much power as possible from the wind. As mentioned in the aerodynamic model, to achieve the maximum P_M, the c_p must have the maximum value and thus the pitch angle control is to keep the pitch angle at its optimum value in the wind turbine variable speed operations to have the maximum c_p. When the wind is above the rated speed, the pitch angle is controlled to increase to make the wind turbine operate at lower efficiency and shed excessive aerodynamic power. In consequence, the output power of the wind turbine is restricted to its rated power and the mechanical stress is reduced as well. A generic pitch angle controller is presented in Figure 2.7.

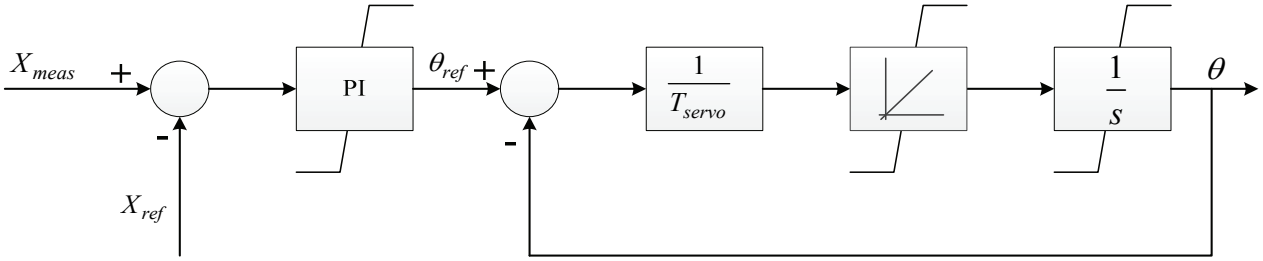

Figure 2.7 Generic pitch angle controller for variable speed wind turbines.

The controlling parameter X could be: a) an electric value, e.g. the electric power P_e; b) a mechanical torque, e.g. the mechanical torque T_t or the generator rotor speed ω_g; c) a combination of electrical and mechanical values [6]. The servo time constant T_{servo} corresponds to the servomechanism that adjusts the pitch angle to its reference. Both the pitch angle range and its rate of change are limited.

2.2.4 Power Converter model and control

DIgSILENT provides standardized built-in model for PWM converters. Based on a fundamental frequency approach, the model is self-commutated and voltage sourced, and is appropriate and sufficient for power system stability studies [10]. Therefore, the back-to-back voltage source converter system for the wind turbine has been developed based on this fundamental frequency model. Moreover, since the sub-transient process inside the converter are not concerned, the VSC converters have been modelled ideally by a DC-voltage controlled AC-voltage source conserving active power between AC- and DC- side [10].

The back-to-back voltage converter system consists of a PWM rectifier (generator-side converter), an intermediate DC circuit and a PWM inverter (grid-side converter). Correspondingly, the converter control also represents two controllers: the generator-side converter controller and the grid-side converter controller. These two controllers are using vector controls, which allow decoupled active and reactive power control. Figure 2.8 illustrates the rotor oriented reference frame (RRF) and the stator voltage oriented reference frame (SVRF), in which E is the internal voltage induced by the permanent magnet field; L_d is the d-axis component of the stator inductance and δ is the load angle.

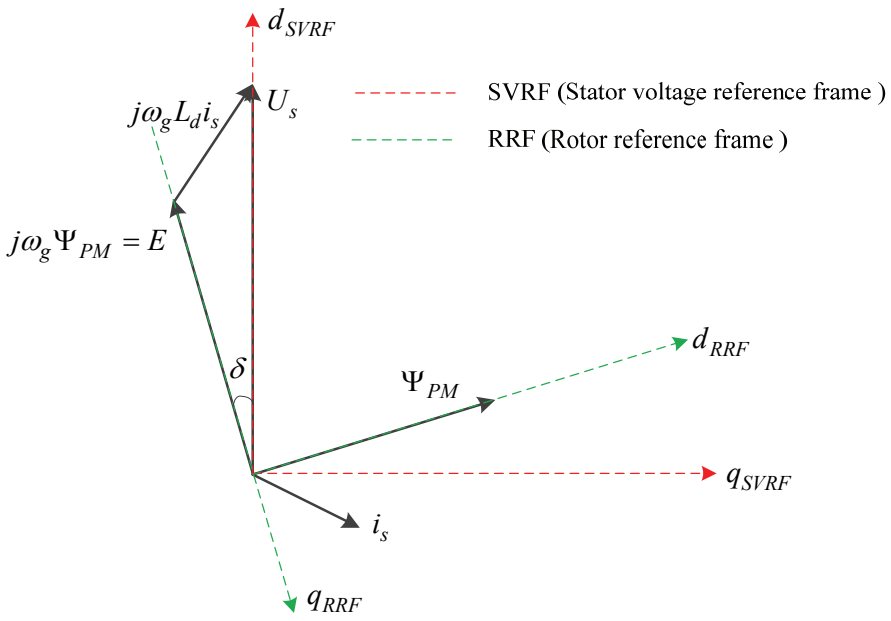

Figure 2.8 Illustration of RRF and SVRF.

Different control strategies can be applied to the frequency converters and in [5], [9] and [11], three control strategies, which are commonly used for the PMSG-based wind turbine, are described and compared:

a) *Maximum torque control*. This control uses the RRF that is aligned with its *d*-axis to the permanent magnet flux vector Ψ_{PM}. In this reference frame, the stator current can be controlled to only have the q-axis component i_{sq} ($i_{sd} = 0$). Thus, the maximum electrical torque T_e of the generator can be determined by the *q*-axis current only as:

$$T_e = \frac{3}{2} p \Psi_{PM} i_{sq} . \tag{2.7}$$

The active and reactive power of the generator can then be expressed as:

$$P_g = \frac{3}{2} u_{sq} i_{sq} \tag{2.8}$$

$$Q_g = -\frac{3}{2} u_{sd} i_{sq} . \tag{2.9}$$

This control strategy uses the total stator current for producing the electrical torque to achieve optimal utilization of the generator. However, since the converter must also meet the reactive power demand of the generator as given by equation (2.9), a larger converter rating is needed.

The grid-side converter maintains a constant DC-link voltage to make sure maximum active power transmission through the DC-link. It also controls the reactive power supplied to the grid.

b) *Constant stator voltage control of the generator*. This control uses the SVRF which is aligned with its *d*-axis to the generator stator voltage U_s. This means that the stator voltage is controlled to only have the *d*-axis component. Thus, the active and reactive power of the generator can be expressed as:

$$P_g = \frac{3}{2} u_{sd} i_{sd} \tag{2.10}$$

$$Q_g = -\frac{3}{2} u_{sd} i_{sq} . \tag{2.11}$$

It can be seen that the active and reactive power of the generator are determined by the *d*-axis and *q*-axis component of the stator current respectively. This control strategy ensures that the generator and generator-side converter always operate at rated voltage and thus the converter has a constant ratio between its DC voltage and AC voltage. In consequent, the converter can avoid overvoltage and saturation at high generator speeds. However, the demand of reactive power of the generator increases the converter rating.

The grid-side converter controls the reactive power to the grid and DC-link voltage as the previous control strategy.

c) *Unity power factor control*. It aims to operate the generator with unity power factor and to control its active power output in accordance with the MPPT. To achieve this, the *d*-axis component of the stator current in RRF can be used to compensate the reactive

power demand of the generator. Thus, the active power of the generator depends on the *q*-axis component of the stator current in RRF as:

$$P_g = \omega_g \cdot T_e = \omega_g \cdot \frac{3}{2} p\Psi_{PM} i_{sq} . \tag{2.12}$$

And the reactive power of the generator is controlled to Zero. In this control strategy, the converter doesn't need to provide reactive power for the generator, which minimizes the converter rating.

In this control, the grid-side converter controls the reactive power to the grid and DC-link voltage as the previous control strategy.

A. Control of the generator-side converter

In this project, the constant stator voltage control strategy is chosen for the generator-side converter. Thus, as above mentioned, the generator-side converter aims to control the active power output of the generator and keeps the stator voltage constant. The generic control scheme of the generator-side converter is shown in Figure 2.9.

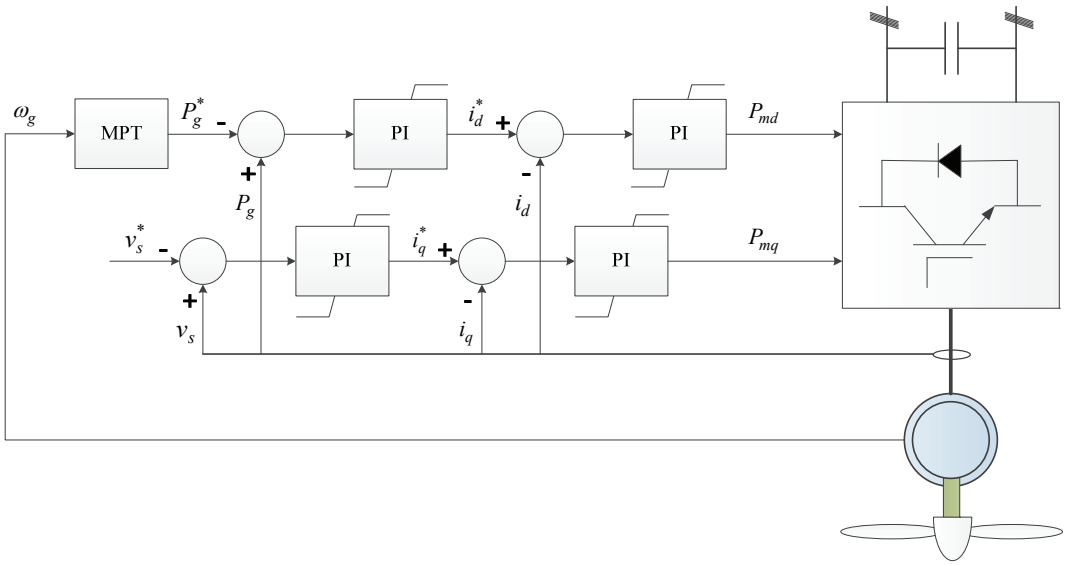

Figure 2.9 Generic control of the generator-side converter.

As can be seen, each control loop uses a cascaded control structure. The fast inner current control regulates the converter AC current (i_d & i_q). The slow outer loop of *d*-axis controls the generator active power generation. The maximum power tracking (MPT) is used to produce the power reference P_g^* in terms of the generator speed, which guarantees that the generator operates at

its highest efficiency. Instead of controlling the active power, the generator-side converter can also be implemented to control the torque or generator speed through the *d*-axis current [12]. The slow outer loop of *q*-axis controls the generator stator voltage to its rated value v_s^* by regulating the reactive power of the generator-side converter. The P_{md} and P_{mq} in Figure 2.9 represent the pulse-width modulation index of *d*- and *q*-axis respectively.

B. Control of the grid-side converter

A steady DC voltage ensures all active power of the generator to be transmitted to the grid regardless of the converter loss. Therefore, the grid-side converter aims to maintain a constant DC voltage and control the reactive power exchange with the grid in a grid voltage oriented reference frame. The generic control of the grid-side converter is presented in Figure 2.10.

The control also employs a cascaded control structure as does the generator-side converter control. The grid-side converter controls the DC voltage to its rated value v_{dc}^* through *d*-axis current and the reactive power output through *q*-axis current. The reactive power reference Q_{grid}^* can be set to zero to enable a unity power factor power transmission or to be a reference value that is imposed by the TSO. Alternatively, the *q*-axis control loop can also be used to control the grid voltage.

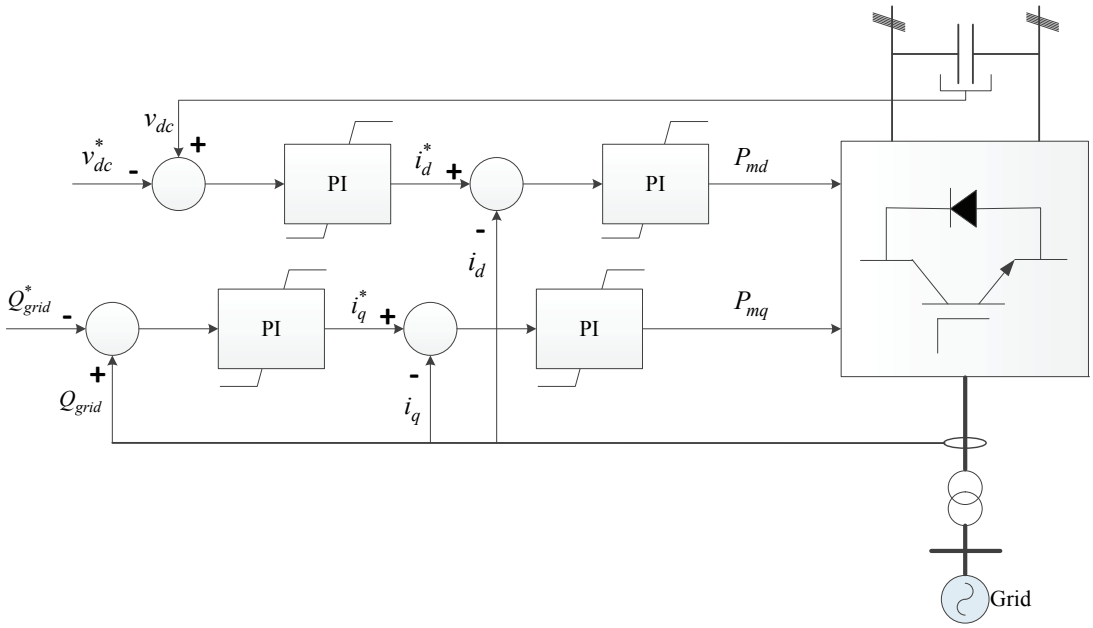

Figure 2.10 Generic control of grid-side converter.

2.3 VSC-HVDC modeling

2.3.1 Overall structure

In this project, a bipolar VSC-HVDC transmission system with a ±150kV DC link has been used to connect the offshore wind farm to the onshore power grid. The schematic single line diagram and the actual layout designed in DIgSILENT are shown in Figure 2.11. Similar to the converter model used in the wind turbine with full converter, the offshore and onshore converters of VSC-HVDC have been using the built-in fundamental frequency converter model in DIgSILENT. To calculate load flow and study power system stabilities, this model is not only valid for two-level converters but also for three-level or multi-level converters [10].

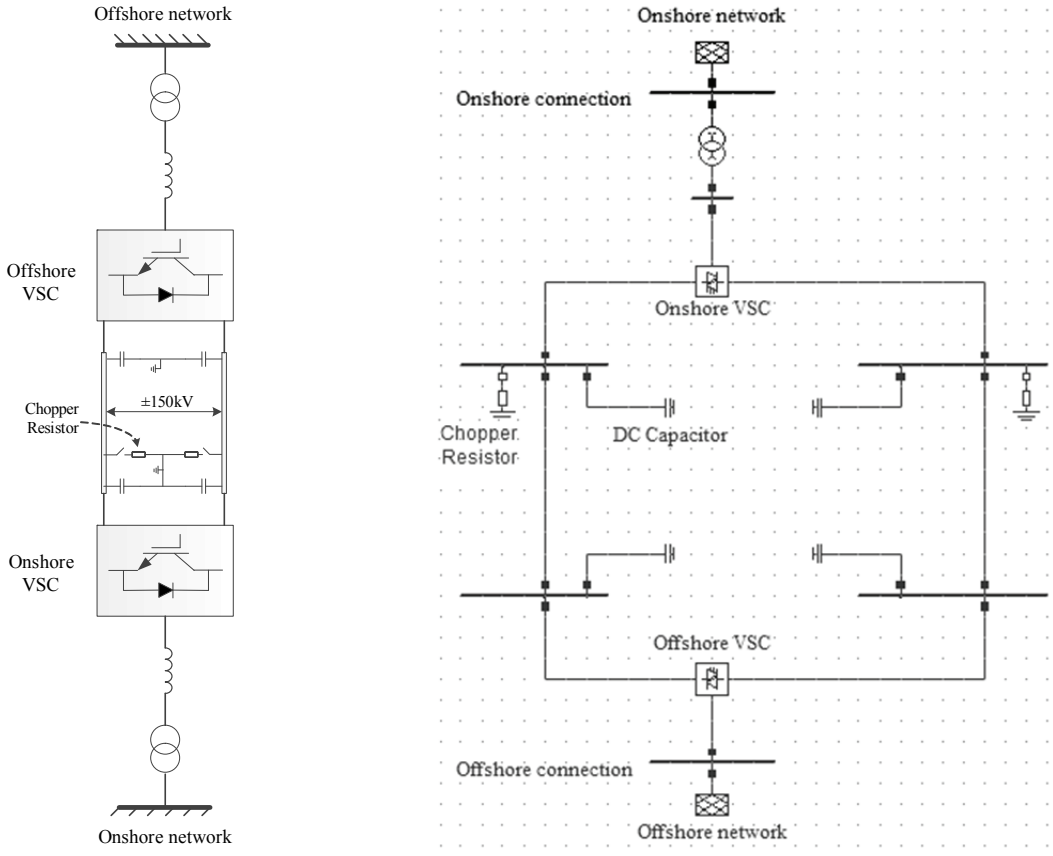

(a) (b)

Figure 2.11 VSC-HVDC system: (a) Single line diagram; (b) Layout in DIgSILENT.

2.3.2 Control system

Voltage source converters have a four-quadrant operation in the *d-q* plane and decoupled control for active and reactive power [9]. That provides the VSC-HVDC transmission with the capability of fast and bidirectional active power flow control and the capability of absorbing or delivering reactive power to the connected network. This flexible controllability of active and reactive power is beneficial to improve the power system stability.

In general, the control of the VSC-HVDC is also based on the cascaded control structure that consists of a slow outer control loop and a fast inner current control loop. Various electrical variables can be used as the control objectives of the converters. However, under normal conditions, one of the converters must be used to maintain a constant DC link voltage to keep a balanced active power flow along the DC link. Fluctuations on the DC link voltage represents that the power that flows into the VSC-HVDC is not equal to the power that flows out of the VSC-HVDC without regard to the losses.

A. Offshore VSC control

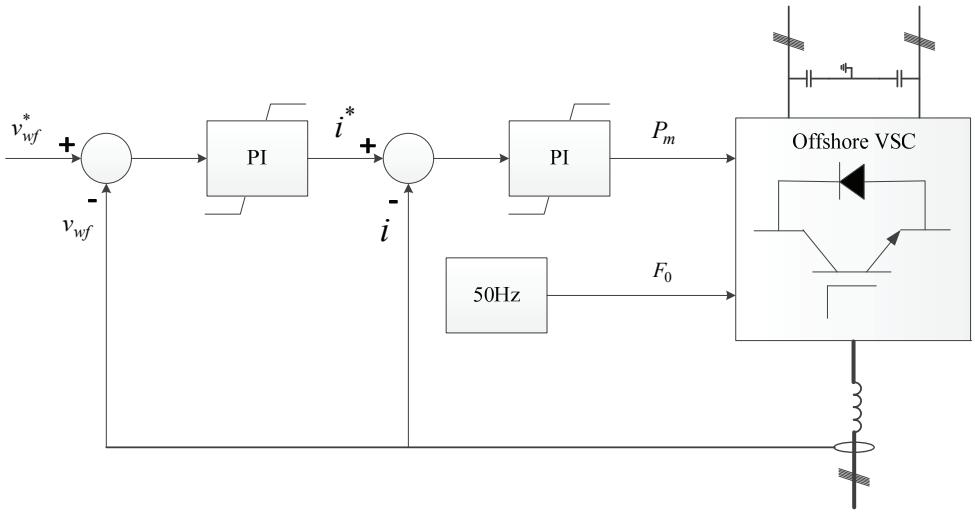

Figure 2.12 Control of offshore VSC.

While linked with the offshore wind farm with FCWTs, the offshore VSC is responsible for collecting the active power generated by the FCWTs and providing constant voltage and frequency for the offshore wind farm network as a reference machine during normal operations [13], [14]. Since the offshore VSC is not required to control the power flow, a simple control method is

adopted to keep the voltage magnitude at a desired value and the frequency is directly regulated without using a feedback loop. Without identifying whether the power is active or reactive, the control strategy allows the offshore VSC to transmit the offshore wind farm power generation automatically [15]. However, the converter may be overcurrent during offshore grid disturbances as there is no current control [14]. The control scheme is presented in Fig. 2.12, in which i is the measured offshore VSC current, and P_m and F_0 stand for the PWM index magnitude and the frequency input to the offshore-VSC respectively.

B. Onshore VSC control

The primary responsibility of the onshore VSC is to deliver the active power transmitted from the offshore VSC into the onshore power grid. The control of the onshore VSC uses the grid voltage oriented reference frame which is aligned with its d-axis to the grid voltage. In consequence, the decoupled active and reactive power control is achieved, in which the active power is controlled by the d-axis component of the converter current and the reactive power is controlled by the q-axis component of the converter current as [16]:

$$\begin{bmatrix} P \\ Q \end{bmatrix} = \frac{3}{2} i_d \begin{bmatrix} v_d \\ v_q \end{bmatrix} + \frac{3}{2} i_q \begin{bmatrix} v_q \\ -v_d \end{bmatrix}. \tag{2.11}$$

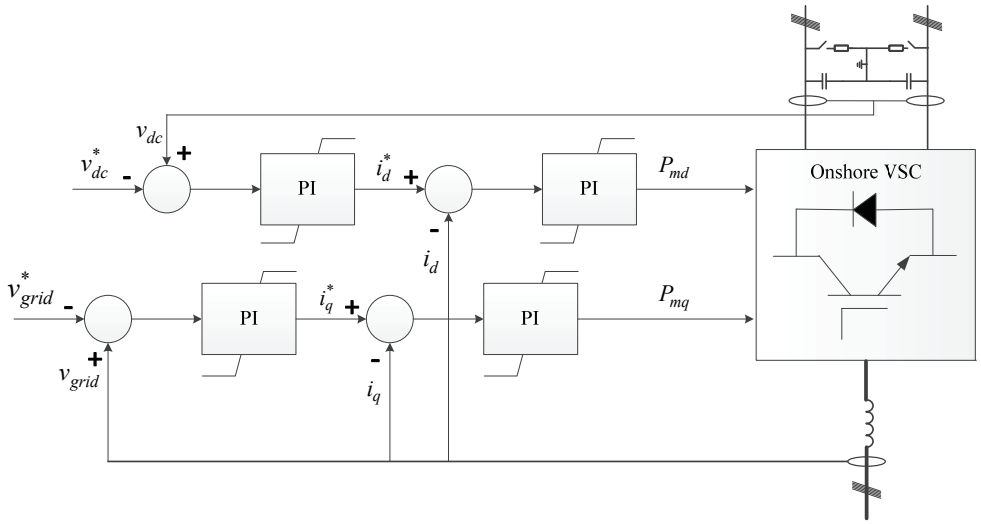

Figure 2.13 Control of onshore VSC.

As aforementioned, the DC link voltage must be maintained to guarantee the active power transmission balance between the offshore and onshore converters. The onshore VSC is, therefore,

used to control the DC link voltage and either the reactive power infeed or the grid voltage magnitude at the connection point. Figure 2.13 shows the onshore VSC control scheme with cascaded PI control loops.

2.4 Summary

In this chapter, the popular used wind turbine concepts have been introduced briefly. Compared with other wind turbine concepts, the full converter wind turbine concept appears to be more suitable for offshore wind applications. For transmitting the great amount of energy generation of remotely located large offshore wind farms, the selection of transmission system is prone to VSC-HVDC. Hence, the modelling of FCWT and VSC-HVDC has also been described in detail as well as their basic control principles. The FCWT-based offshore wind farm and VSC-HVDC are then used for further studies in this project. Appendix A presents the converter control frames of VSC-HVDC and FCWT.

Bibliography

[1] T. Ackermann (Editor), *Wind Power in Power Systems (First Edition)*. John Wiley & Sons, Ltd, 2005.

[2] V. Akhmatov, H. Knudsen, "An aggregate model of a grid-connected, largescale, offshore wind farm for power stability investigations-importance of windmill mechanical system", *International Journal of Electrical Power and Energy Systems*, Volume 24, Number 9, pp. 709-717(9), November, 2002.

[3] M. Pöller, S. Achilles., "Aggregated Wind Park Models for Analyzing Power System Dynamics", in *Processing of Fourth International Workshop on Large-scale Integration of Wind Power and Transmission Networks for Offshore Wind Farms*, Billund, Denmark, 2003.

[4] J. Conroy, R. Watson, "Aggregate modelling of wind farms containing full-converter wind turbine generators with permanent magnet synchronous machines: transient stability studies," *IET Renewable Power Generation*, vol.3, no.1, pp.39-52, March 2009.

[5] G. Michalke, "Variable speed wind turbines – modeling, control, and impact on power systems," PhD thesis, Darmstadt University of Technology, Germany, 2008.

[6] V. Akhmatov, "Analysis of dynamic behavior of electric power systems with large amount of wind power," PhD thesis, ØRSTED-DTU, Denmark, 2003.

[7] J. Conroy and T. Watson, "Torsional damping control of gearless full-converter large wind turbine generators with permanent magnet synchronous machines", *Wind Energy*, Vol. 31, no. 5, pp. 325-340, 2007.

[8] G. Michalke, and A.D. Hansen, "Modelling and control of variable speed wind turbines for power system studies" *Wind Energy*, vol. 13, no. 4, pp. 307-322, 2010.

[9] A.D. Hansen, F. Iov, P. Sørensen *et al*, "Dynamic wind turbine models in power system simulation tool DIgSILENT," RISØ Report R-1400 (EN), RISØ national Laboratory, Denmark, 2003.

[10] DIgSILENT GmbH, “PWM Converter – DIgSILENT technical documentation”, March 2008.

[11] G. Michalke, A. D. Hansen and T. Hartkopf, “Control strategy of a variable speed wind turbine with multipole permanent magnet synchronous generator,” in *EWEA Conference proceedings*, Brussels, 2007.

[12] S. Achilles and M. Pöller, “Direct drive synchronous machine models for stability assessment of wind farms,” in *Processing of Fourth International Workshop on Large-scale Integration of Wind Power and Transmission Networks for Offshore Wind Farms*, Billund, Denmark, 2003.

[13] L. Xu and B. R. Andersen, "Grid connection of large offshore wind farms using HVDC," *Wind Energy*, vol. 9, no. 4, pp. 371-382, 2006.

[14] C. Feltes, H. Wrede, F. W. Koch, and I. Erlich, "Enhanced Fault Ride-Through Method for Wind Farms Connected to the Grid Through VSC-Based HVDC Transmission," *IEEE Transactions on Power Systems*, vol. 24, no. 3, pp. 1537-1546, 2009.

[15] L. Xu, L. Z. Yao, and C. Sasse, "Grid Integration of Large DFIG-Based Wind Farms Using VSC Transmission," *IEEE Transactions on Power Systems*, vol. 22, no. 3, pp. 976-984, 2007.

[16] Y. Liu, “The study on Hybrid multi-infeed HVDC systems connecting with offshore wind farm”, PhD thesis, Aalborg University, Denmark, 2013.

Chapter 3

Impact of VSC-HVDC based Offshore Wind Farm Integration on Power System Stability

A large offshore wind farm normally has a capacity of hundreds of MW. The long distance to shore of large offshore wind farms makes it more realistic and effective to use VSC-HVDC transmission instead of HVAC. This chapter presents the impact of VSC-HVDC based large-scale offshore wind farm integration on power system stability. First, the voltage support control of VSC-HVDC during voltage dips is described. Then, the stability issues of the studied system with offshore wind farm integration via VSC-HVDC are analysed regarding steady-state voltage stability, dynamic voltage stability and transient stability.

3.1 Introduction

Power system stability is *the ability of an electric power system, for a given initial operating condition, to regain a state of operating equilibrium after being subjected to a physical disturbance, with most system variables bounded so that practically the entire system remains intact* [1]. It is a complex problem that can be influenced by a wide range of factors and can be exhibited by different forms. On the basis of several essential considerations, the power system stability problem can be categorized into different classes as shown in Figure 3.1 [1], [2]:

Traditional power systems rely on synchronous generators for supplying electrical power and the power systems stability is, therefore, mainly determined by these synchronous machines. However, wind energy conversion systems have dynamical characteristics quite different from conventional power generation units. With the increasing penetration of wind power and the integration of large-scale wind farms, power systems will undoubtedly witness significant changes in their structures and operations since conventional power plants will be gradually withdrawn from operation. Accordingly, detailed analysis of the impact of wind power on power system stability becomes substantial necessary and critical. Numerous studies have been carried out on power system stability with regard to wind power integration, e.g. [3]-[9]. Most of these studies were dealing with SCIG- or DFIG- based wind farms connected to the power grid via HVAC links.

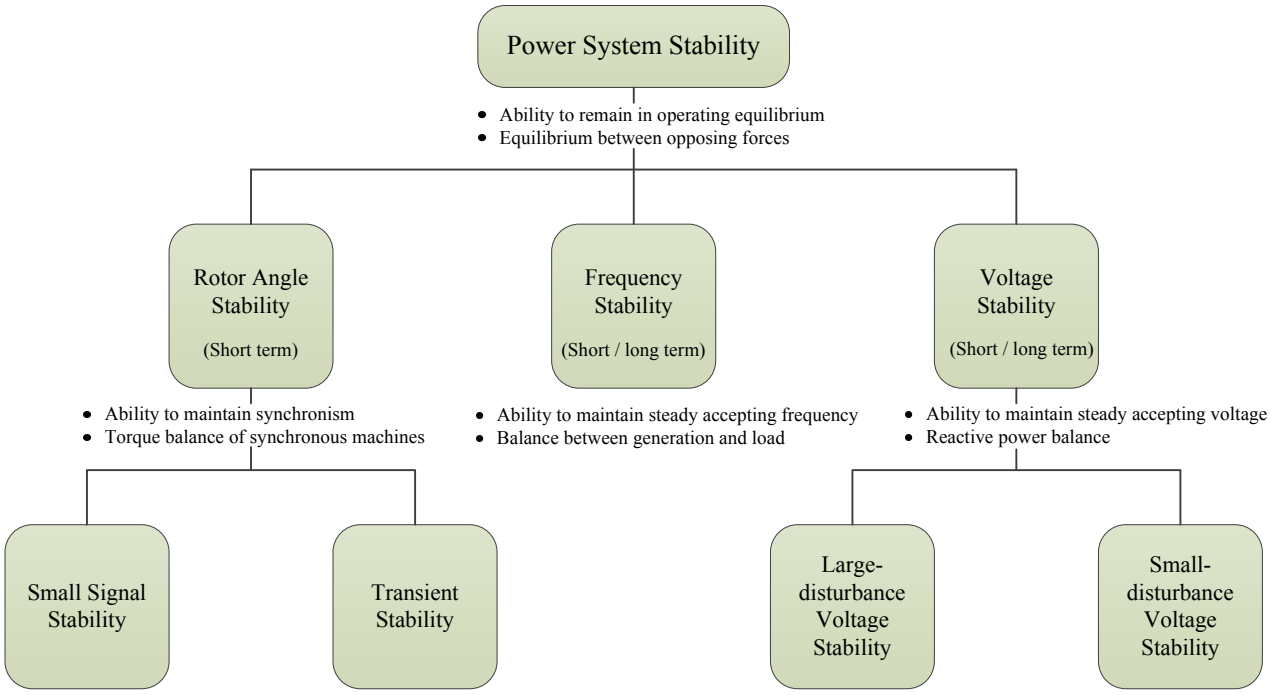

Figure 3.1 Classification of power system stability [1], [2].

By means of the advantages mentioned in Chapter 1 and 2, VSC-HVDC transmission becomes the primary choice for connecting large-scale offshore wind farms over long distances. Furthermore, its fast independent control for active and reactive power can also be utilized to support the interconnected grid during stressed conditions. In [10], the benefits of VSC-HVDC for power system stability were presented regarding to voltage stability and transient stability in three different grid configurations: a) series connection of the VSC converter and the AC-system; b) parallel connection of the VSC link and the AC-system and c) asynchronous infeed from the VSC converter into the AC-system. Based on a winter peak load Irish transmission network, it has been concluded in [11] that VSC-HVDC can efficiently protect the FCWT-based offshore wind farm from the onshore grid fault and provide fault ride-through (FRT) for the wind farm compared to the HVAC connection. The transient stability of PMSG-based offshore wind farm was analyzed in [12] based on HVAC and VSC-HVDC transmission respectively. The offshore wind farm with VSC-HVDC was proved to be more robust during the given onshore grid fault. However, the impact on power system stability of large-scale offshore wind farm interconnected via VSC-HVDC has not been thoroughly investigated.

Therefore, this chapter presents the impact of VSC-HVDC based large-scale offshore wind farm integration on power system voltage and transient stability. The voltage control of VSC-HVDC is

derived from E.ON grid code and the VSC-HVDC support to power system stability is also addressed.

3.2 Voltage support control of VSC-HVDC

Due to the decoupling of VSC-HVDC, the offshore wind farm cannot directly detect and respond to the onshore grid disturbances in time. Moreover, reactive current/power cannot be transmitted by DC links. Therefore, for the offshore wind farm connected to the AC grid via VSC-HVDC, the voltage support is basically provided by the onshore VSC of VSC-HVDC.

3.2.1 Reactive current support requirement of E.ON grid code

As aforementioned in Chapter 1, a generating unit is required to provide reactive current infeed of at least 2% of its rated current for each per cent of the voltage dip. Accordingly, the slope of the reactive current support line is equal to at least 2. Figure 3.2 illustrates the principle of voltage support during the grid faults according to E.ON code. The detailed information can be found in [13].

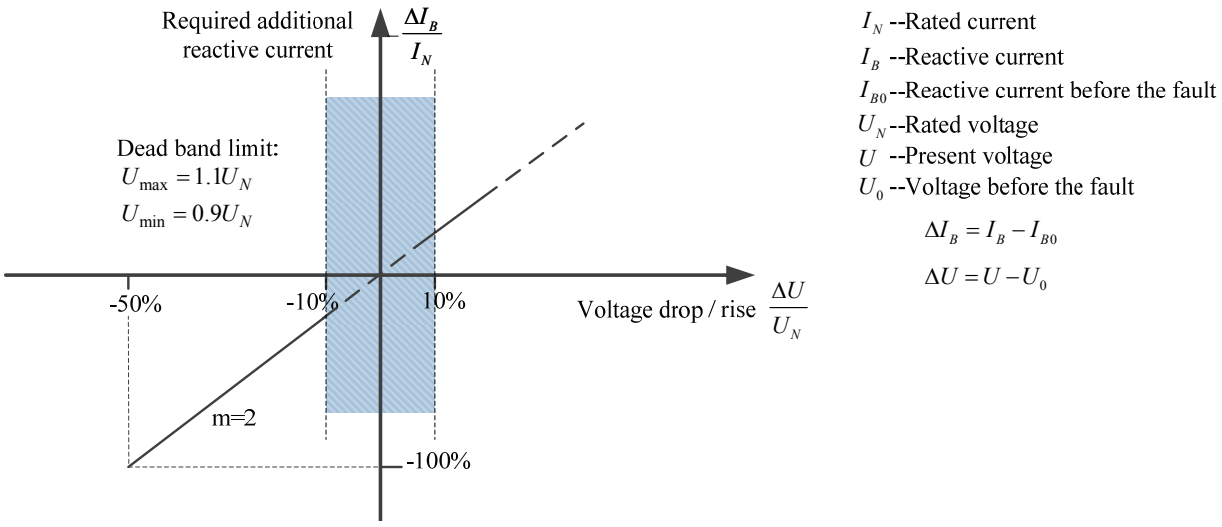

Figure 3.2 Fundamental voltage support requirement during grid faults according to E.ON code [13].

3.2.2 VSC control strategy under fault conditions

As depicted in Chapter 2, under normal conditions, the offshore VSC is responsible for collecting and transmitting the active power generated by the offshore wind farm, while maintaining the AC

voltage magnitude and frequency of the offshore network. At the same time, the onshore VSC is responsible for feeding the active power transmitted from the offshore VSC into the onshore power grid, while maintaining a constant DC link voltage of VSC-HVDC to guarantee the power balance between VSCs.

During onshore grid faults, the voltage drop leads to the reduction of the power transmission capacity of VSC-HVDC. That means that the onshore VSC cannot inject all the received active power into the onshore grid. If no countermeasures are implemented, the power differences between offshore and onshore VSCs would cause a rapid increase in DC-link voltage since the DC capacitance is over-charged. To cope with this issue, there are generally two methods [14] - [16]:

1) *Fast reduction of the offshore wind farm output power.* The objective using this method is gained by employing coordinated control strategies between the offshore wind farm and VSC-HVDC, e.g. [16], [17].

2) *DC chopper*. The abnormal DC-link voltage activates the DC chopper to dissipate the excess energy that cannot be transmitted by the onshore VSC in a large resistor as in [14], [18].

The main advantage of the first method is that it can avoid the use of the chopper or reduce the chopper size so as to cut down the investment for additional equipment. However, it may introduce high mechanical stress for the wind turbine drive train and electrical stress for the converters. The communication delay and measurement sensitivity are also critical for some control strategies. By comparison, the DC chopper solution is very robust and easier to be implemented though it is expensive. The main advantage of the DC chopper solution is that the offshore wind farm is immune from the onshore grid voltage disturbances. The grid faults will hardly affect the operation speed and output power of the offshore wind turbine generators.

To simplify the design, the DC chopper solution is used in this study. Therefore, the control of wind turbines and the offshore VSC remains the same as described in Chapter 2. The control of the onshore VSC must be modified to enable the onshore VSC to provide voltage support during grid voltage disturbances. The modified control based on E.ON grid code is shown in Figure 3.3.

When the onshore grid voltage deviates out of the dead band (see Figure 3.2) due to faults, a simple P controller is activated instead of the PI controller functioning in normal operations. It

enables the onshore VSC to make a fast response to the grid voltage deviations. The maximum reactive current output depends on the current limit of the onshore VSC. Besides, to meet the voltage support requirements of the grid code, the reactive current (q-axis component) has a higher priority than the active current (d-axis component) during grid faults. It means that if necessary, the onshore VSC would sacrifice its active power output to meet the needs of reactive current output. The relation of active and reactive current output in case of grid faults was defined in the Current Limiter and can be expressed as:

$$\begin{aligned} & i_{d\max} = \sqrt{i_{\max}^2 - i_q^2} \\ & i_d \le i_{\max} \\ & -i_{\max} \le i_q \le i_{\max} \end{aligned} , \tag{3.1}$$

where i_d and i_q are the active and reactive current respectively, i_{dmax} is the active current limit and i_{max} is the current limit of the onshore VSC. The i_{max} represents the maximum allowed current of the onshore VSC, which is 1.1 times of the rated current in this study. The voltage supportive reactive current during grid voltage drops is calculated according to:

$$\begin{aligned} & i_q = m \cdot (v_{grid} - v_{grid}^* - v_{db}) \\ & -i_{\max} < i_q < i_{\max} \end{aligned} , \tag{3.2}$$

where m is the slope of the reactive current support line, v_{grid} is the AC voltage at the onshore VSC in pu, v^*_{grid} is the reference AC voltage at the onshore VSC in pu and v_{db} is the threshold of the deadband.

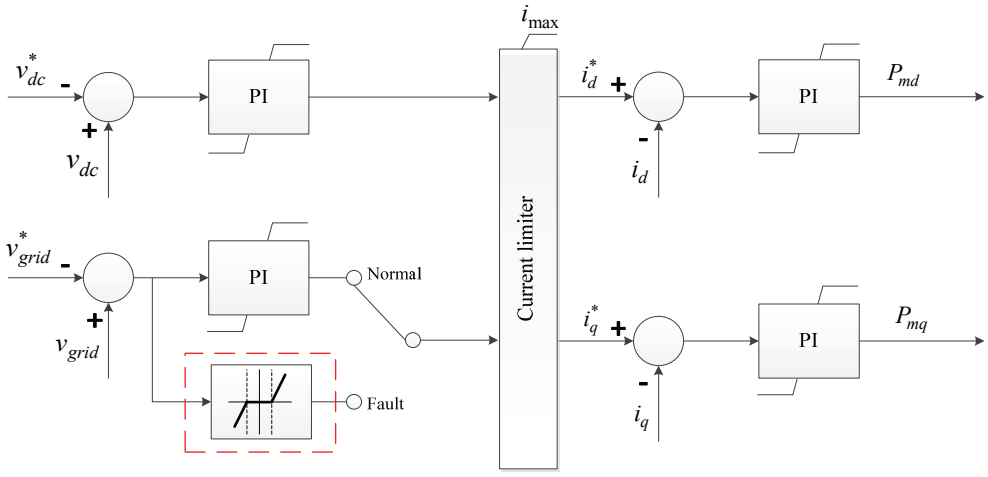

Figure 3.3 Modified control of onshore VSC for voltage support.

3.2.3 Control of DC chopper

The DC chopper is installed at the DC-side of the onshore VSC and its control is independent of VSCs control. Therefore, a simple hysteresis function is used to control the DC chopper based on the DC-link voltage. The DC chopper is activated when the DC voltage reaches 1.1 *pu*, and it is deactivated when the DC voltage drops below 1.02 *pu*. The thermal capacity of the chopper resistor is not considered in this study. As the highest steady DC overvoltage is controlled to be 1.1 pu, the chopper resistance is given by:

$$R \approx \frac{(1.1 \times v_{dc}^{*})^2}{\mathrm{P}_{rated}}. \tag{3.3}$$

3.3 Studied transmission system

The transmission system used to carry out the studies is shown in Figure 3.4. This system model is originally derived from [19] and has been modified to suit the requirements of this study. It consists of four conventional synchronous generators, in which G1 is an external grid equivalent with a large inertia. Several constant impedance loads are connected to different buses and the load center is at Bus9 together with shunt capacitor banks of 1500 Mvar. Shunt reactors are connected to Bus6 and Bus 5 for compensating the capacitive charging current of the 400 kV lines. The aggregated offshore wind farm with FCWT-based wind turbines is connected to the transmission system through the VSC-HVDC link at Bus11. As shown in Figure 3.4, the point of common coupling (PCC) is Bus11. More details of this transmission grid are given in Appendix B.

3.4 System stability analysis

3.4.1 Steady state voltage profile

The steady state voltage profile is represented by P-V curve, which are drawn by increasing the offshore wind power injection but keeping the system loads constant. The power balance in grid is achieved by the reference generator G1, while the active power generations of G2-G4 are not changed. Here, two wind power injection modes are considered:

1) Unity power factor wind power supply: Assume that the onshore VSC operates at unity power factor and only active power is delivered into the main grid.

2) Rated PCC voltage wind power supply: Assume that the onshore VSC has the capability to provide enough reactive power support to keep a rated PCC voltage while delivering wind power.

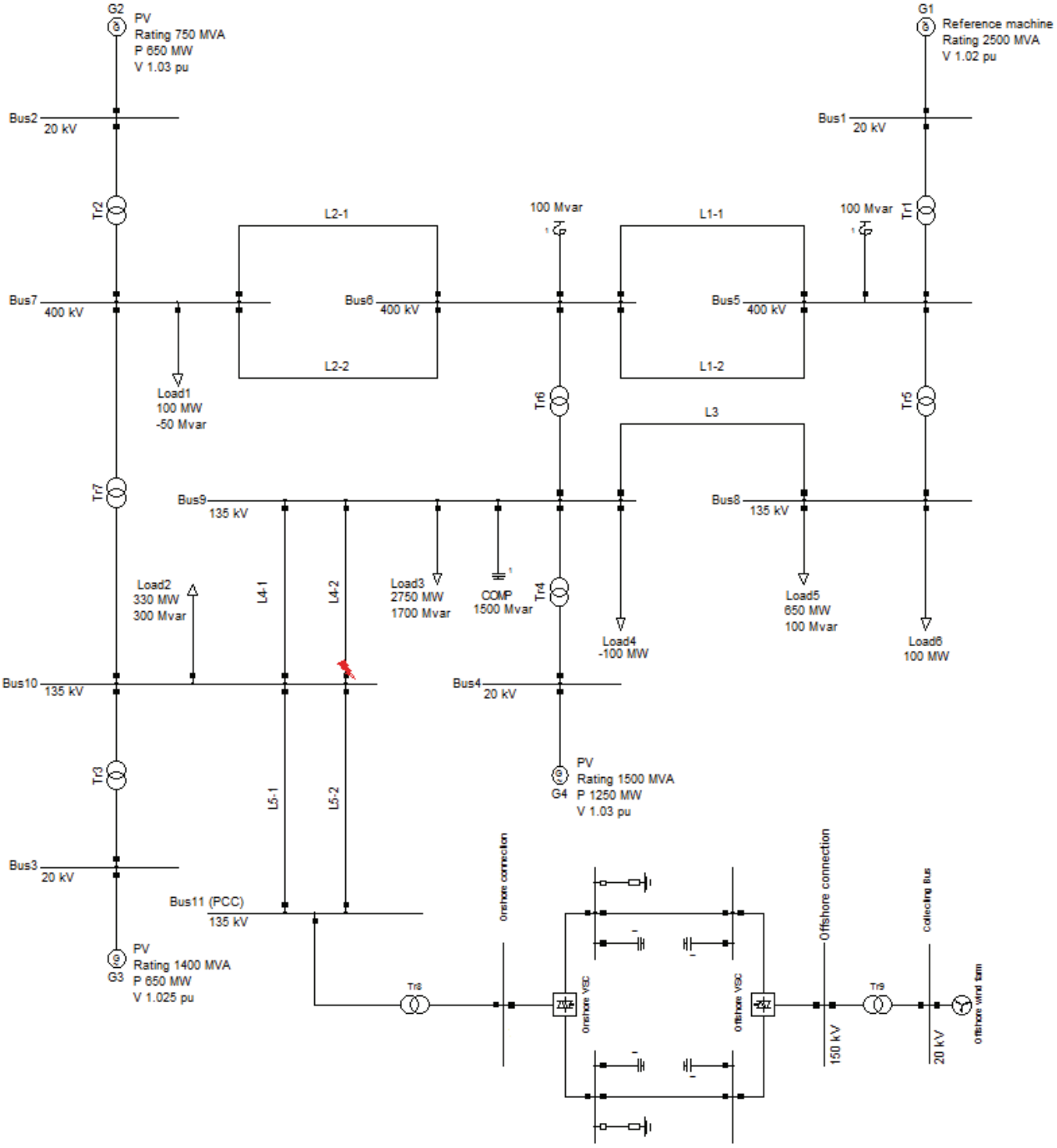

Figure 3.4 Single line diagram of the test transmission system [19].

Figure 3.5 shows the P-V curves of PCC with unity power factor wind power supply and Bus10 with rated PCC voltage wind power supply. It can be seen that the higher the wind penetration, the

lower the voltage of the selected buses. In this study, the wind power injection leads to the increase in loading of all the transmission lines except L3. Clearly, the loading of the lines close to the wind farm increases faster than the lines far from the wind farm. The increase in the active power transmission results in greater reactive power demand of the lines, especially when the line is overloaded. When the reactive power demand of the lines cannot be met, the voltage of the buses attached to the lines starts to drop as shown in Figure 3.5.

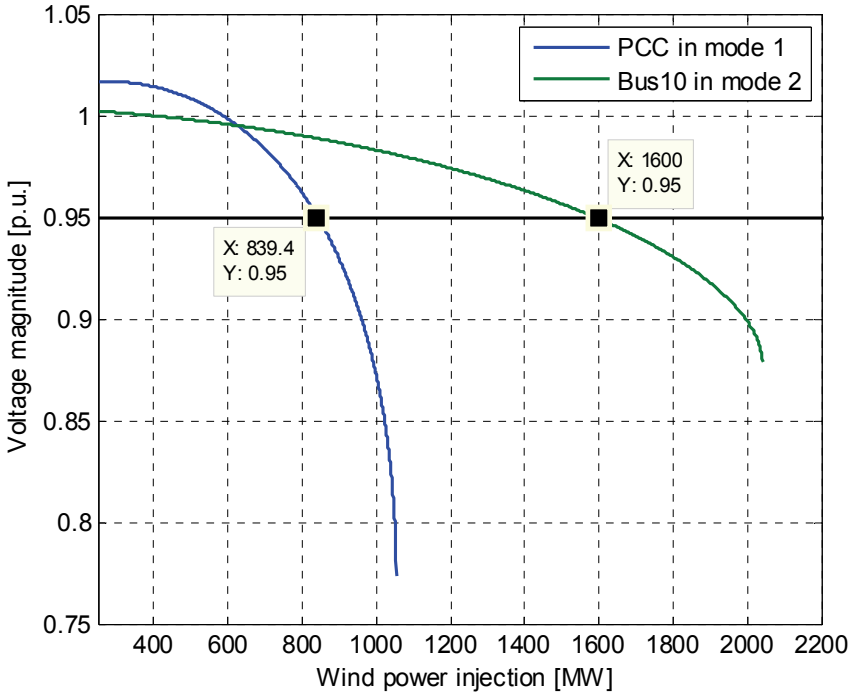

Figure 3.5 P-V curves of PCC with unity power factor wind power supply and Bus10 with rated PCC voltage wind power supply.

Moreover, the wind power penetration limit (WPPL) is directly related to the reactive power support capability of the onshore VSC. In this study, the WPPL is defined as the maximum wind power injection with which the connection node voltage reaches 0.95 pu. In mode 2, the connection node is thought as Bus10 since the PCC voltage is always set constant. From Figure 3.5, we can see that the WPPL in mode 2 is almost doubled compared with that in mode 1.

3.4.2 Dynamic voltage stability

To investigate the dynamic behavior of grid voltages, a severe three-phase ground fault is simulated at 90% of the line L4-2 near Bus10 (see red lighting mark in Figure 3.4). This fault lasts

for 200ms and is cleared by tripping L4-2 without consideration of line reclosing. Two levels of wind power penetration are studied: 270MW and 450MW, and their corresponding VSC-HVDC rating are 300MVA and 500MVA respectively. Figure 3.6 shows the dynamic voltages of Bus10 and PCC at different penetration levels in the event of the given fault.

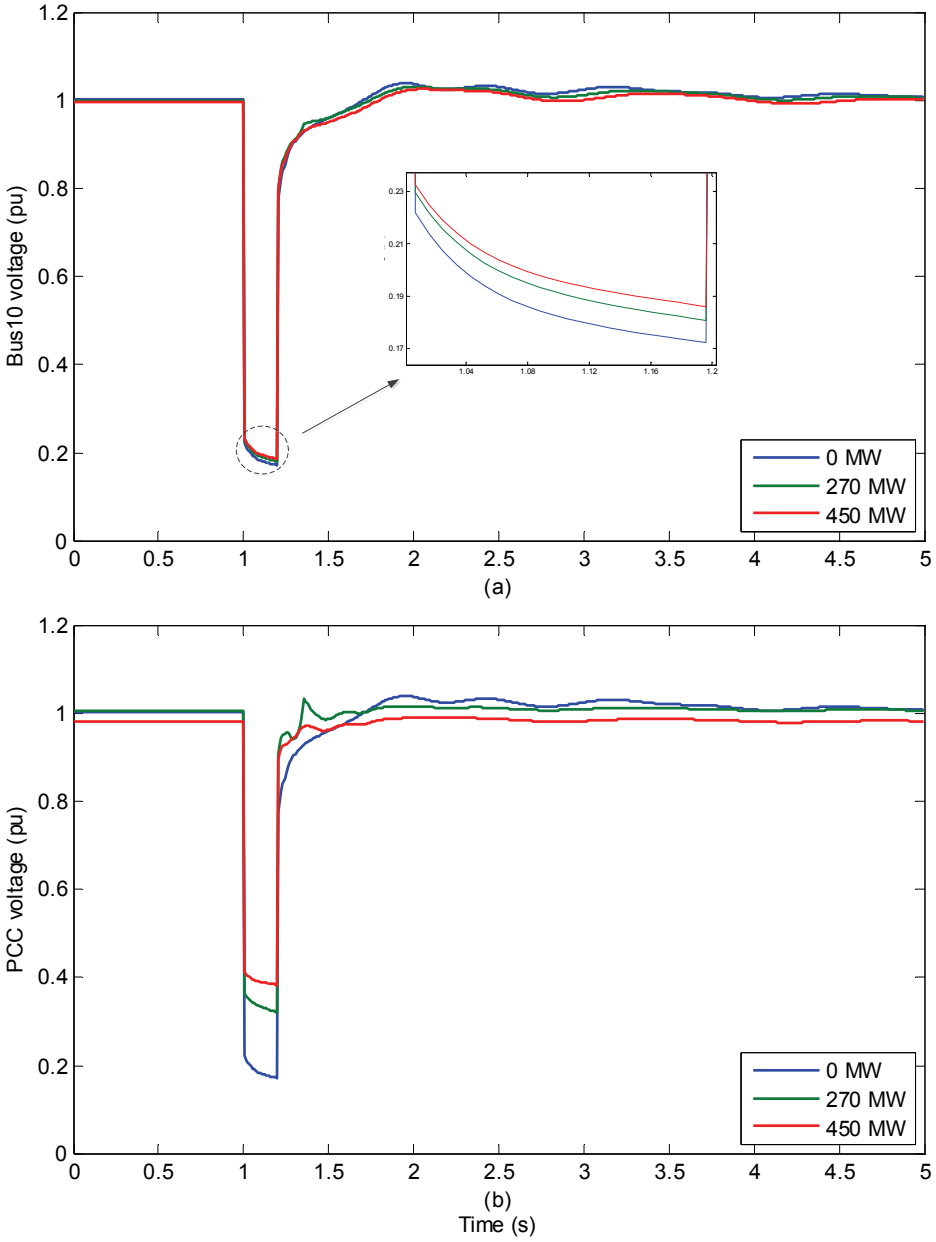

Figure 3.6 Dynamic voltages of Bus10 and PCC at different wind penetration levels: (a) Voltage magnitude of Bus10; (b) Voltage magnitude of PCC.

It can be seen from Figure 3.6 that under normal conditions, the voltages of PCC and Bus10 are a bit lower when the wind power is higher as described before. During the fault period, the voltage profile is on the contrary. The highest voltage is observed during the gird disturbance in the maximum wind power injection case, whereas the voltage is the lowest with no wind power penetration. These distinct voltage profiles are caused by the fact that the onshore VSC adopts a different control strategy during grid disturbances.

In normal operations, the onshore VSC is controlled to transfer as much active power as it receives (within its rated capacity). However, when a grid fault is detected and the onshore VSC terminal voltage drops below the threshold value of the dead band, the control of the onshore VSC is changed to guarantee reactive power support with the reduction of active power output if necessary. The active and reactive power outputs of the onshore VSC are shown in Figure 3.7. It is clear that during the voltage dip, the reactive power output increases significantly together with the sharp decrease in active power output. As seen from Figure 3.7a, the active power output restores instant after the fault is cleared. The overshoots of the *P* curves are caused by the discharging of DC-link capacitance. In Figure 3.7b, the sudden restored voltage of PCC leads to the overshoots of the *Q* curves at 1.2 s. Obviously, a larger converter is able to provide a larger amount of reactive power and thus has better voltage support capability during grid faults as could be observed.

3.4.3 Transient angle stability

Transient angle stability here is characterized by critical clearing time (CCT), which is defined as maximal fault duration for which the system remains synchronous operation. It highly depends on system configuration and network parameters. Therefore, before analyzing the impact of wind integration on system transient angle stability, the steady-state operation of synchronous generators is firstly investigated at different wind penetration levels.

We have already known that the increase in wind penetration would lead to a decrease in the connection node voltage as depicted in Figure 3.5. As a consequence, more reactive power is needed to compensate for this voltage drop and thus the synchronous generators in the grid will take this responsibility assuming that no more ancillary equipment is deployed for wind integration. Figure 3.8 presents the loading and rotor angle of synchronous generators of the grid at different wind penetration levels.

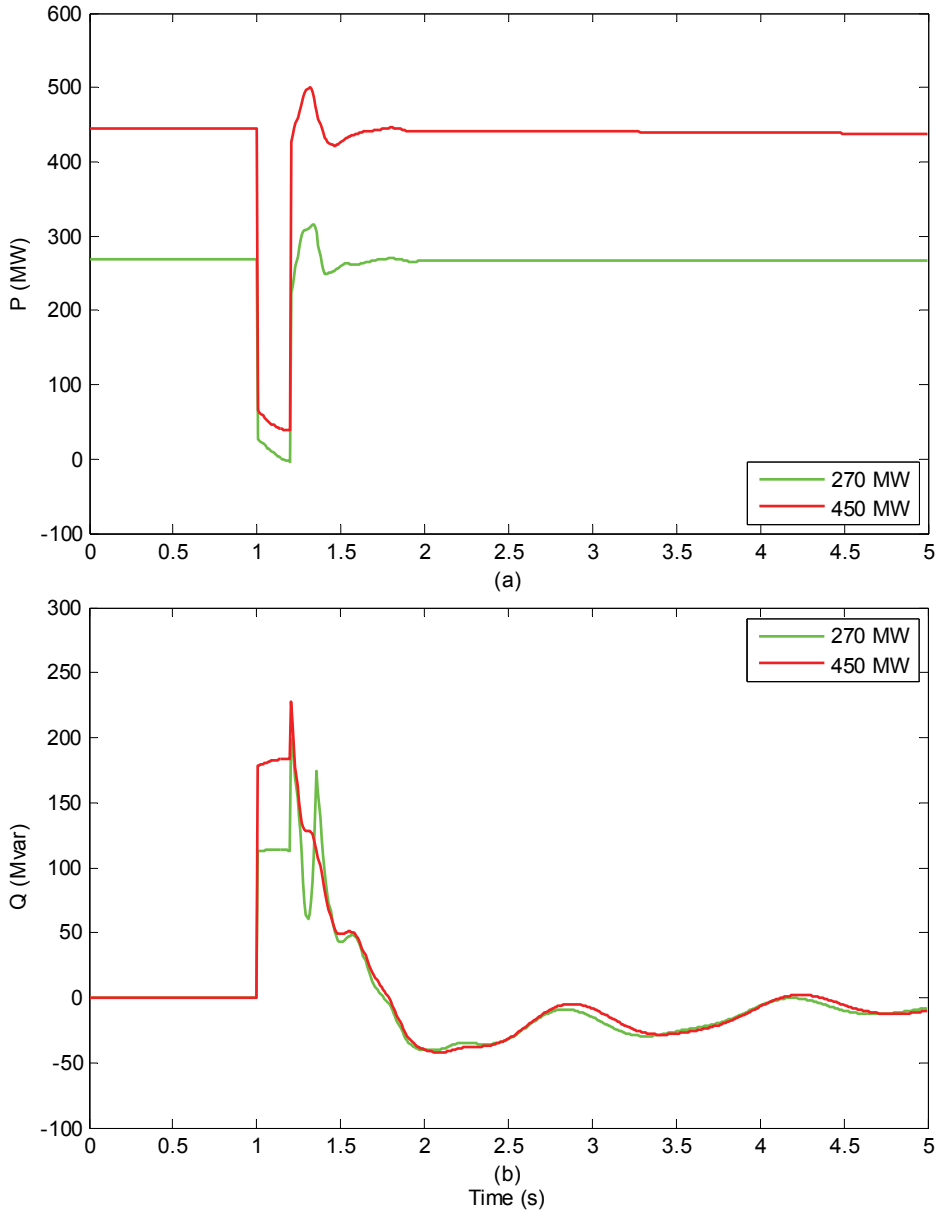

Figure 3.7 Active and reactive power output of the onshore VSC: (a) Active power output; (b) Reactive power output.

In the proposed power grid, G1 is set as the reference machine and the system loads are constant. So, the loading levels of G2, G3 and G4 climb slightly (Figure 3.8a) together with an obvious increase in their rotor angles (Figure 3.8b) while the wind penetration level gets higher, whereas G1's loading declines as its active power generation is offseted by wind power. Clearly, G2 is the most vulnerable to lose synchronism since its loading is very high and rotor angle is the biggest. The loading of a synchronous generator is defined as:

$$Loading = \frac{\sqrt{P_{gen}{}^2 + Q_{gen}{}^2}}{S_N} \times 100\% \tag{3.4}$$

where P_{gen} and Q_{gen} are the active and reactive power generation respectively, and S_N is the generator's nominal apparent power.

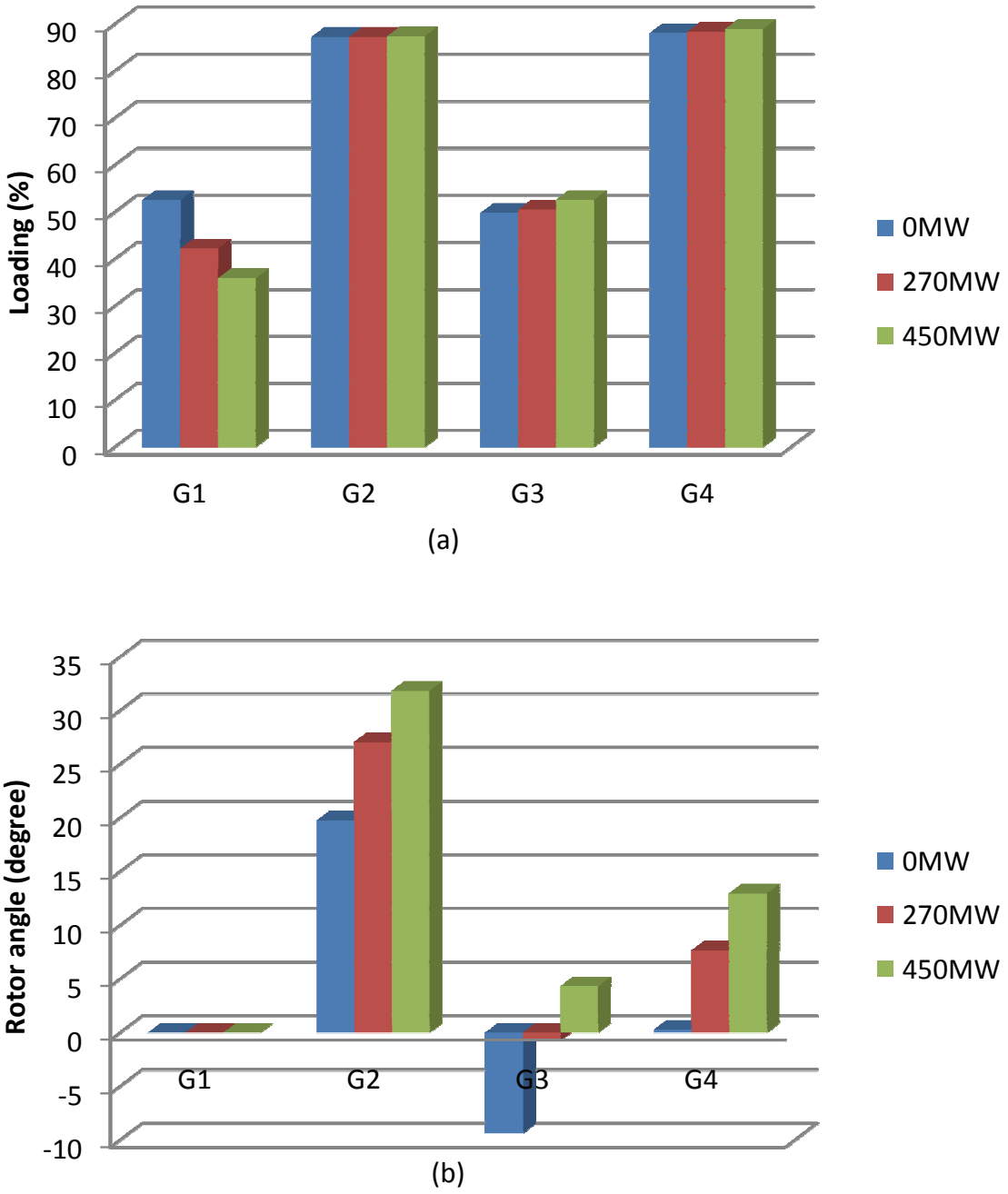

Figure 3.8 Loading and rotor angle of synchronous generators in steady-state.

To calculate CCT, three-phase short circuit fault has been simulated at different individual lines and been cleared afterwards by tripping the faulted line. The simulation results are illustrated in Figure 3.9 for given fault locations and given wind integration levels. It is observed that the integration of wind power into the studied power grid via VSC-HVDC could result in enhanced or weakened transient angle stability depending on the fault locations. In all cases, G2 is always the first one who falls out of synchronism as expected.

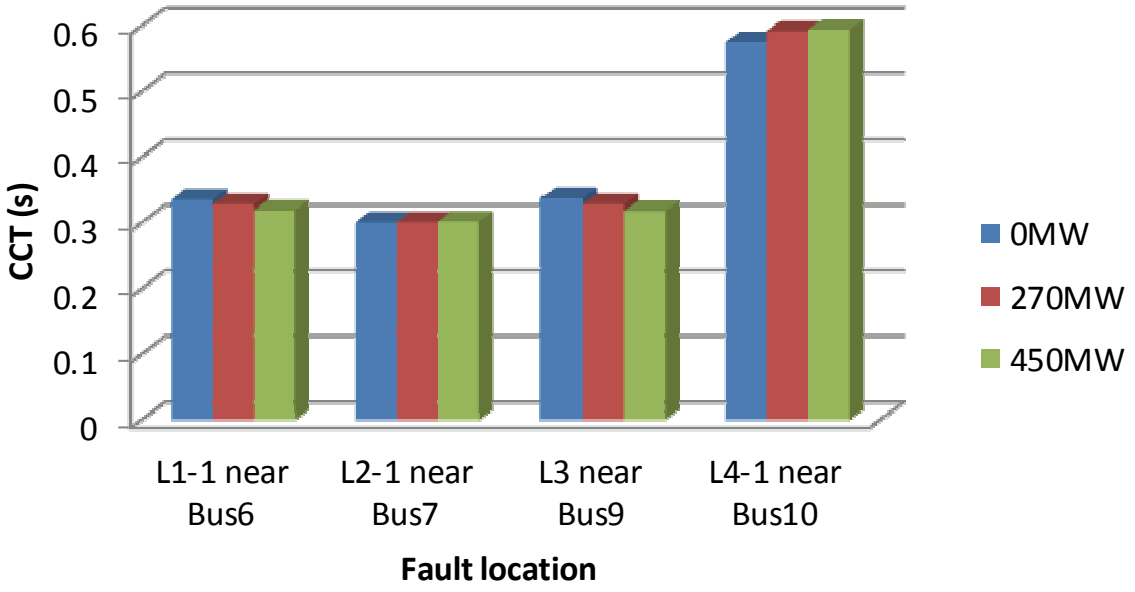

Figure 3.9 Critical clearing time for different fault locations with increasing wind penetration.

Due to a short electrical distance, the given fault at L2-1 near Bus7 causes instant and disastrous voltage drop on G2 terminal. Therefore, regardless of wind penetration levels, the CCT for this study scenario is the shortest and keeps almost fixed. For scenarios in which the given fault occurs at L1-1 near Bus6 or at L3 near Bus 9, the system becomes less transient angle stable with higher wind penetration. The reason is that the wind power injection has changed the system power flow and assigned more loads on L1-1 and L1-2. During given grid disturbances, low voltage on Bus6 or Bus9 makes L1-1 and L1-2 overloaded, causes shunt reactors and capacitor banks ineffective and thus deteriorates the transient angle stability. However, the wind integration exerts a positive impact on transient angle stability while the given fault happens at L4-1 near Bus10 due to the reactive power support capability of the onshore VSC as explained above.

3.5 Summary

In this chapter, the impact of VSC-HVDC based large offshore wind farm integration on power system stability has been studied. In addition to steady-state voltage profile analysis, dynamic voltage stability and transient angle stability simulations have also been conducted at different wind penetration levels.

Basically, the P-V curves indicate the impact of the increasing wind power injection on steady-state voltages of the studied power system and the maximum wind power capacity that the given grid can bear. It can be drawn that the grid voltages experience a decrease with an increase in wind power in general, if no ancillary reactive power compensation equipment is provided. However, with rated PCC voltage wind power supply, the WPPL can be greatly enhanced compared to that with unity power factor wind power supply for the given power grid. It proves that the VSC-HVDC plays a very important role in wind power transfer owing to its reactive power support capability.

The relation between wind power penetration and steady-state grid voltages could be also inferred in the dynamic voltage simulation. However, during grid disturbances, the bus voltage is higher with higher wind penetration. It is due to the independent active and reactive power controllability of VSC-HVDC link, the proposed control strategy of the onshore VSC and the fact that higher wind injection brings higher rating converters that can provide more reactive power support.

The analysis of transient angle stability is actually a case-by-case issue, which is strongly influenced by system configuration and network parameters. The wind power integration changes the system power flow, loading of generators and lines, generators' rotor angles etc. For the studied transmission grid, the transient angle stability generally becomes worsen with higher wind penetration that results in higher loading of transmission lines (except L3). However, owing to the control strategy of VSC-HVDC during grid faults, the VSC-HVDC is able to limit its active power output and, at the same time, enhance its reactive current output when it detects grid voltage faults. Therefore, an improvement in transient angle stability has actually been achieved when the given fault occurs at the line close to PCC.

Bibliography

[1] P. Kundur, J. Paserba, V. Ajjarapu, G. Andersson, A. Bose, C. Canizares*, et al.*, "Definition and classification of power system stability IEEE/CIGRE joint task force on stability terms and definitions," *IEEE Transactions on Power Systems,* vol. 19, no.3, pp. 1387-1401, 2004.

[2] P. Kundur, *Power System Stability and Control*. New York: McGraw-Hill, Inc., 1994.

[3] I. Erlich, C. Feltes, F. Shewarega, M. Wilch, "Interaction of large offshore wind parks with the electrical grid," in *Third International Conference on Electric Utility Deregulation and Restructuring and Power Technologies,* pp.2658-2663, April 2008.

[4] F. Shewarega, I. Erlich, J.L. Rueda, "Impact of large offshore wind farms on power system transient stability," in *Power Systems Conference and Exposition,* pp.1-8, March 2009.

[5] I.S. Naser, O. Anaya-Lara, K.L. Lo, "Study of the impact of wind generation on voltage stability in transmission networks," in *4th International Conference on Electric Utility Deregulation and Restructuring and Power Technologies (DRPT)*, pp.39-44, July 2011.

[6] Y. Liu, Y. Chi, W. Wang, H. Dai, "Impacts of large scale wind power integration on power system," in *4th International Conference on Electric Utility Deregulation and Restructuring and Power Technologies (DRPT)*, pp.1301-1305, July 2011.

[7] Ch. Eping, J. Stenzel, M. Pöller, H. Müller, "Impact of large scale wind power on power system stability," DIgSILENT GmbH. [online]. Available at: http://www.digsilent.org/ .

[8] Akhmatov, V..; Eriksen, P.B., "A Large Wind Power System in Almost Island Operation—A Danish Case Study," *IEEE Transactions on Power Systems*, vol.22, no.3, pp.937-943, Aug. 2007.

[9] N. R. Ullah, T. Thiringer, and D. Karlsson, "Voltage and Transient Stability Support by Wind Farms Complying With the E.ON Netz Grid Code," *IEEE Transactions on Power Systems,* vol. 22, no. 4, pp. 1647-1656, 2007.

[10] S. G. Johansson, G. Asplund, E. Jansson, R. Rudervall, "Power system stability benefits with VSC DC-transmission systems," in *Proceedings of Cigré conference in Paris*, Session B4-

204, 2004. [online]. Available: http://library.abb.com/.

[11] A. Reidy and R. Watson, "Comparison of VSC based HVDC and HVAC interconnections to a large offshore wind farm," in *IEEE Power Engineering Society General Meeting,* vol. 1, pp. 1-8, June 2005.

[12] N. Inaba, R. Takahashi, J. Tamura, M. Kimura, A. Komura, and K. Takeda, "Transient stability analysis of HVAC or HVDC transmission system based offshore wind farm," in *15th International Conference on Electrical Machines and Systems (ICEMS)*, pp. 1-6, 2012.

[13] Grid code: High and Extra High Voltage, E.ON Netz GmbH Tehc, Rep., 2006, Status: 1.

[14] P. Sandeberg, L. Stendius, "Large scale offshore wind power evacuation by HVDC light®", in *Proceedings of EWEC*, 2008. [online]. Available: http://www05.abb.com/global/

[15] R. L. Hendriks, R. Völzke, W. L. Kling, "Fault ride-through strategies for VSC-connected wind parks," in *Proceedings of EWEC*, 2009. [online]. Available: http://proceedings.ewea.org/ewec2009/

[16] C. Feltes, H. Wrede, F. W. Koch, and I. Erlich, "Enhanced Fault Ride-Through Method for Wind Farms Connected to the Grid Through VSC-Based HVDC Transmission," *IEEE Transactions on Power Systems*, vol. 24, no. 3, pp. 1537-1546, 2009.

[17] L. Xu, L. Z. Yao, and C. Sasse, "Grid Integration of Large DFIG-Based Wind Farms Using VSC Transmission," *IEEE Transactions on Power Systems*, vol. 22, no. 2, pp. 976-984, 2007.

[18] Chaudhary, S.K.; Teodorescu, R.; Rodriguez, P.; Kjar, P.C., "Chopper controlled resistors in VSC-HVDC transmission for WPP with full-scale converters," in *IEEE PES/IAS Conference on Sustainable Alternative Energy (SAE),* pp. 1-8, Sept. 2009.

[19] V. Akhmatov and A. H. Nielsen, "Simulation Model of the Transmission Grid for a Large Offshore Windfarm, Used in Education and Research at the Technical University of Denmark," *Wind Engineering*, vol. 30, no. 3, pp. 255-263, 2006.

Chapter 4

Enhancement of Voltage Support Capability of VSC-HVDC for Offshore Wind Applications Using Trajectory Sensitivity Analysis

VSC-HVDC is characterized by independent active and reactive power control and hence is able to provide reactive power / voltage support during grid voltage disturbances. The voltage support capability of VSC-HVDC depends on both its VSC capacity and the control scheme. In this chapter, a TSA-based approximation is proposed as a method to identify the minimum onshore VSC capacity with which the VSC-HVDC is able to provide effective support for stabilizing the grid voltage following a grid disturbance. The proposed TSA-based method implements a two-stage approximation strategy to improve the accuracy of the linear approximation. Both reactive power-based and voltage-based trajectory sensitivities are used to verify the effectiveness of the proposed method. This proposed method avoids running large amount of repeated time-domain simulations.

4.1 Introduction

The integration of large-scale offshore wind farms could influence the power system operation and stability significantly. Power system voltage stability refers to the ability of a power system to maintain steady voltages at all buses in the system after being subjected to a disturbance from a give initial operating condition [1]. The main factor causing voltage instability is that the power system is unable to meet the reactive power demand during heavy load or by the occurrence of large disturbances [2], [3]. One of the widely used preventive measures to avoid voltage instability is the application of reactive power compensating devices, such as Static Synchronous Compensator (STATCOM), Static Var Compensator (SVC). The VSC-HVDC link is characterized by independent reactive and active power control and therefore is able to provide reactive current/voltage support and improve system voltage stability.

For offshore wind farms integrated through VSC-HVDC link, the interaction of offshore wind farms and the onshore power system is mainly determined by the VSC-HVDC link itself. Therefore, during grid faults, the requirement for wind farms to ride through low grid voltage and to provide reactive current to support grid voltage during and after the faults is actually fulfilled by VSC-HVDC

link then. The capability of reactive current / voltage support of VSC-HVDC depends on both its control strategy and VSC capacity. A reliable combination of control strategy and VSC capacity could meet the fault ride-through requirement and maintain the post-fault grid dynamic voltage stability. This study proposes a trajectory sensitivity based method to design the onshore VSC capacity of VSC-HVDC with the fault ride-through control strategy based on E.ON grid code [4].

Trajectory sensitivity analysis is a technique based on linearizing the system around a nominal trajectory [5]-[7]. It can effectively complement time domain simulation and provide valuable insights into the behavior of the dynamic system in accordance with the changes in parameters and operating conditions. TSA was originally used to cope with issues in control systems and parameter estimation [5], [9], and has also been successfully applied in analysis of power system dynamics in recent decades, such as parametric influences on system dynamics, parameter uncertainty, parameter estimation and stability assessment [10].

TSA was applied in [11] to investigate a real major disturbance of the Nordel power system. In [12], two techniques based on trajectory sensitivities were proposed to estimate critical values of parameters of interest in a power system. A trajectory sensitivity based control method was developed in [13], while various optimal preventive control strategies were determined in [14] by utilizing trajectory sensitivity method. The location of dynamic Var support in power systems were identified using trajectory sensitivities for improving transient stability in [15], [16] and for mitigating short-term voltage instability in [17]. The TSA technique was also employed to design robust PSS parameters to damp low frequency power oscillation and enhance the overall performance of both transient and small signal stability in [18].

In this study, VSC-HVDC transmission is used to link a large-scale offshore wind farm to the onshore power system. Following a severe grid fault, the effect of voltage support capability of VSC-HVDC in improving short-term dynamic voltage stability is investigated. To satisfy the short-term voltage stability criteria during the post-fault period, a TSA-based two-stage approximation strategy is developed to identify the minimum onshore VSC capacity for the studied control approaches. The proposed two-stage design strategy improves the accuracy of the TSA-based linear approximation. Both reactive power-based and voltage-based trajectory sensitivities are used to verify the effectiveness of the proposed method.

4.2 Trajectory sensitivity analysis

4.2.1 Theoretical basis

Power systems are complex hybrid systems consisting of continuous time subsystems and event driven discrete subsystems. In general, a power system can be modelled by a set of differential-algebraic equations (DAE) as [5], [9], [12]:

$$\dot{x} = f(x, y, \lambda), \tag{4.1}$$

$$0 = \begin{cases} g^{-}(x, y, \lambda) & s(x, y, \lambda) < 0 \\ g^{+}(x, y, \lambda) & s(x, y, \lambda) > 0 \end{cases}. \tag{4.2}$$

where f represents the dynamics of the generator, load, HVDC and SVC etc.; g represents the instantaneous power flow in the system; x is the vector of dynamic state variables, e.g. generator rotor angles, velocities and fluxes; y is the vector of algebraic variables, e.g. voltage magnitudes and angles; λ is the vector of system parameters, e.g. line reactance, generator mechanical input power and HVDC capacities.

In the above model, the differential equation represents the dynamics of the equipment and the algebraic equations represent the power transfer relationships between the buses of the transmission network. A switching occurs when the switch function $s(x, y, \lambda) = 0$ and causes discontinuity of the power system. This discontinuity can be ignored when only the post-fault dynamics of the power system are concerned. The dynamic model of a power system can then be expressed by:

$$\dot{x} = f(x, y, \lambda), \tag{4.3}$$

$$0 = g(x, y, \lambda). \tag{4.4}$$

The initial conditions for the state variables of equation (4.3) and the algebraic variables of equation (4.2) are given by:

$$x(t_0) = x_0, \tag{4.5}$$

$$y(t_0) = y_0. \tag{4.6}$$

Accordingly, the trajectories of the variables starting from x_0 and y_0 can be defined as:

$$x(t) = \phi_x(x_0, t, \lambda), \tag{4.7}$$

$$y(t) = \phi_y(y_0, t, \lambda). \tag{4.8}$$

The trajectory change $\Delta x(t)$ and $\Delta y(t)$ at time t to a given parameter variation $\Delta\lambda$ is then obtained by forming the Taylor series expansions of equations (4.7) and (4.8) as:

$$\Delta x(t) = \Delta\phi_x(x_0, t, \lambda) = \frac{\partial\phi_x(x_0, t, \lambda)}{\partial\lambda}\Delta\lambda + \textit{higher order terms}, \tag{4.9}$$

$$\Delta y(t) = \Delta\phi_y(y_0, t, \lambda) = \frac{\partial\phi_y(y_0, t, \lambda)}{\partial\lambda}\Delta\lambda + \textit{higher order terms}. \tag{4.10}$$

Neglecting the higher order terms and using equations (4.7) and (4.8), we can get:

$$\Delta x(t) \approx \frac{\partial\phi_x(x_0, t, \lambda)}{\partial\lambda}\Delta\lambda = \frac{\partial x(t)}{\partial\lambda}\Delta\lambda \equiv x_\lambda(t)\Delta\lambda, \tag{4.11}$$

$$\Delta y(t) \approx \frac{\partial\phi_y(y_0, t, \lambda)}{\partial\lambda}\Delta\lambda = \frac{\partial y(t)}{\partial\lambda}\Delta\lambda \equiv y_\lambda(t)\Delta\lambda. \tag{4.12}$$

The time-varying partial derivatives x_λ and y_λ are called trajectory sensitivities. They can be derived by differentiating equations (4.3) and (4.4) with respect to λ as the following:

$$\dot{x}_\lambda = \frac{\partial f(t)}{\partial x}\frac{\partial x}{\partial\lambda} + \frac{\partial f(t)}{\partial y}\frac{\partial y}{\partial\lambda} + \frac{\partial f(t)}{\partial\lambda} = f_x(t)x_\lambda + f_y(t)y_\lambda + f_\lambda(t), \tag{4.13}$$

$$0 = \frac{\partial g(t)}{\partial x}\frac{\partial x}{\partial\lambda} + \frac{\partial g(t)}{\partial y}\frac{\partial y}{\partial\lambda} + \frac{\partial g(t)}{\partial\lambda} = g_x(t)x_\lambda + g_y(t)y_\lambda + g_\lambda(t). \tag{4.14}$$

Solving the two simultaneous equations (4.13) and (4.14), we obtain:

$$\dot{x}_\lambda = [f_x(t) - f_y(t)\cdot g_x(t)\cdot g_y^{-1}(t)]\cdot x_\lambda - f_y(t)\cdot g_\lambda(t)\cdot g_y^{-1}(t) + f_\lambda(t), \tag{4.15}$$

$$y_\lambda = -\frac{g_x(t)x_\lambda + g_\lambda(t)}{g_y(t)}. \tag{4.16}$$

The initial conditions for x_λ and y_λ are given by:

$$x_\lambda(0) = 0, \tag{4.17}$$

$$y_\lambda(0) = g_y(0)y_\lambda(0) + g_\lambda(0). \tag{4.18}$$

Basically, implicit integration methods, e.g. trapezoidal integration, are used to solve the differential and algebraic equations, and obtain the system trajectory and sensitivities.

Using equations (4.15) and (4.16) needs all the state variables and algebraic variables from the system and involves solving of differential and algebraic equations. In power systems, however, most of the state variables in equation (4.3) are hard to be measured. Alternatively, the trajectory sensitivities can also be calculated by a simple numerical approximation approach. Considering a small parameter perturbation $\Delta\lambda$ over the nominal parameter λ, the sensitivities with respect to λ can then be given as:

$$x_\lambda = \frac{\partial x}{\partial \lambda} \approx \frac{\Delta x}{\Delta \lambda} = \frac{\phi_x(x_0, t, \lambda + \Delta\lambda) - \phi_x(x_0, t, \lambda)}{\Delta\lambda}, \tag{4.19}$$

$$y_\lambda = \frac{\partial y}{\partial \lambda} \approx \frac{\Delta y}{\Delta \lambda} = \frac{\phi_y(y_0, t, \lambda + \Delta\lambda) - \phi_y(y_0, t, \lambda)}{\Delta\lambda}. \tag{4.20}$$

As can be seen, the sensitivities at a given time t are computed by subtracting the perturbed and nominal trajectories that can be obtained from time domain simulations, and then by dividing the trajectory variations over the parameter perturbation $\Delta\lambda$. Compared with the direct calculation of the sensitivities using equations (4.15) and (4.16), this numerical approximation approach involves greater computation but is much easier to implement.

4.2.2 Trajectory estimation

In case that the trajectory sensitivities are known, the new values of the system variables for a small parameter perturbation can be linearly approximated based on the base case [6], [7], [12]. It is given by:

$$x_{new}(t) = x_{base}(t) + x_{\lambda}(t)\Delta\lambda \ . \tag{4.21}$$

where $x_{new}(t)$ is the approximated variable trajectory and $x_{base}(t)$ is the base case variable trajectory.

Consequently, the effect of parameter changes on the dynamic behavior of the system can be evaluated using (4.21) in agreement with trajectory sensitivities. However, if the parameter change is large, errors in the approximation given by high-order terms of the Taylor series will also be large and further evaluation of the approximation is necessary.

In the case that the expected variable trajectory $x_{exp}(t)$ has already been determined, then the parameter perturbation $\Delta\lambda$ is also able to be approximated according to:

$$\Delta\lambda = \frac{x_{\exp}(t) - x_{base}(t)}{x_{\lambda}(t)} . \tag{4.22}$$

4.3 Studied system

The test power system presented in Figure 4.1 was originally derived from [19] and has been modified to meet the requirements of this study. It consists of three conventional power plants: one hydropower plant, one gas turbine plant and one coal-fired power plant. All synchronous generators are equipped with a turbine governor and an exciter. Load A, B and C are aggregated static loads and Load D is induction motor load. The total load capacity is 336MW.

A large variable-speed wind turbine-based offshore wind farm is integrated into the grid via VSC-HVDC on Bus 5. Therefore, Bus 5 is the PCC as shown in Figure 4.1. The rated capacity of the offshore wind farm is 135 MW and the base capacity of VSC-HVDC is 150 MVA. It means that wind power supplies about 40% of the grid's load consumption. The offshore wind farm operates at rated wind speed for the duration of the simulating time. In the short-term voltage stability analysis, it is practical to assume a constant wind speed for the investigated period only lasts for a few seconds. The parameters of the VSC-HVDC transmission are listed in Table 4.1 and more details of this studies system can be found in Appendix C.

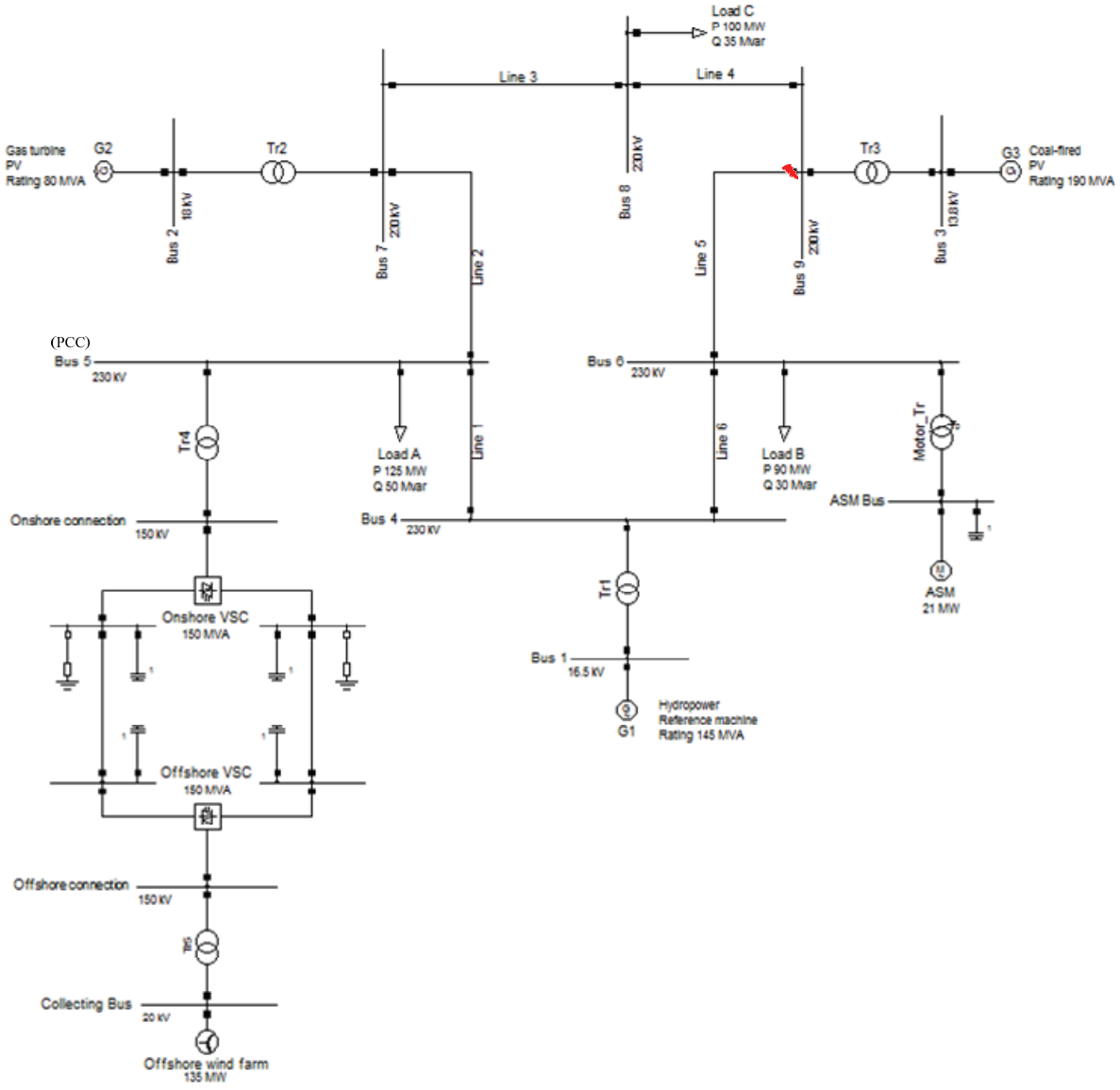

Figure 4.1 Single line diagram of the test power system.

TABLE 4.1

Parameters of VSC-HVDC transmission system

Parameter	Value
VSC rated power S_{vsc}	150 MVA
VSC rated AC rms voltage V_{vsc}	150 kV
VSC rated DC voltage V_{dc}	±150 kV
DC capacitor C_{dc}	450 μF × 4
Chopper resistance R	400 ohm × 2

4.4 Voltage support strategies of VSC-HVDC

As described in the previous chapters, the offshore VSC sets reference frequency, voltage amplitude and phase angle for the offshore network. The onshore VSC manages the power flow to the onshore grid by controlling the DC-link voltage and the grid voltage amplitude. Explicitly, the voltage support of VSC-HVDC during grid disturbances is fulfilled by the onshore VSC. The control structure of the onshore VSC is shown in Figure 3.3 of Chapter 3. To guarantee balanced power flow and avoid overcharging of the DC-link capacitor during grid voltage drops, the DC chopper is applied to dissipate the excess power on the DC link.

The voltage support control strategy used here is derived from E.ON Netz fault response code [4]. The details about the voltage support requirement of E.ON code can be found in Chapter 3.2.1. Modifications have been made as shown in Figure 4.2. The maximum reactive current is limited to the maximum current of the converter instead of the rated current as can be seen from equation (3.2). In base case, the slope of the reactive current support line is '$m = 2$'. Moreover, '$m = 3$' and '$m = 4$' are all evaluated as well. In the case of '$m=3$', the reactive current support reaches its maximum when the voltage drops down to 0.67 pu without considering the dead band. Similarly, in case of '$m=4$', the maximum reactive current output is obtained when the voltage is below 0.75 pu without considering the dead band.

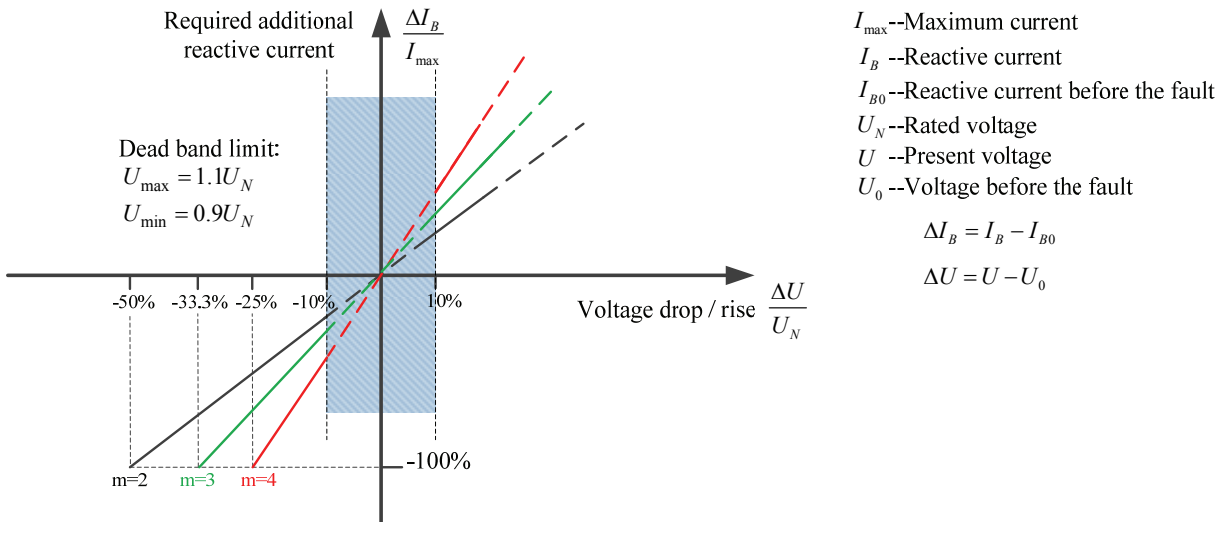

Figure 4.2 Modified E.ON code.

4.5 Simulation and discussion

System modelling and simulations are based on power system analysis software DIgSILENT/ PowerFactory. The fault considered is a three-phase ground fault occurred at t = 1s on Line5 close to Bus 9. The fault lasts for 100 ms and is cleared by tripping Line5 between Bus 6 and Bus 9 without reclosing. The step size of time-domain simulations in this study is set to 1ms.

4.5.1 Simulation of Voltage Disturbance

Given the above fault and three different values of m, the voltage magnitude of Bus 5 (PCC) is shown in Figure 4.3a and the reactive power output of onshore VSC is presented in Figure 4.3b. It can be seen that during the fault period, the reactive power output of the onshore VSC is larger for a bigger value of m, and thus the larger reactive power support results in a higher voltage of Bus 5. However, it is not the case after the fault is cleared. At the time that the fault is cleared (1.1s), the voltage curves increase steeply to about 0.85 pu and then begins to drop gradually again. At around 1.35s, the voltage curves hit the ground and grows steadily to 0.9 pu at around 1.55s. During the period of around 1.1s to 1.3s, the voltage curve with a bigger m has higher magnitude. From around 1.3s to 1.55s, it is observed that the higher the m, the lower the voltage. However, from Figure 4.3b, we can see that though the reactive power output curves fluctuate, the reactive power curve with a higher m has a higher value during the period of about 1.1s to 1.55s. The reason of this mismatch between the voltage and reactive power is that in a power system the voltage of a bus is determined by many factors, such as system structure and load characteristics etc.

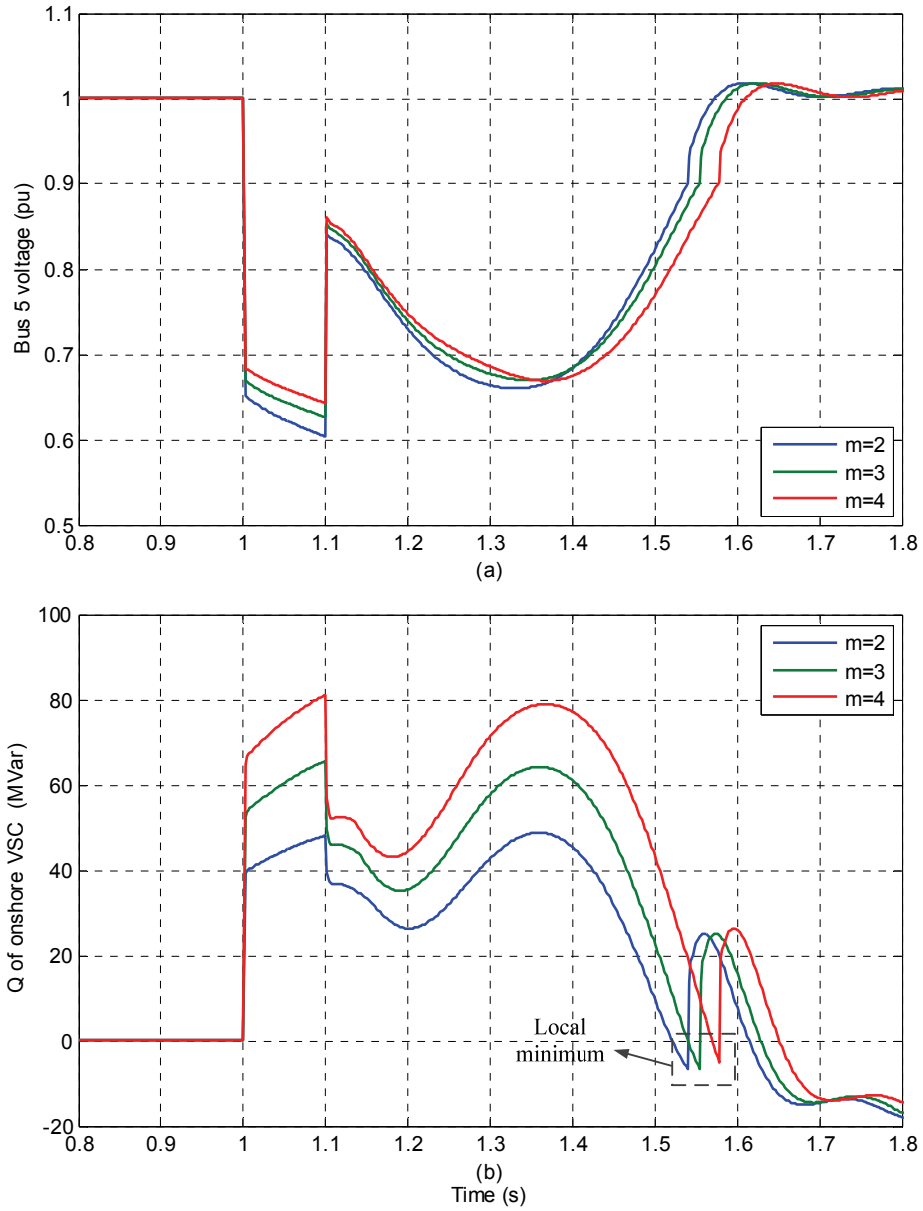

Figure 4.3 System dynamics for the given fault in the case of different m with 150 MVA onshore VSC: (a) Voltage magnitude of Bus 5; (b) Reactive power output of onshore VSC.

TABLE 4.2
Data for local minimum points based on the base onshore VSC capacity

m	VSC S (MVA)	Bus5 V (pu)	VSC Q (MVar)	Time (s)
2	150	0.90	-6.7362	1.54
3	150	0.90	-6.5536	1.55
4	150	0.90	-5.0555	1.58

By comparison of Figure 4.3a and 4.3b, we can further notice that during the post-fault period, the voltage of Bus 5 restores to 0.9 pu in Figure 4.3a, when the corresponding reactive power output of the onshore VSC reaches the local minimum point in Figure 4.3b. The explanation for this phenomenon can be revealed from the way the onshore VSC provides the voltage support. Table 4.2 lists the onshore VSC rating, Bus5 voltage and reactive power output of onshore VSC and time instant corresponding to local minimum points for *m=2, 3* and *4*.

As aforementioned in Chapter 3.2, when the onshore VSC terminal voltage is below the threshold voltage of the dead band (0.9 pu), the *q*-axis control switches from *Normal* state to *Fault* state and the fast *P* controller takes the place of the *PI*. The reactive current output of onshore VSC is then controlled to be proportional (*m*) to the absolute deviation from normal voltage operating range and to have a higher priority than active power output as presented by (3.1) and (3.2). Similarly, when the disturbed voltage restores to 0.9 pu, the *q*-axis control of the onshore VSC switches back from *Fault* state to *Normal* state and the active current output gets back the priority. Therefore, due to the control switching, we can expect that the reactive power output of the onshore VSC will experience a dramatic change when the voltage is across 0.9 pu in any direction as shown in Figure 4.3. If the voltage restores from a lower value to equal or more than 0.9 pu, the reactive power output of the onshore VSC may reduce to less than zero as can be deduced from equation (3.2).

In this study, it is recognized as short-term voltage instability if the voltage magnitude is below 0.9 pu for more than 500ms. It can be seen from Figure 4.3a that for all three values of *m*, the voltage of Bus 5 is less than 0.9 pu at t = 1.5s. Hence, it can be drawn that VSC-HVDC with the base capacity is unable to provide enough reactive power / voltage support to stabilize the PCC (Bus5) voltage by adopting the given values of *m* for the studied control strategies.

4.5.2 Two-stage approximation based on TSA

The objective of using trajectory sensitivities is to identify the minimum capacity of onshore VSC for the given *m* values to ascertain that the entire range of the voltage magnitude of Bus5 satisfies the above voltage stability criterion. For this purpose, two types of trajectory sensitivity are selected for each given *m* value. One is the sensitivity ($Sen_Q(t)$) of the change in reactive power output of onshore VSC to VSC capacity increment, and the other is the sensitivity ($Sen_V(t)$) of the change in Bus5 voltage to the onshore VSC capacity increment. And the suitable VSC capacity is identified with each sensitivity index separately. Comparison studies are conducted afterwards.

The approach is based on equation (4.22). When the expected reactive power of the VSC and the expected Bus5 voltage are already known, the VSC capacity increment ΔS can then be approximated based on $Sen_Q(t)$ or $Sen_V(t)$ as:

$$\Delta S_Q = \frac{Q_{\exp}(t) - Q_{base}(t)}{Sen_Q(t)}. \tag{4.23}$$

or

$$\Delta S_V = \frac{V_{\exp}(t) - V_{base}(t)}{Sen_V(t)}. \tag{4.24}$$

To find the suitable VSC capacity with which the reactive power output of VSC could enhance the Bus5 voltage up to 0.9 pu at t=1.5 s, the reactive power listed in Table 4.1 is considered as the expected reactive power output of the VSC at t=1.5s following the grid fault. And it is obvious that the expected Bus5 voltage at t=1.5s is 0.9 pu. The design steps are depicted in Figure 4.4, in which X represents reactive power of onshore VSC or Bus5 voltage. The details associated with these steps are as follows:

1) For $m = 2, 3$ and 4, perform time-domain simulations based on 150 MVA (base capacity) and 155MVA VSC respectively.

2) Calculate sensitivities $Sen_Q(t)$ and $Sen_V(t)$ towards its capacity increase (5 MVA) at t=1.5s according to equation (4.19) and (4.20):

$$Sen(1.5s) = \frac{X_{155MVA}(1.5s) - X_{base}(1.5s)}{155 - 150}. \tag{4.25}$$

3) Use the trajectory sensitivity information to approximate the VSC capacity increment ΔS by equation (4.23) and (4.24) with

$$Q_{\exp}(1.5s) = \begin{cases} -6.7362MV\text{ar}, m = 2 \\ -6.5536MV\text{ar}, m = 3 \\ -5.0555MV\text{ar}, m = 4 \end{cases} \text{ and } V_{\exp}(1.5s) = 0.9\,pu.$$

4) Get the new VSC capacity S_{new}.

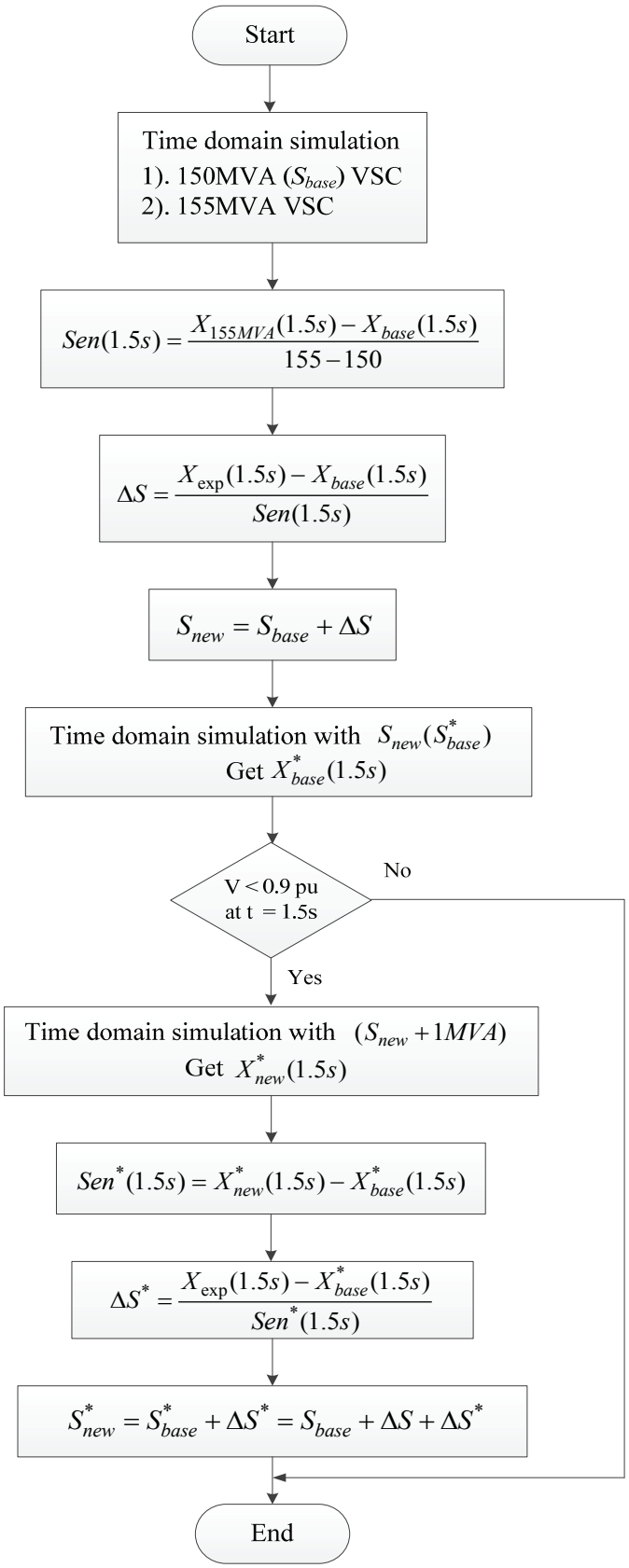

Figure 4.4 Flowchart for estimating the onshore VSC capacity.

5) Run time domain simulation with the VSC with S_{new}. The S_{new} is also the base capacity S^*_{base} for further trajectory sensitivity calculation, if necessary.

6) If the Bus5 voltage at 1.5s is still lower than 0.9 pu, run time domain simulation with the VSC with S_{new}+1MVA.

7) Calculate sensitivities $Sen_Q(t)$ and $Sen_V(t)$ towards the capacity increment 1MVA at t=1.5s.

8) Use the new trajectory sensitivities to calculate the further VSC capacity increment ΔS^*.

9) Get the desirable VSC capacity S^*_{new} by

$$S^*_{new} = S^*_{base} + \Delta S^* = S_{base} + \Delta S + \Delta S^* . \tag{4.26}$$

In step 2, the trajectory sensitivities are calculated on a relatively large capacity change (5MVA) and then the first approximation is obtained. This is considered as the first stage approximation in this study. If the result of the first approximation cannot satisfy the requirements, then the trajectory sensitivities are updated on a much small capacity change (1MVA) to improve the accuracy of the linear approximation as in step 7. Based on the new trajectory sensitivities, the second approximation is conducted to complete the design procedure. This is, of course, the second stage approximation.

4.5.3 Results and analysis

Table 4.3 present the $Sen_Q(1.5s)$-based design results for both stage including trajectory sensitivities at 1.5s, approximated capacity increments and the desirable capacities. The $Sen_V(1.5s)$-based approximation results are listed in Table 4.4. It can be seen from Table 4.3-4.4 that it requires a bigger VSC capacity to satisfy the voltage stability criteria for a bigger value of *m*, but the capacity gap is very narrow.

The results in these two tables are also compared in Figure 4.5. It can be seen from the bottom plot of Figure 4.5 that the $Sen_Q(1.5s)$-based approximations leads to a smaller VSC capacity than the $Sen_V(1.5s)$-based approximation. Though the difference is not significant, a bigger value of *m* results in a bigger difference. From the top plot of Figure 4.5, it can be observed that $Sen_V(1.5s)$-based first stage approximation gains almost the same results for all values of *m*, but it tends to yield more

conservative results compared to $Sen_Q(1.5s)$-based first stage approximation with the increase of *m*. The middle plot of Figure 4.5 shows that $Sen_V(1.5s)$-based second stage approximation gains larger VSC capacities than those of $Sen_Q(1.5s)$-based second stage approximation, and the bigger the value of *m*, the larger the approximation result.

The short-term voltage stability of Bus5 with the desirable VSC capacities is verified by running time domain simulations. Figure 4.5 shows the simulation results with $Sen_Q(1.5s)$-based design and Figure 4.6 shows the simulation results with $Sen_V(1.5s)$-based design. The Bus5 voltage magnitude and the reactive power of onshore VSC at t=1.5s are presented in Table 4.5-4.6 with respect to $Sen_Q(1.5s)$- and $Sen_V(1.5s)$-based designs respectively.

From Figure 4.6 and Table 4.5, it can be seen that the Bus5 voltage reaches 0.9 pu at 1.5s for m=2, and 0.89 pu (1% error to 0.9 pu) at 1.5s for m=3 and 4. From Figure 4.7 and Table 4.6, it can be observed that the Bus5 voltage reaches 0.9 pu at 1.5s for all given values of m. Thus, it can be deduced that the Bus5 voltages of simulations based on both $Sen_Q(1.5s)$- and $Sen_V(1.5s)$-based designs are acceptable with regard to the short-term voltage stability criteria used in this study. However, the $Sen_V(1.5s)$-based design yields more accurate results than the $Sen_Q(1.5s)$-based design. The reason is that the expected voltage magnitudes used in the design procedures are definite and accurate, but the expected reactive power output of onshore VSC are estimated values based on the time domain simulation with base VSC capacity (150MVA).

TABLE 4.3
Design results based on $Sen_Q(1.5s)$

m	**First stage approximation**			**Second stage approximation**		
	$Sen_Q(1.5s)$	$\Delta S_Q(MVA)$	$S_{Qnew}(MVA)$	$Sen_Q^*(1.5s)$	$\Delta S_Q^*(MVA)$	$S_{Qnew}^*(MVA)$
2	-0.7948	20.6	171	-0.3711	6.5	178
3	-1.2161	24.0	174	-0.7667	4.0	178
4	-2.0069	24.1	174	-1.2286	6.7	181

TABLE 4.4
Design results based on $Sen_V(1.5s)$

m	First stage approximation			Second stage approximation		
	$Sen_V(1.5s)$	$\Delta S_V(MVA)$	$S_{Vnew}(MVA)$	$Sen_V^*(1.5s)$	$\Delta S_V^*(MVA)$	$S_{Vnew}^*(MVA)$
2	0.0036	21.2	171	0.0022	8.0	179
3	0.0045	21.3	171	0.0024	9.9	181
4	0.0060	21.7	172	0.0027	12.5	185

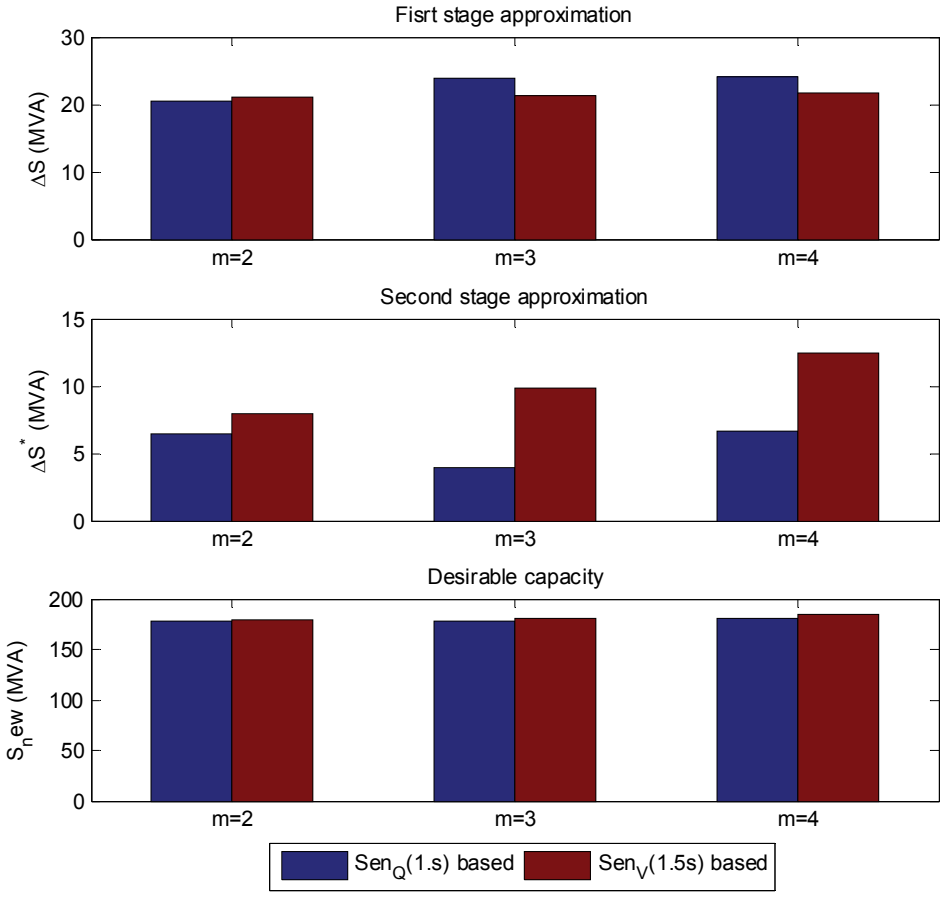

Figure 4.5 Result comparison between $Sen_Q(1.5s)$- and $Sen_V(1.5s)$-based design.

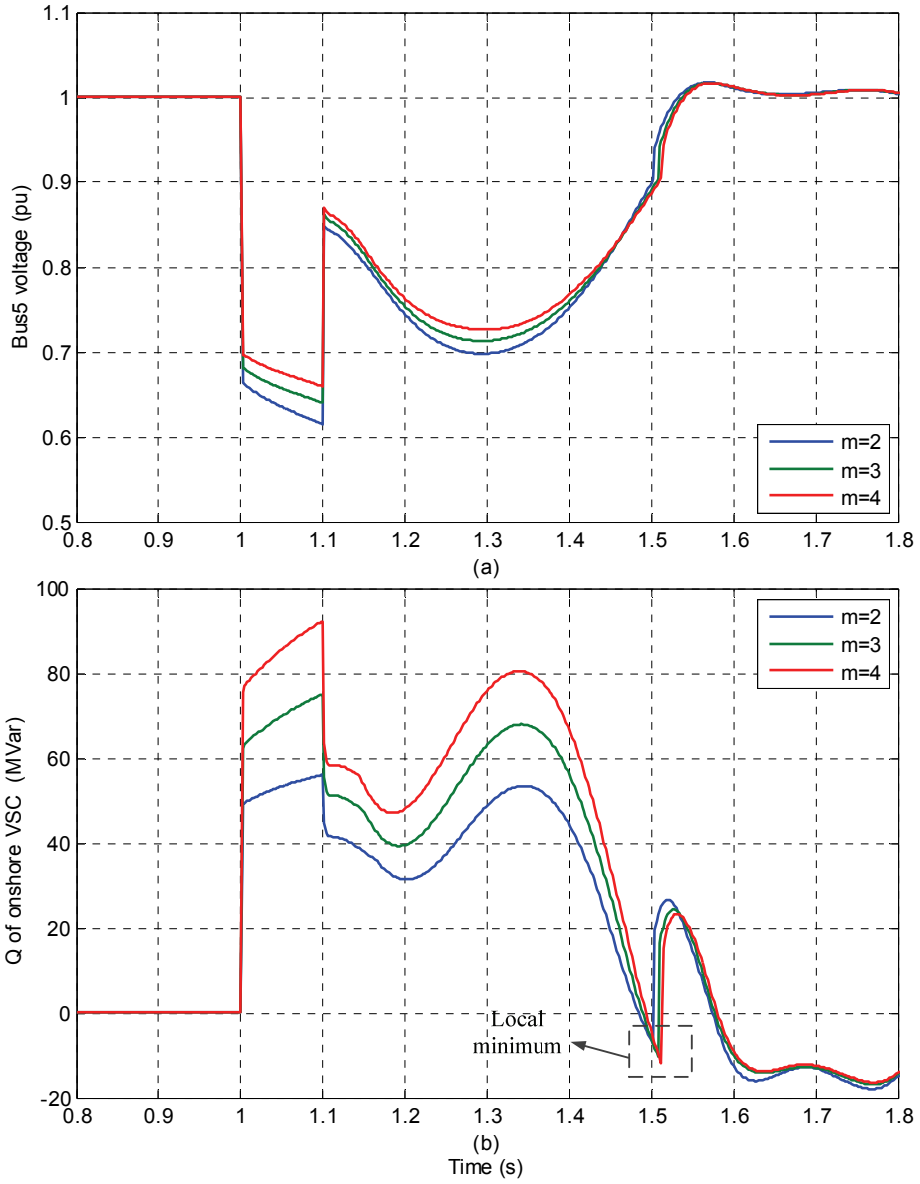

Figure 4.6 Bus5 voltage and reactive power output of onshore VSC based on $Sen_Q(1.5s)$-based design: (a) Voltage magnitude of Bus 5; (b) Reactive power output of onshore VSC.

TABLE 4.5
Results at t=1.5s based on $Sen_Q(1.5s)$-based design

m	VSC S (MVA)	Bus5 V (pu)	VSC Q (MVar)	Time (s)
2	178	0.90	-6.6448	1.50
3	178	0.89	-6.3313	1.50
4	181	0.89	-4.6114	1.50

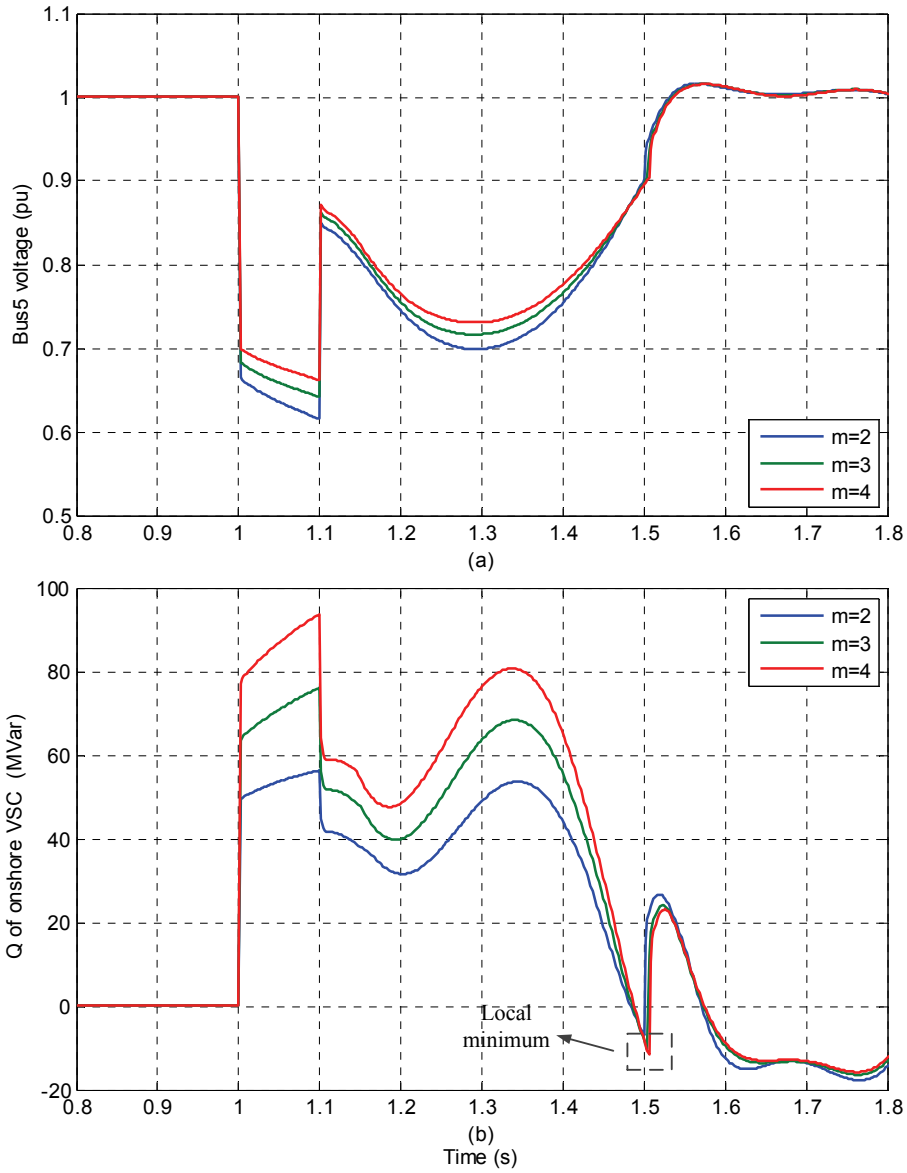

Figure 4.7 Bus5 voltage and reactive power output of onshore VSC based on $Sen_V(1.5s)$-based design: (a) Voltage magnitude of Bus 5; (b) Reactive power output of onshore VSC.

TABLE 4.6
Results at t=1.5s based on $Sen_V(1.5s)$-based design

m	VSC S (MVA)	Bus5 V (pu)	VSC Q (MVar)	Time (s)
2	179	0.90	-6.9836	1.50
3	181	0.90	-8.2172	1.50
4	185	0.90	-8.1823	1.50

Figure 4.8 compares the expected reactive power output (t=1.5s) of onshore VSC with the simulation results (t=1.5s) based on $Sen_Q(1.5s)$- and $Sen_V(1.5s)$-based designs respectively. It is obvious that the difference between the expected values and simulation values is bigger for $Sen_V(1.5s)$-based design compared to the $Sen_Q(1.5s)$-based design.

The Bus5 voltage for a longer time scale is also shown in Figure 4.9 for $Sen_Q(1.5s)$-based design. It can be observed from Figure 4.9 that the voltage of Bus 5 is stabilized from 1.5s on. Apparently, the voltage stability can also be guaranteed for $Sen_V(1.5s)$-based design.

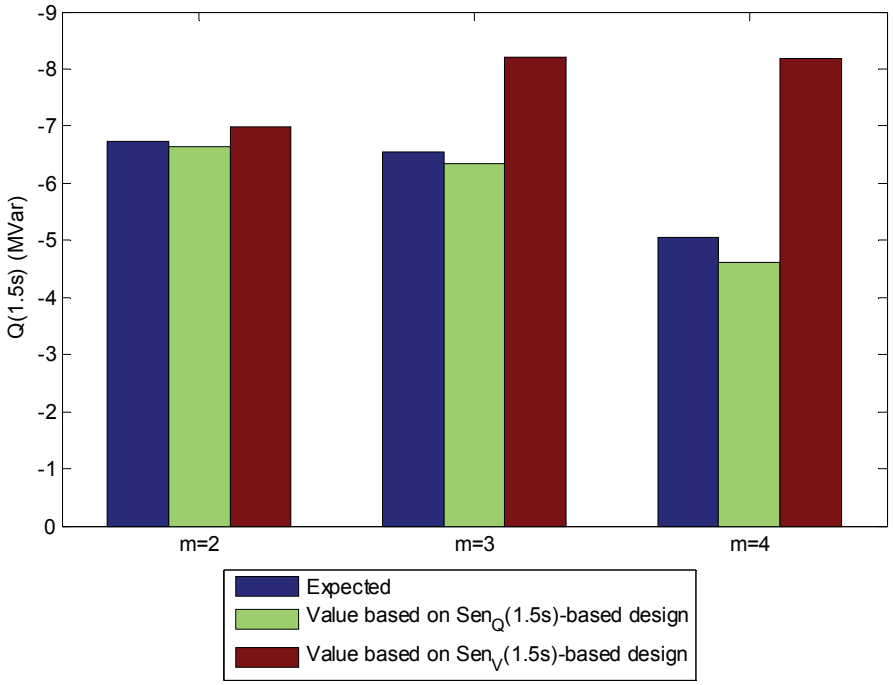

Figure 4.8 Comparison of reactive power output of onshore VSC at t=1.5s between expected values and simulation results with desirable VSC capacities.

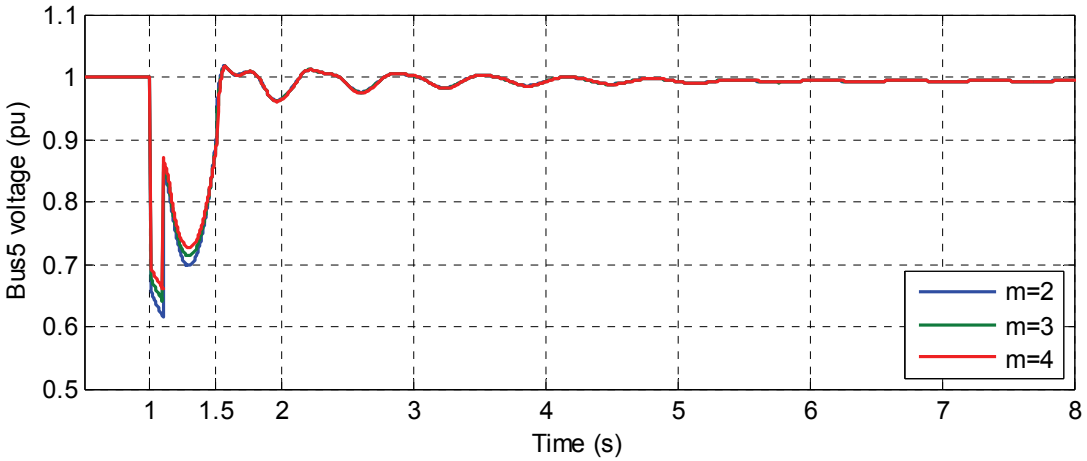

Figure 4.9 Bus5 voltage for a longer time scale for $Sen_Q(1.5s)$-based design.

For the given grid disturbance, Figure 4.10 presents the Bus5 voltage magnitude and the reactive power of onshore VSC at 1.5s with respect to various onshore VSC capacities. It can be seen that the Bus5 voltage and reactive power of onshore VSC at 1.5s are almost linearly dependent on the onshore VSC capacity. This nearly linear relationship, from another point of view, also reflects the reasonability of the proposed method.

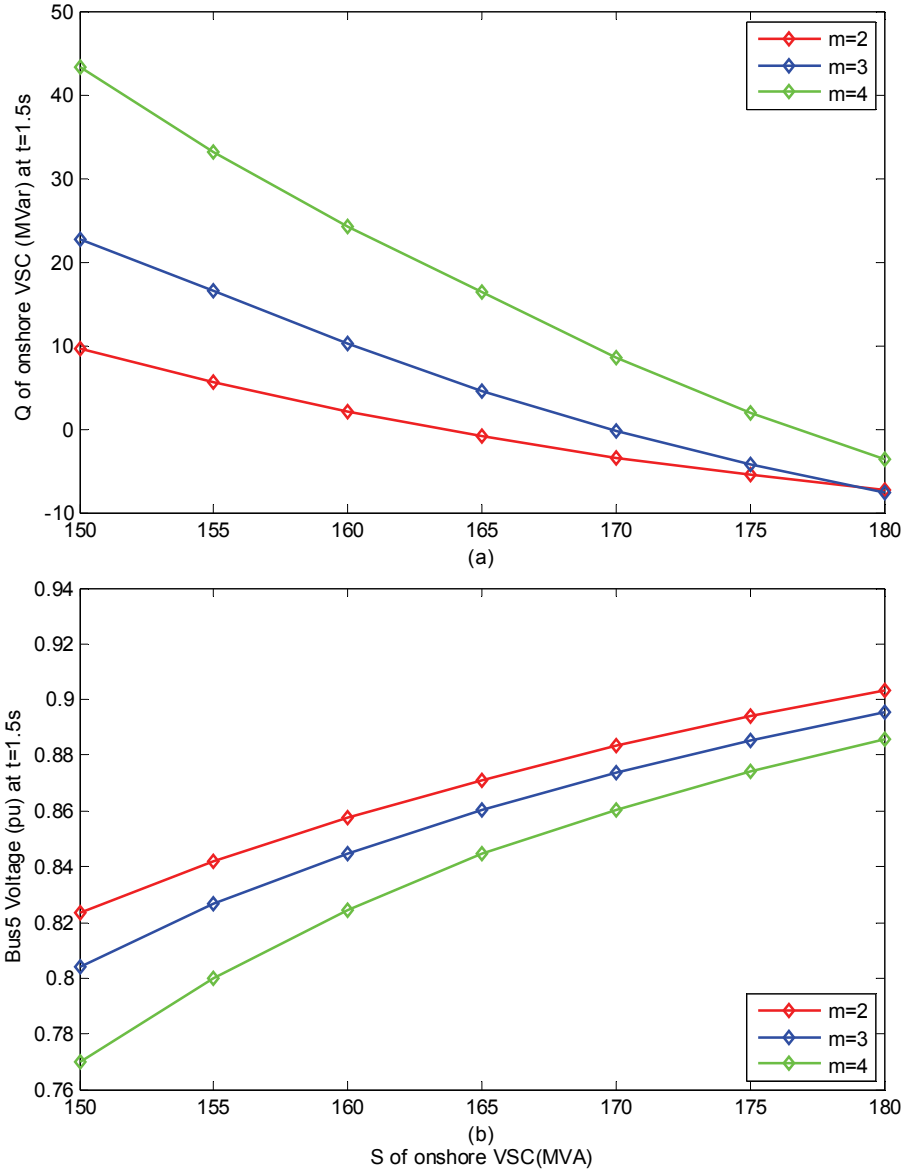

Figure 4.10 Bus5 voltage and reactive power of onshore VSC at 1.5s towards various onshore VSC capacities: (a) Bus5 voltage magnitude at 1.5s; (b) Reactive power of onshore VSC at 1.5s.

4.6 Summary

In this chapter, VSC-HVDC transmission system is used to integrate a large-scale wind power plant into the onshore power grid. For the studied voltage support strategies of VSC-HVDC, a TSA-based two-stage design method is developed to identify the minimum onshore VSC capacity with which VSC-HVDC can provide enough support for stabilizing the PCC voltage following a grid disturbance.

By using the proposed TSA-based two-stage method, the design is accomplished by numerical calculations based on only a few time domain simulations. The two-stage approximation strategy also improves the accuracy of the TSA-based linear approximation. Both reactive power-based and voltage-based trajectory sensitivities are applied to the design procedures. And the effectiveness of the proposed method is finally verified by results based on time-domain simulations.

Bibliography

[1] P. Kundur, J. Paserba, V. Ajjarapu, G. Andersson, A. Bose, C. Canizares *et al.*, "Definition and classification of power system stability IEEE/CIGRE joint task force on stability terms and definitions," *IEEE Transactions on Power Systems,* vol. 19, no. 3, pp. 1387-1401, Aug. 2004.

[2] P. Kundur, *Power System Stability and Control*. New York: McGraw-Hill, Inc., 1994.

[3] T. V. Cutsem, C. Vournas, *Voltage Stability of Electric Power Systems*. Springer Science+Business Media, LLC, 1998.

[4] Grid Code: High and Extra High Voltage, E.ON Netz GmbH Tech. Rep., April 2006, Status:1.

[5] I. A. Hiskens and M. A. Pai, "Sensitivity analysis of power system trajectories: recent results," in *Proceedings of the 1998 IEEE International Symposium on Circuits and Systems*, vol.3, pp. 439-443, June 1998.

[6] I. A. Hiskens and M. A. Pai, "Trajectory sensitivity analysis of hybrid systems," *IEEE Transactions on Circuits and Systems I: Fundamental Theory and Applications,* vol. 47, no. 2, pp. 204-220, Feb. 2000.

[7] I. A. Hiskens and J. Alseddiqui, "Sensitivity, Approximation, and Uncertainty in Power System Dynamic Simulation," *IEEE Transactions on Power Systems,* vol. 21, no. 4, pp. 1808-1820, Nov. 2006.

[8] M. J. Laufenberg and M. A. Pai, "A new approach to dynamic security assessment using trajectory sensitivities," *IEEE Transactions on Power Systems,* vol. 13, no. 3, pp. 953-958, Aug. 1998.

[9] M. A. Pai and T. Nguyen, "Trajectory Sensitivity Theory in Nonlinear Dynamical Systems: Some Power System Applications," in *Stability and Control of Dynamical Systems with Applications*, Ed: Birkhäuser Boston, pp. 271-292, 2003.

[10] I. A. Hiskens and M. A. Pai, "Power system applications of trajectory sensitivities," in *IEEE Power Engineering Society Winter Meeting,* vol. 2, pp. 1200-1205, 2002.

[11] I. A. Hiskens and M. Akke, "Analysis of the Nordel power grid disturbance of January 1, 1997 using trajectory sensitivities," *IEEE Transactions on Power Systems,* vol. 14, no. 3, pp. 987-994, Aug. 1999.

[12] T. B. Nguyen, M. A. Pai, and I. A. Hiskens, "Sensitivity approaches for direct computation of critical parameters in a power system," *International Journal of Electrical Power & Energy Systems,* vol. 24, no. 5, pp. 337-343, June 2002.

[13] M. Zima and G. Andersson, "Stability assessment and emergency control method using trajectory sensitivities," in *IEEE Bologna Power Tech Conference Proceedings*, vol. 2, pp. 1-7, June 2003.

[14] H. Guanji and V. Vittal, "Trajectory Sensitivity Based Preventive Control of Voltage Instability Considering Load Uncertainties," *IEEE Transactions on Power Systems,* vol. 27, no. 4, pp. 2280-2288, Nov. 2012.

[15] D. Chatterjee and A. Ghosh, "Application of Trajectory Sensitivity for the Evaluation of the Effect of TCSC Placement on Transient Stability," *International Journal of Emerging Electric Power Systems,* vol. 8, no. 1, 2007.

[16] D. Chatterjee and A. Ghosh, "Improvement of transient stability of power systems with STATCOM-controller using trajectory sensitivity," *International Journal of Electrical Power & Energy Systems,* vol. 33, no. 3, pp. 531-539, March 2011.

[17] B. Sapkota and V. Vittal, "Dynamic VAr Planning in a Large Power System Using Trajectory Sensitivities," *IEEE Transactions on Power Systems,* vol. 25, no. 1, pp. 461-469, Feb. 2010.

[18] S. Q. Yuan and D. Z. Fang, "Robust PSS Parameters Design Using a Trajectory Sensitivity Approach," *IEEE Transactions on Power Systems,,* vol. 24, no. 2, pp. 1011-1018, May 2009.

[19] Application Manual: Battery Energy Storing Systems in PowerFacory, DIgSILENT GmbH, 30 Nov. 2010.

Chapter 5

Coordinated Frequency Regulation by Offshore Wind Farm and VSC-HVDC Transmission

Modern offshore wind farms are generally required to provide ancillary services, such as voltage support and frequency regulation, as conventional synchronous generation units. The VSC-HVDC inherently doesn't contribute to grid frequency regulation, and may block or delay the offshore wind turbines' responding to grid frequency disturbances. This chapter presents a new control strategy that reduces the time of transmitting onshore frequency signal to offshore wind turbines and enable VSC-HVDC to provide inertial response by means of partially charging / discharging of its DC capacitors. To further improve the system frequency response, the cooperation with the frequency support from offshore wind turbines is also considered with respect to the latency of offshore wind turbines responding to onshore grid frequency disturbances.

5.1 Introduction

Power system frequency stability refers to *the ability of a power system to maintain stable frequency following a severe system upset resulting in a significant imbalance between generation and load* [1]. In the event of a sudden loss of a large power supply or a sudden increase in power demand, synchronous generators will release their kinetic energy stored in their large rotating masses immediately to slow down the initial rate of change of the frequency (ROCOF). This response is known as inertial response. Soon afterwards, the speed governors of synchronous generators will detect the frequency deviation and then start to provide additional power to balance the load. When the generation once again meets the power demand, the frequency will then be stabilized at a steady-state value that deviates from the nominal frequency. During this dynamic process, the frequency hits the nadir at some point. This response is known as primary frequency control. As primary frequency control is not sufficient to restore the frequency back to its nominal value, the response known as secondary frequency control is, therefore, required to accomplish the frequency regulation. The secondary frequency control is generally provided by automatic generation control (AGC). Figure 5.1 shows the normal frequency response of a power system following a large disturbance.

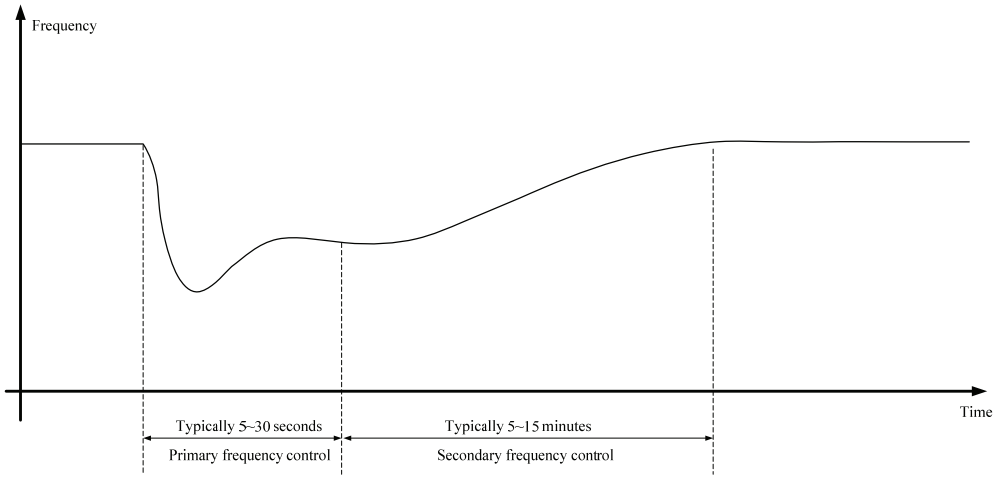

Figure 5.1 Normal frequency response following a large disturbance.

The generation of a large-scale offshore wind farm could be hundreds of MW, which well matches the generation of conventional power plants. With the increasing penetration level, the behavior of large-scale offshore wind farms will exert significant impact on the operation and control of the interconnected power system. In fact, modern large-scale offshore wind farms are not merely required to supply active power generation, but also to provide ancillary voltage and frequency regulation as conventional power plants, especially under the conditions that the offshore wind farms are displacing conventional power plants [2], [3].

However, the electromechanical behavior of variable speed wind turbines (VSWTs), which comprise modern offshore wind farms, differs fundamentally from that of conventional synchronous generators (SGs). VSWTs that are interfaced with AC power grid via voltage source converters (VSCs) are naturally considered inertia-less to AC power systems [4], [5] and have no primary control reserve as the wind is not controllable [6]. Thus, the integration of large offshore wind farms along with the de-commissioning of conventional power plants is bound to reduce the system inertia and primary control reserve. Without countermeasures, this would put power system security at high risk. To solve this problem, ancillary frequency support schemes need to be equipped to VSWTs for active power control. In [6]-[9], control methods for converters were proposed to provide short-term frequency support by utilizing the rotational kinetic energy of VSWT's generator. The implementation of energy reserve was also reported in [10], [11] by forcing VSWT to operate in a de-loading mode by means of converter control and pitch angle control.

As already known, a large-scale offshore wind farm is probably located far away from the

onshore connection point and is connected into the onshore grid via VSC-HVDC transmission system. Due to the decoupling of the VSC-HVDC link, the offshore wind farm would not be directly affected by onshore grid disturbances. However, this decoupling would also reduce the sensitivity of the offshore wind farm to the onshore network disturbances and prevent the offshore wind farm from timely response. For a grid frequency deviation, it is apparent that the offshore wind farm is not able to provide immediate frequency support following the frequency transient due to the communication delay. As for the VSC-HVDC transmission itself, though it performs well on voltage support [12], [13], it doesn't respond to the frequency deviation inherently. Yet, efforts have been made to allow the VSC-HVDC to participate in grid system frequency regulation.

In [14], a supplementary control loop was added to the onshore VSC for frequency regulation. However, this supplementary control loop was only responsible for generating a simple raise / lower signal in line with the onshore grid frequency absolute deviation, and sending the signal to the offshore wind farm via communication interface. The signal activated the de-loading control of offshore wind turbines to provide frequency support. In [15]-[17], the participation of VSC-HVDC connected wind farms in system frequency regulation was also investigated. However, all these studies focused only on developing artificial coupling methods between the wind farm grid and the onshore grid frequencies. The magnitude of DC link voltage of VSC-HVDC was controlled by the onshore VSC to reflect the onshore grid frequency deviation and the offshore VSC adjusted the offshore grid frequency based on the variation of the DC link voltage. Therefore, the offshore wind turbines could detect the onshore grid frequency disturbance without communication interface, and participate in frequency control. However, the above studies did not probe into the potential frequency support capability of VSC-HVDC itself. An inertia emulation control (INEC) strategy for VSC-HVDC transmission systems was proposed in [18], [19]. It allowed a VSC-HVDC system with a fixed capacitance to emulate a wide range of inertia constants by specifying the amount of permissible DC voltage [19]. The stored energy in the HVDC DC capacitors was utilized to provide inertial response and contribute to primary frequency control of the studied AC network. However, the DFIG-based wind farm connected via the VSC-HVDC did not provide frequency support in this work and the effectiveness of the proposed INEC strategy was not evaluated while coordinating with the frequency control of the offshore wind farm.

This chapter explores the frequency regulation capability of VSC-HVDC that is used to integrate a large offshore wind farm into the onshore power grid. The offshore wind farm is comprised of

FCWTs. A coordinated control strategy is proposed to reduce the time of transmitting onshore frequency signal to offshore wind turbines and enable VSC-HVDC to provide inertial response by means of partially charging / discharging of its DC capacitors. To further improve the system frequency response, the cooperation with the frequency support from offshore wind turbines is also considered with respect to the latency of offshore wind turbines responding to onshore grid frequency disturbances.

5.2 Frequency support strategies

5.2.1 Frequency support strategy for wind turbine

For clear demonstration, Figure 5.2 shows the generic structure and control of the FCWT. The generator-side converter regulates the generator active power output and stator voltage, while the grid-side converter stabilizes the DC voltage and maintains a unity power factor operation. The blade angle is controlled through a pitch angle controller. The detailed modelling has been described in Chapter 2.2.

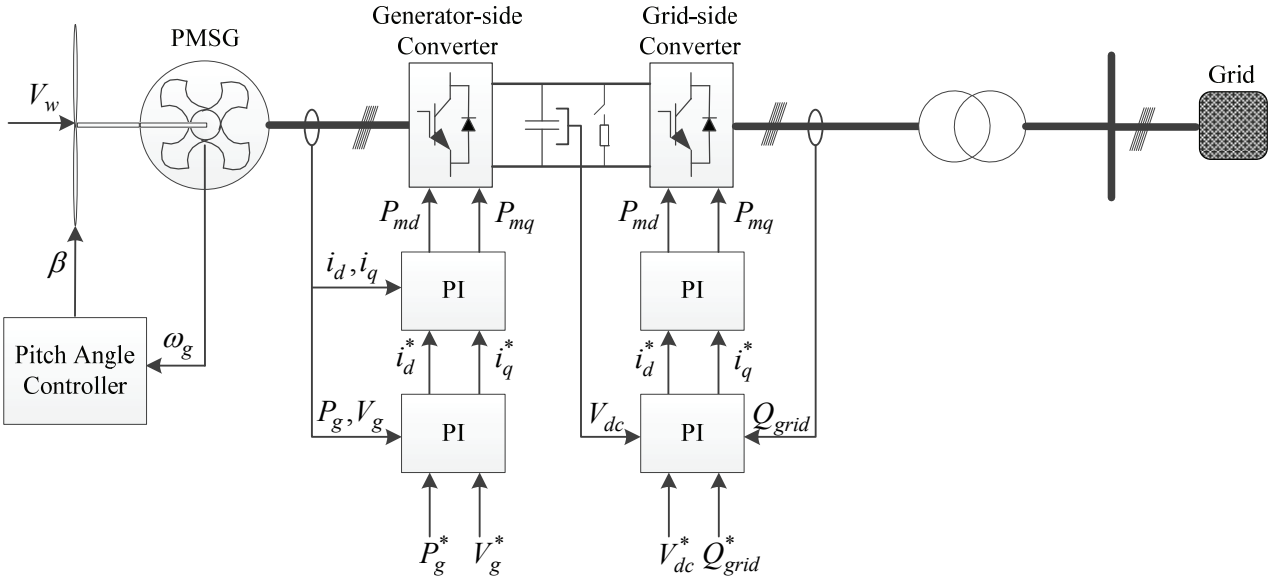

Figure 5.2 Generic structure and control of FCWT.

To fulfill frequency support capability, an ancillary frequency controller is designed and shown in Figure 5.3. It can be divided into two parts: *under-frequency controller* that is activated if the measured frequency is below 49.8Hz, and *over-frequency controller* that is activated if the

measured frequency is over 50.2Hz. In Figure 5.3, the active power reference P_{ω_ref} is determined by the wind turbine generator speed via MPT. The active power reference P_{under} (pu) and P_{over} (%) are generated by the under-and over- frequency controllers respectively. The total active power reference value P_g^* to the wind turbine generator is then given as

$$P_g^* = P_{\omega\_ref} \times P_{over} + P_{under}. \tag{5.1}$$

The Low-pass filter is used to eliminate the measurement noise of the frequency signal.

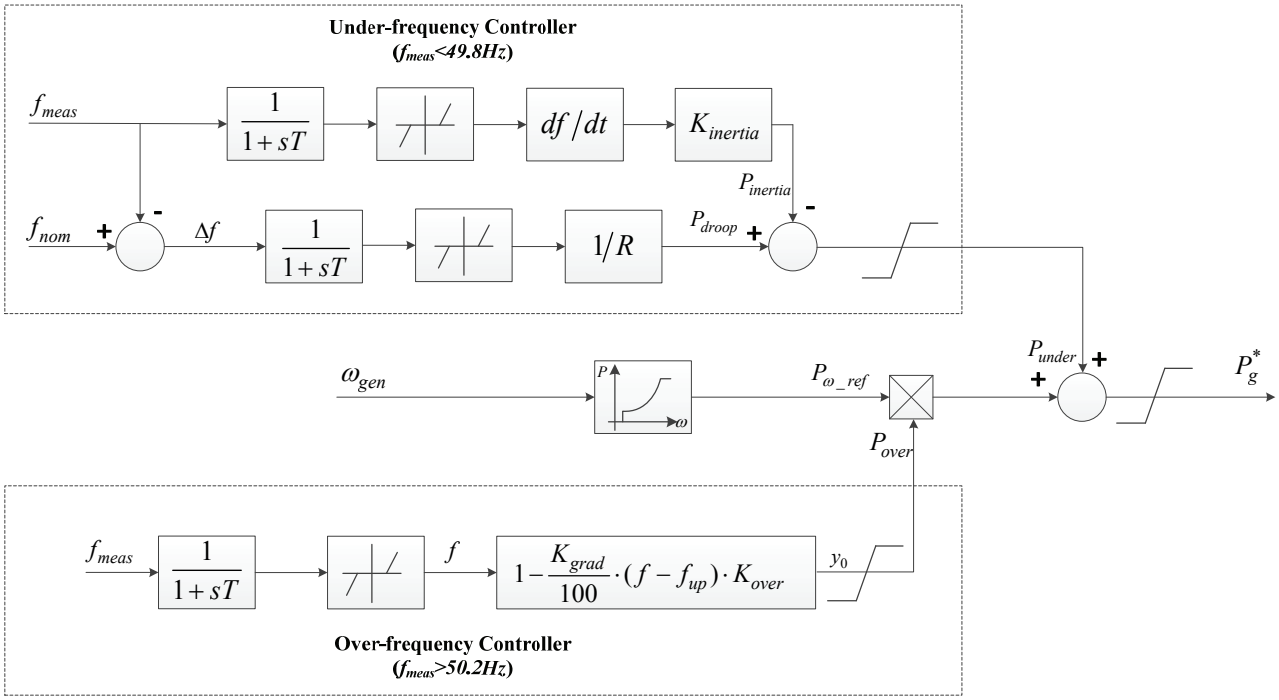

Figure 5.3 Ancillary frequency control for FCWT.

A. Under-frequency controller

The under-frequency controller is used to enable the FCWT to provide inertial response and release active power reserve if applicable, when the system frequency drops lower than 49.8Hz (nominal 50Hz) that is determined by the author in the simulation experiments. From Figure 5.3, it can be seen that the under-frequency controller is also composed of two components: *inertia controller* and *droop controller*. A demonstrative diagram of the under-frequency controller is shown in Figure 5.4.

The inertia controller is applied to emulate the inertial response of synchronous generators and

its output active power reference $P_{inertia}$ is proportional to the derivative of the system frequency. The droop controller is applied to emulate the response of the speed governor of a synchronous generator and its output active power reference P_{droop} is proportional to the absolute deviation of the system nominal frequency. Hence, the output P_{under} of the under-frequency controller can be given as

$$P_{under} = -K_{inertia} \cdot \frac{df_{meas}}{dt} + \frac{f_{nom} - f_{meas}}{R}, \tag{5.2}$$

where $K_{inertia}$ is the gain of the inertia controller, R is the adjusting coefficient of the droop controller, f_{meas} is the measured system frequency and f_{nom} is the nominal frequency of the power system. Similar discussions of this under-frequency regulation strategy can be found in detail in [6]-[11].

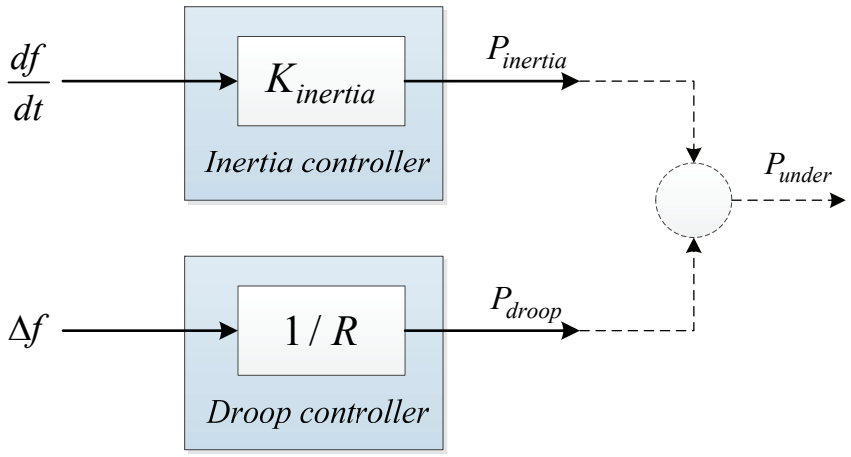

Figure 5.4 Demonstrative diagram of under-frequency controller.

B. Over-frequency controller

Fundamentally, the over-frequency controller reduces the current active power generation with a 40% gradient of the presently available power per Hz if the measured frequency exceeds 50.2Hz in terms of E.ON Grid Code [20]. While coordinated with the ancillary frequency control of VSC-HVDC, a participation coefficient K_{over} has been employed to offset the influence of regulation of VSC-HVDC on the peak frequency during over-frequency disturbances. The control is described as

$$y_o = 1 - K_{grad} \cdot (f - f_{up}) \cdot K_{over}. \tag{5.3}$$

where y_o is the output control signal, f is the system frequency and f_{up} is equal to 50.2 Hz, which is the activating threshold value. The value of K_{over} is determined according to the wind capacity penetration level (WCPL), which is defined as

$$WCPL = \frac{total\ installed\ wind\ capacity\ (MW)}{total\ load\ capacity\ (MW)} \times 100\%. \quad (5.4)$$

Since the VSC-HVDC capacity as well as its DC capacitance is directly related to the connected wind farm rating, the *WCPL* can then be thought as an index to reflect the frequency support level of VSC-HVDC using the proposed control. In this study, the WCPL is around 40% and thus K_{over} is assigned to '1.4'. The reduction of generation of FCWT is achieved by increasing the pitch angle.

C. Primary frequency reserve implementation

Conventional synchronous generating units are able to provide primary frequency reserve within 30 seconds. As mentioned above, when a frequency disruption occurs, the governor of a convention synchronous generator detects the frequency decline and then increases its mechanical power output to drive the synchronous generator to generate additional active power. As a result, the imbalance between the power demand and supply is reduced or eliminated and the system frequency is stabilized at an off-nominal point.

Dissimilarly, variable speed wind turbines are inherently non-capable of providing primary frequency reserve due to the un-controllability of wind speed. However, with customized control strategies, the FCWT can generate less active power than its available capability as described in Chapter 1.2. The margin between the actual generation and available generation can be considered as primary frequency reserve. To obtain the active power reserve margin, the FCWT must operate in a de-loading mode instead of in the maximum power extraction mode. The de-loading operation can be achieved by wind turbine generator speed control and / or pitch angle control [10], [11], [21].

In this study, rated wind speed is applied and only pitch angle control is implemented to realize primary frequency reserve of FCWT. The generic pitch angle controller has been depicted in Chapter 2.2.3. To enable FCWT to provide active power reserve margin for frequency support, an angle increment $\Delta\beta$ is added to force the FCWT to operate in the de-loading mode. The value of $\Delta\beta$ determines the de-loading level, namely, the capacity of active power reserve. A 10% de-loading level ($\Delta\beta \approx 1.7^{\circ}$) is set for frequency regulation study and the modified pitch angle controller is

shown in Figure 5.5.

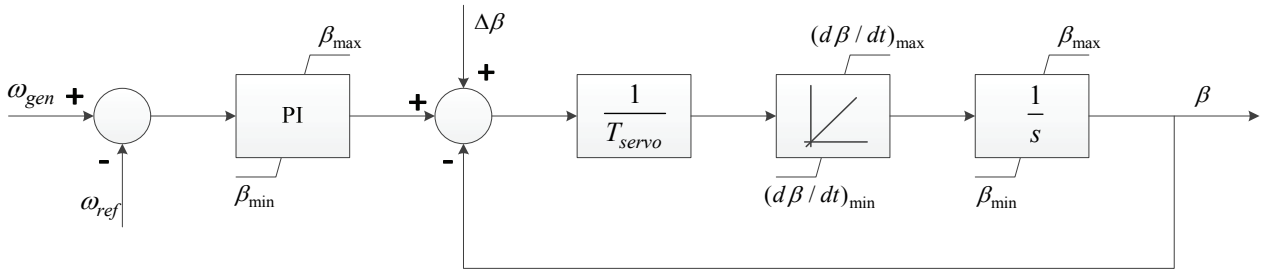

Figure 5.5 Modified pitch angle controller.

5.2.2 Frequency support strategy for VSC-HVDC

VSC-HVDC transmission system is attractive for connecting remotely located offshore wind farms to the onshore main grid. From the point of view of a power system, it acts as a zero-inertia generator that can control active and reactive power instantaneously and independently. The generic scheme of the VSC-HVDC system is shown in Figure 5.6.

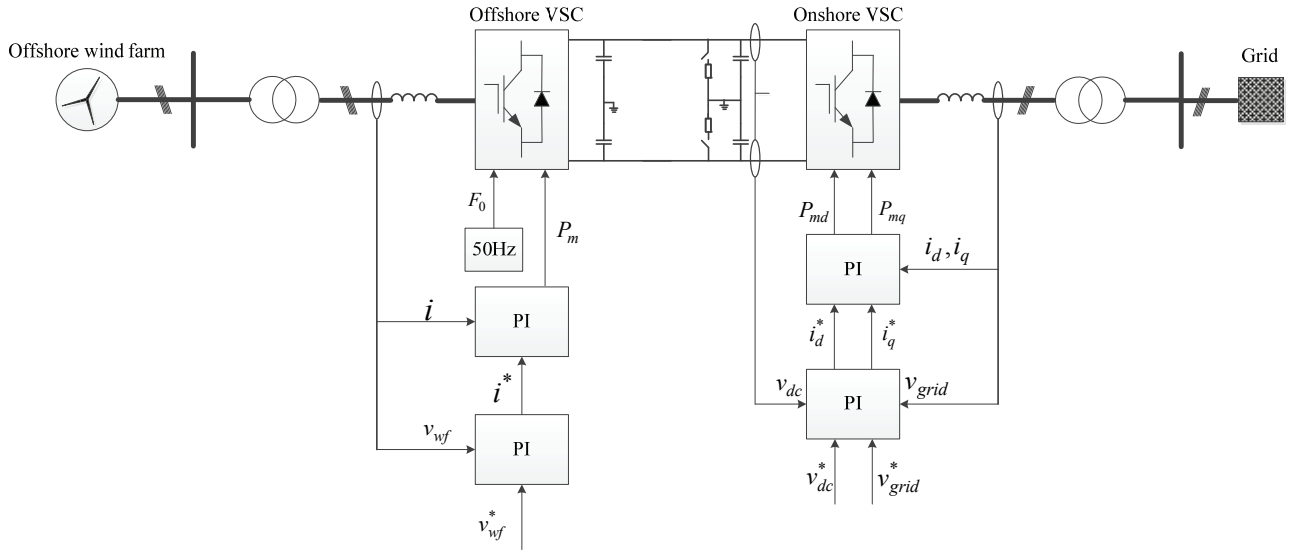

Figure 5.6 Generic scheme of VSC-HVDC.

The offshore VSC is responsible for collecting power generated by the offshore wind farm. Due to the decoupling of VSC-HVDC, it operates as a reference machine to set reference frequency, voltage amplitude and phase angle for the offshore network. The onshore VSC controls the power flow to the onshore grid by controlling the DC-link voltage and voltage amplitude at the connection point. A constant DC-link voltage indicates active power balance between onshore and offshore

VSCs, which means that the active power entering VSC-HVDC is equal to the active power leaving it.

Basically, VSC-HVDC system itself does not generate any active power, nor consume active power if ignoring converter and cable losses. Hence, it cannot provide frequency support inherently. Moreover, it even blocks offshore wind farm from directly responding to the state changes of the onshore grid. In other words, the existence of VSC-HVDC actually deteriorates the participation of FCWT-based offshore wind farm in system frequency regulation. Therefore, to cope with this impairment, a new frequency support strategy for VSC-HVDC is developed.

A. Frequency signaling

Generally, the control and measurement data is transmitted to individual FCWTs via standard SCADA-link. However, this direct communication method has a relatively longer latency that is not suitable for events that FCWTs are required to respond instantly.

Therefore, instead of setting the reference frequency at a constant value for the offshore grid, the offshore VSC is controlled to vary the reference frequency f_{wf} along with the onshore grid frequency f_{grid} by adding an ancillary control loop as shown in Figure 5.7, in which P_m is magnitude of the pulse-width modulation index and F_0 is the input frequency to VSC which allows varying the frequency of the output voltage. In the ancillary frequency signaling loop, the grid frequency f_{grid} is transmitted via the communication interface of VSC-HVDC. In this way, the onshore grid frequency

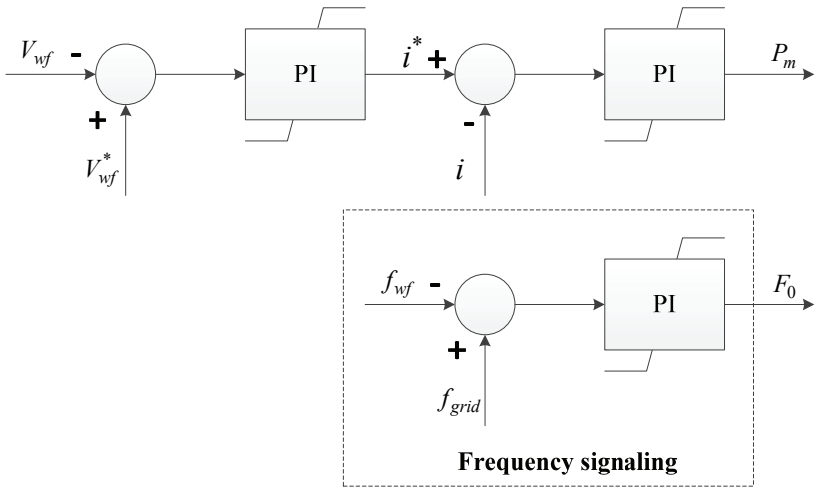

Figure 5.7 Modified Offshore VSC control with ancillary frequency control.

signal is contained in the offshore electrical waveforms. Thus, individual offshore FCWTs can detect the onshore grid frequency disturbance by monitoring the offshore grid frequency and react swiftly.

B. Ancillary DC voltage control

Figure 5.8 shows the equivalent ac-side and dc-side circuits of a VSC, in which R represents the loss of the VSC and the VSC reactor, L is the reactor inductance, V_s is the grid bus voltage and V_c is the VSC output voltage [22], [23]. The two sides are coupled each other with a controlled voltage source and a controlled current source.

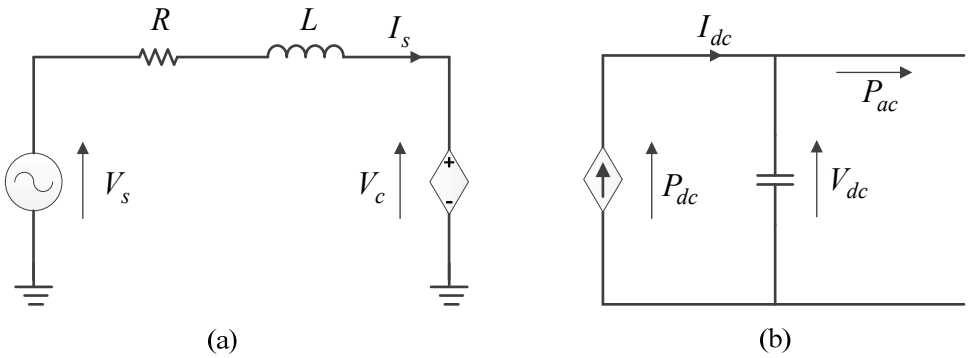

Figure 5.8 Equivalent circuit of a VSC: (a) ac-side; (b) dc-side.

Referred to [22]-[24], the mathematical model of ac-side in the synchronous *d-q* reference frame, in which the d-axis is aligned with grid voltage V_s, can be presents as

$$\frac{d}{dt}\begin{bmatrix} i_{sd} \\ i_{sq} \end{bmatrix} = \begin{bmatrix} -R/L & \omega \\ -\omega & -R/L \end{bmatrix}\begin{bmatrix} i_{sd} \\ i_{sq} \end{bmatrix} + \frac{1}{L}\begin{bmatrix} -v_{sd} + v_{cd} \\ -v_{sq} + v_{cq} \end{bmatrix} \tag{5.5}$$

$$P_{ac} = \frac{3}{2}(v_{cd} \cdot i_{sd} + v_{cq} \cdot i_{sq}). \tag{5.6}$$

And the dc-side can be given as

$$P_{dc} = I_{dc} \cdot V_{dc}. \tag{5.7}$$

According to the law of energy conservation and from Figure 5.8b, we can get

$$P_{dc} = P_{ac} + C \cdot \frac{dV_{dc}}{dt} \cdot V_{dc}. \tag{5.8}$$

Then, by substituting (5.6) and (5.7) into (5.8), we can have

$$I_{dc} \cdot V_{dc} = \frac{3}{2}(v_{cd} \cdot i_{sd} + v_{cq} \cdot i_{sq}) + C \cdot \frac{dV_{dc}}{dt} \cdot V_{dc} . \tag{5.9}$$

From (5.9), it can be seen that to ensure the power balance between the offshore and onshore VSCs, the DC voltage must be controlled constant. However, since the capacitor is an energy storage element, it is obvious that it can be used to release or absorb power by leveling down or up its voltage. The energy change W_c and power change p_c of a capacitor from t_1 to t_2 can be expressed as

$$W_c = C\int_{V_{dc}(t1)}^{V_{dc}(t_2)} V_{dc} \cdot dV_{dc} \tag{5.10}$$

$$P_c = \frac{dW_c(t_1, t_2)}{dt} . \tag{5.11}$$

Therefore, it is realistic to exploit this characteristic of DC capacitor of VSC-HVDC for grid frequency regulation. By means of adjusting the DC-link voltage, VSC-HVDC is able to inject more or less active power into the onshore grid than that it collects from the offshore wind farm.

For this specific purpose, an ancillary DC voltage controller is proposed and the modified onshore VSC control is shown in Figure 5.9. The additional DC voltage reference V^*_{dcf} is determined by the frequency deviation, which is passed to a first-order lag with gain K_f. To control the energy-releasing speed of the DC capacitors, the time constant T_f of the first-order lag is also tuned in terms of the latency of the communication interface of VSC-HVDC system. This value of V^*_{dcf} is limited to ±0.1 pu of nominal DC voltage, but in realistic applications, it should be determined with respect to insulation requirements, PWM functionality etc. In such a way, when the frequency deviation is recognized, the change rate of DC voltage is controlled according to the communication latency between the stations of VSC-HVDC. The voltage changes faster when the latency is shorter and slower when the latency is longer. That also represents that the DC capacitors are able to release its energy continuously until wind turbines start to react to the grid frequency deviation.

The ancillary DC voltage controller is activated when the grid frequency is out of the range 49.8~50.2Hz. Once the grid frequency is lower than 49.8Hz, the DC voltage is controlled down to 0.9 pu to release part of the stored energy in DC capacitance. When the grid frequency is higher than

50.2Hz, the DC voltage is controlled up to 1.1 pu to absorb energy transmitted from the offshore VSC. Since the DC capacitance and voltage variation for a certain VSC-HVDC are limited, the power released / absorbed by the DC capacitance is also limited. Therefore, in this study, the VSC-HVDC is controlled to provide efficient frequency support until the offshore FCWTs senses the onshore grid frequency disturbance and starts to respond to it.

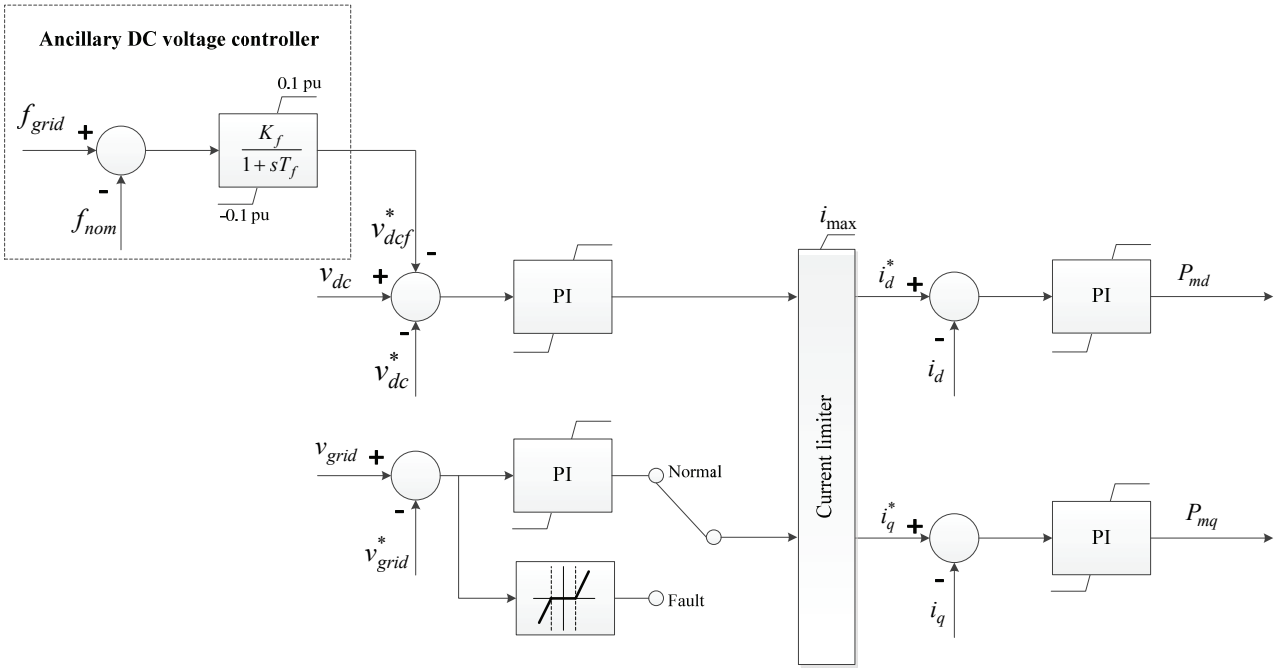

Figure 5.9 Modified onshore VSC control with ancillary frequency control.

5.3 Simulation studies

The simulation study has been carried out on the test power system described in Chapter 4.4 and as shown in Figure 4.1. The system frequency excursions are caused by sudden increase / decrease of Load C. A sudden increase of 46% active power and 10% reactive power of Load C is simulated at 1.0s to cause an under-frequency event. This results in the system frequency to drop to nearly 49.0 Hz without frequency supports from offshore FCWTs and VSC-HVDC. Similarly, the over-frequency event is resulted from a sudden decrease of 20% active power and 5% reactive power of Load C at 1.0s. During the over-frequency event, the maximum frequency is around 50.4Hz if the offshore FCWTs and VSC-HVDC don't participate in frequency regulation. The participation of VSC-HVDC and FCWTs in frequency regulation is activated when the frequency is below 49.8 Hz or beyond 50.2 Hz. The rated wind speed is applied as mentioned before. For different frequency events, cases listed in Table 5.1 are studied in the simulations.

TABLE 5.1
Description of study cases

Case	Description
1	Without frequency support from FCWTs and VSC-HVDC
2	Activating frequency controller of FCWTs only
3	Activating frequency controller of FCWTs and VSC-HVDC

5.3.1 Under-frequency event

Figure 5.10 – 5.13 presents the simulation results for the sudden load increase with 300ms latency of VSC-HVDC communication interface. The frequency response of the AC power system is shown in Figure 5.10. It is observed that the frequency support from offshore wind farm makes up active power for the load increase and reduces the frequency drop significantly. The frequency is also stabilized much faster at a higher steady-state value compared to the case without offshore wind farm frequency support. Moreover, the participation of frequency support from VSC-HVDC improves the nadir frequency further. However, due to the latency of measurement and the VSC-HVDC communication, the initial ROCOF of the frequency decline is not ameliorated evidently though both offshore wind farm and VSC-HVDC provide frequency support.

The response of offshore wind farm for the load increase is shown in Figure 5.11. We can see that if the ancillary frequency controller is not activated, the operation of FCWTs is not affected due to the decoupling of converters. In the cases that the frequency controller of FCWTs is activated, it can be observed that at the instant that the frequency drop is detected by the FCWTs, there is a sudden increase of the active power generation of the offshore wind farm (see Figure 5.11c) as a result of the decrease of both turbine generator speed (see Figure 5.11a) and pitch angle (see Figure 5.11b). The joint action of ancillary frequency controller and pitch angle controller leads to the fluctuation of FCWT generator speed as shown in Figure 5.11a. From Figure 5.11b and 5.11c, it is clear that that the primary frequency reserve is obtained by means of the decrease of pitch angle. The participation of VSC-HVDC in frequency regulation does not exert evident influence on the operation of the offshore wind turbines.

Figure 5.12 presents the response of VSC-HVDC for the load increase. It can be seen from curves of Case2 that the onshore VSC increases its active power output (see Figure 5.12b) as offshore wind farm starts to generate more power to support the frequency (see Figure 5.11c), while only offshore wind farm responds to the frequency decline. Accordingly, the DC voltage (see Figure 5.12a) fluctuates a bit at the time that the active power output of the onshore VSC increases sharply and then maintains at the rated level again. When the ancillary frequency controller of VSC-HVDC is activated, the DC voltage is controlled to drop down to 0.9 pu quickly as shown in Figure 5.12a to release part of the power stored in DC capacitance. In consequence, the onshore VSC is able to infeed more active power into the onshore grid to support the frequency as illustrated in Figure 5.12b. This coordinated frequency regulation of offshore wind farm and VSC-HVDC obtains better frequency response as mentioned above.

The influence of frequency support from offshore wind farm and VSC-HVDC on main grid spinning reserve and active power generation is illustrated in Figure 5.13. The grid spinning reserve is the summation of the spinning reserve of all conventional synchronous generators. It is obvious that enabling frequency support from offshore wind farm has positive effect, whereas the frequency support from VSC-HVDC barely affects the system spinning reserve and the generation of SGs due to its short activation time.

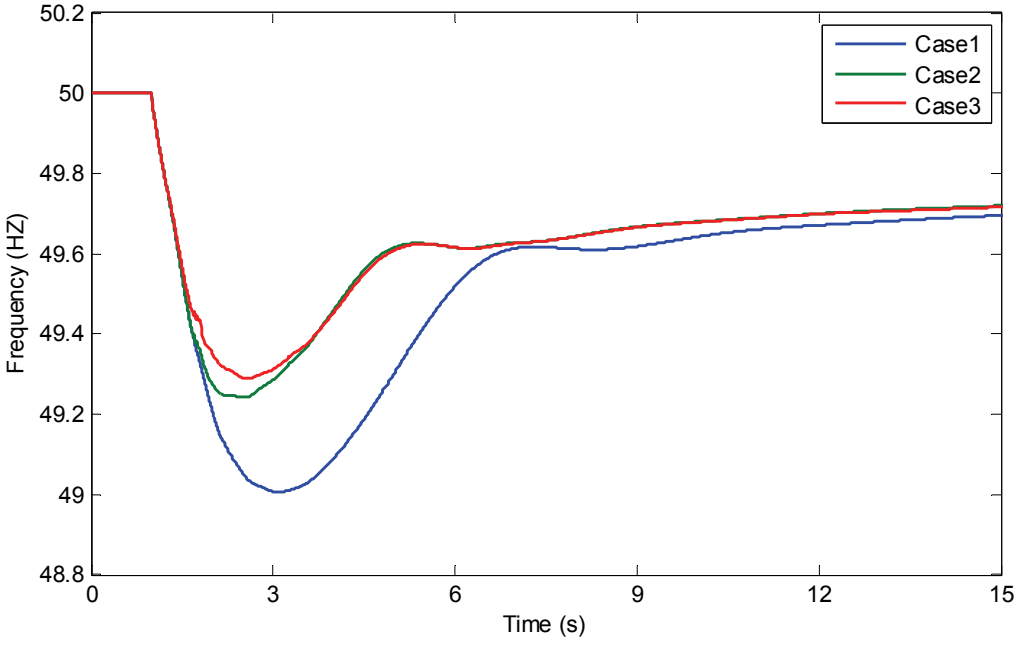

Figure 5.10 System frequency response for the load increase.

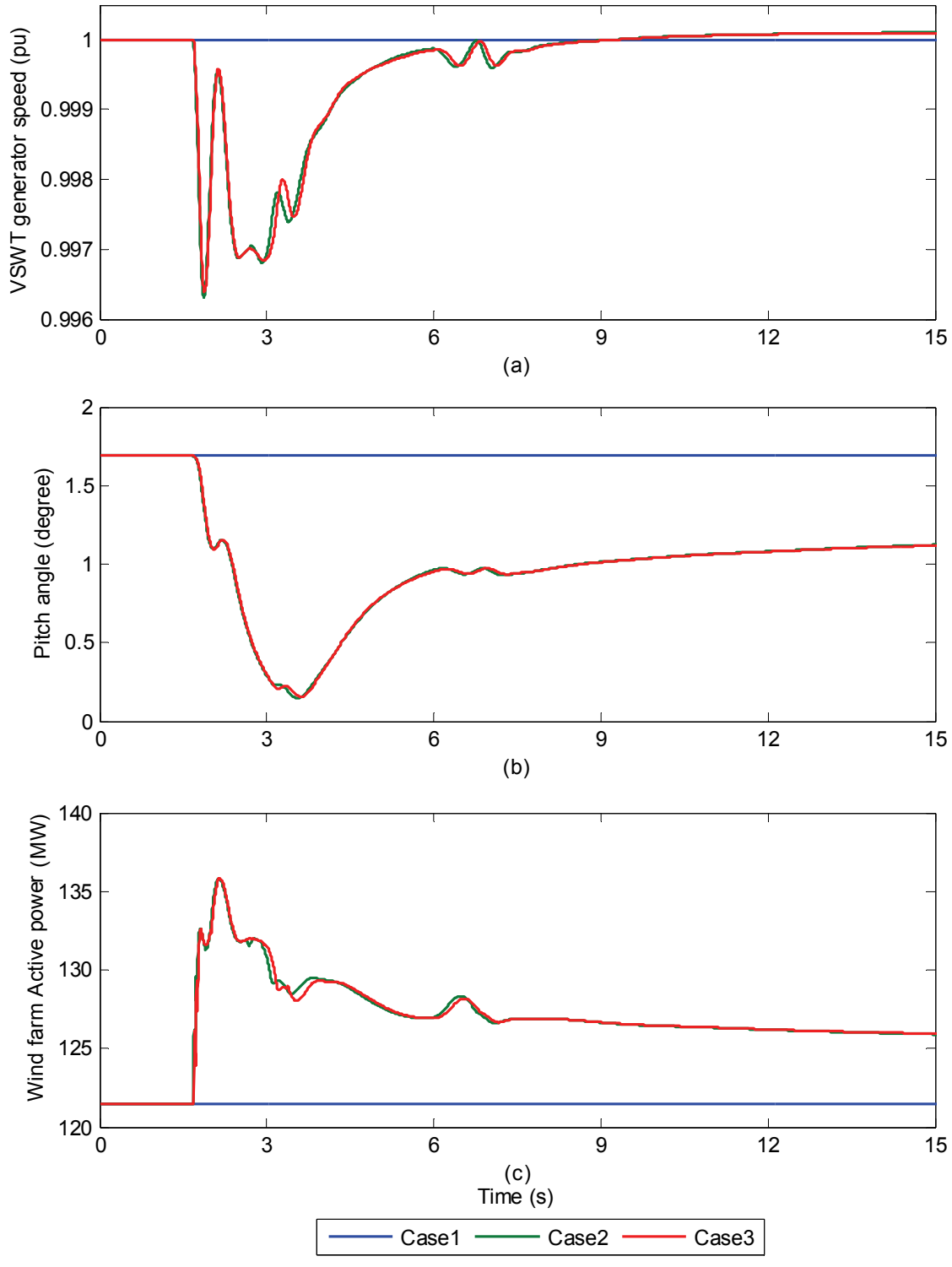

Figure 5.11 Offshore wind farm response for the load increase: (a) FCWT generator speed; (b) Pitch angle; (c) Active power generation of offshore wind farm.

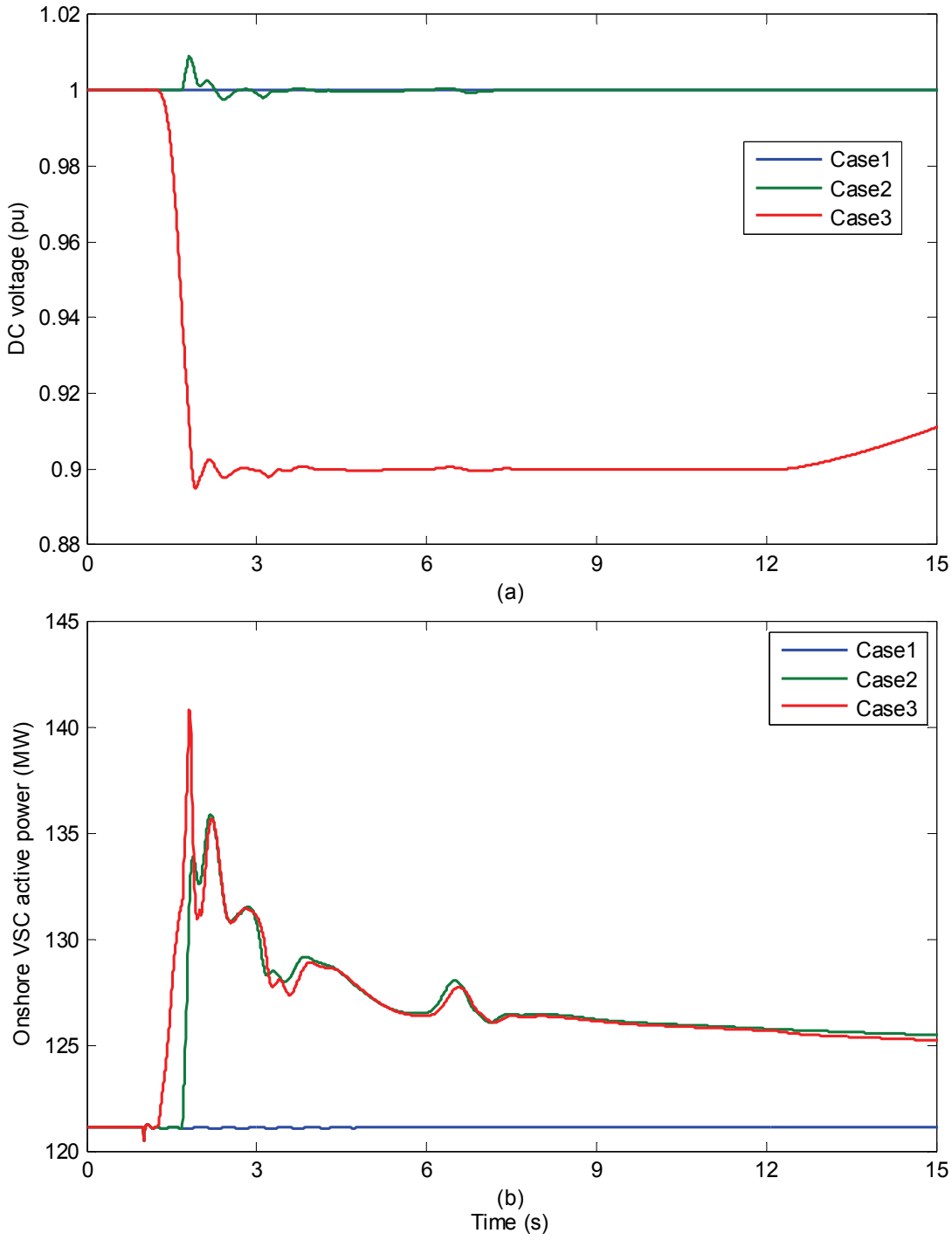

Figure 5.12 VSC-HVDC response for the load increase: (a) DC voltage; (b) Active power output of the onshore VSC.

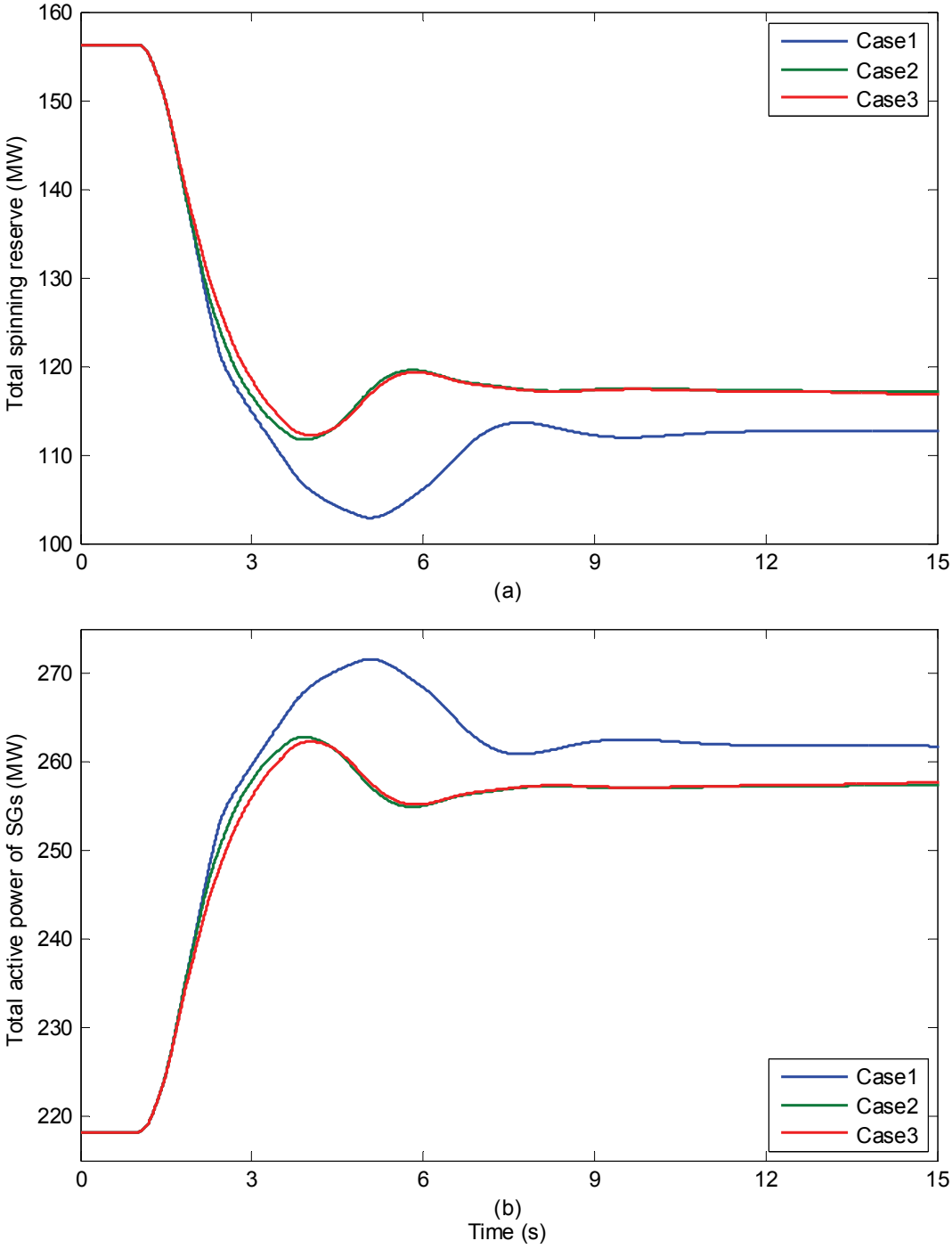

Figure 5.13 Main grid response for the load increase: (a) Total spinning reserve; (b) Total active power generation of conventional synchronous generators.

5.3.2 Over-frequency event

A sudden decrease of Load C results in the frequency to be over the upper acceptable limit (50.2 Hz). The simulation results for the sudden load decrease scenario are shown in Figure 5.14 to Figure 5.17, while the communication delay of VSC-HVDC is also 300ms.

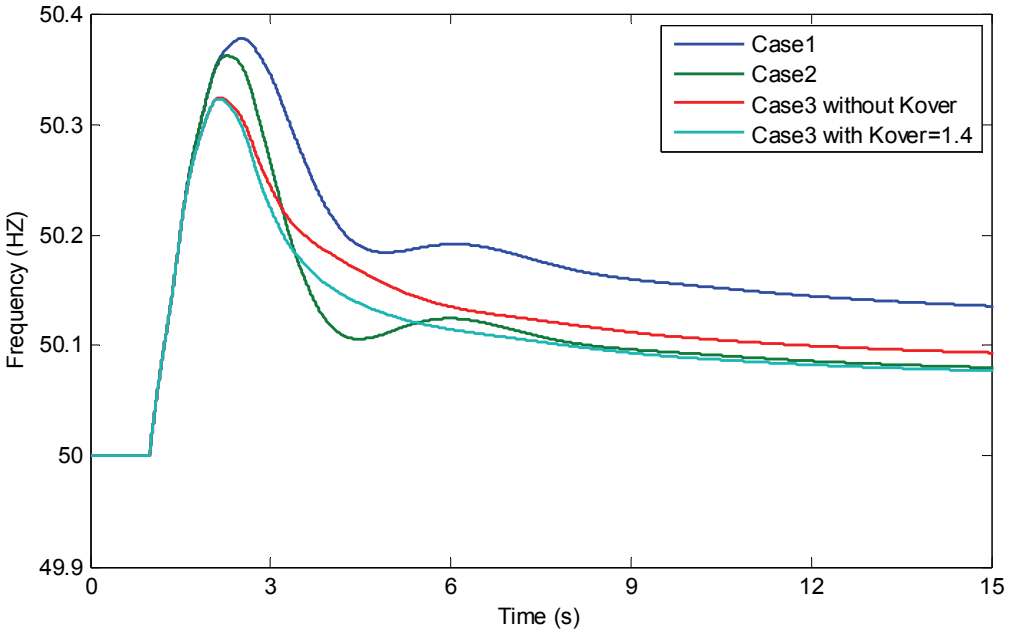

Figure 5.14 System frequency response for the load decrease.

The system frequency response is shown in Figure 5.14. We can see that the frequency support provided only by the offshore wind farm does not improve the initial frequency dynamics but reduces the peak frequency and achieves significant enhancement on the frequency restoration. Comparably, the joint frequency support provided by both offshore wind farm and VSC-HVDC further lowers down the peak frequency more obviously. However, without special coordination, the participation of VSC-HVDC in over-frequency regulation aggravates the restoration of the frequency as observed by comparing '*Case2*' with '*Case3 without* K_{over}'. By introducing the participation coefficient K_{over} to the over-frequency controller of FCWTs in the case '*Case3 with* $K_{over} = 1.4$', it can be seen that the negative impact of the support from VSC-HVDC on frequency restoration is alleviated.

Figure 5.15 presents the offshore wind farm response to the given over-frequency event. According to (5.3), the reduction in offshore wind farm generation is proportional to the over-frequency deviation. From Figure 5.15b and 5.15c, we can see that the pitch angle of FCWTs

increases to cut down the wind power generation, while the over-frequency event occurs. The wind turbine generator also speeds up shortly and then returns to normal operation by means of pitch angle regulation as shown in Figure 5.15a. As above mentioned, the VSC-HVDC support reduces the peak frequency. However, it, in turn, covers the actual severity of the frequency variation to FCWTs and thus weakens the FCWTs' frequency support as the red curves illustrate. The correction is done by the employment of participation coefficient K_{over}. By comparison between '*Case2*' and '*Case3 with* $K_{over} = 1.4$', it is clear that the wind farm active power in '*Case3 with* $K_{over} = 1.4$' is very close to that in '*Case2*'.

Figure 5.16 presents the response of VSC-HVDC for the sudden load reduction. It can be observed from Figure 5.14 - 5.16 that in the frequency-rising period, the DC voltage is controlled to increase to let the DC capacitors charge and absorb the energy that slows down the ROCOF and reduces the absolute frequency deviation. After the offshore wind farm reduces its generation as a response to the over frequency as shown in Figure 5.15c, the DC voltage begins to drop and the DC capacitors then begin to discharge and release energy that impairs the frequency restoring. The charging and discharging of DC capacitance are reflected in the active power output of onshore VSC as shown in Figure 5.16b. The influence of the introduction of K_{over} on DC voltage and onshore VSC active power output are also clearly presented in Figure 5.16a and 5.16b, respectively.

Figure 5.17 shows the changes for the sudden load reduction with respect to main grid spinning reserve and active power generation. By comparison, it is apparent that the frequency support from VSC-HVDC smoothes the fluctuations in spinning reserve (see Figure 5.17a) and system active power generation (see Figure 5.17b).

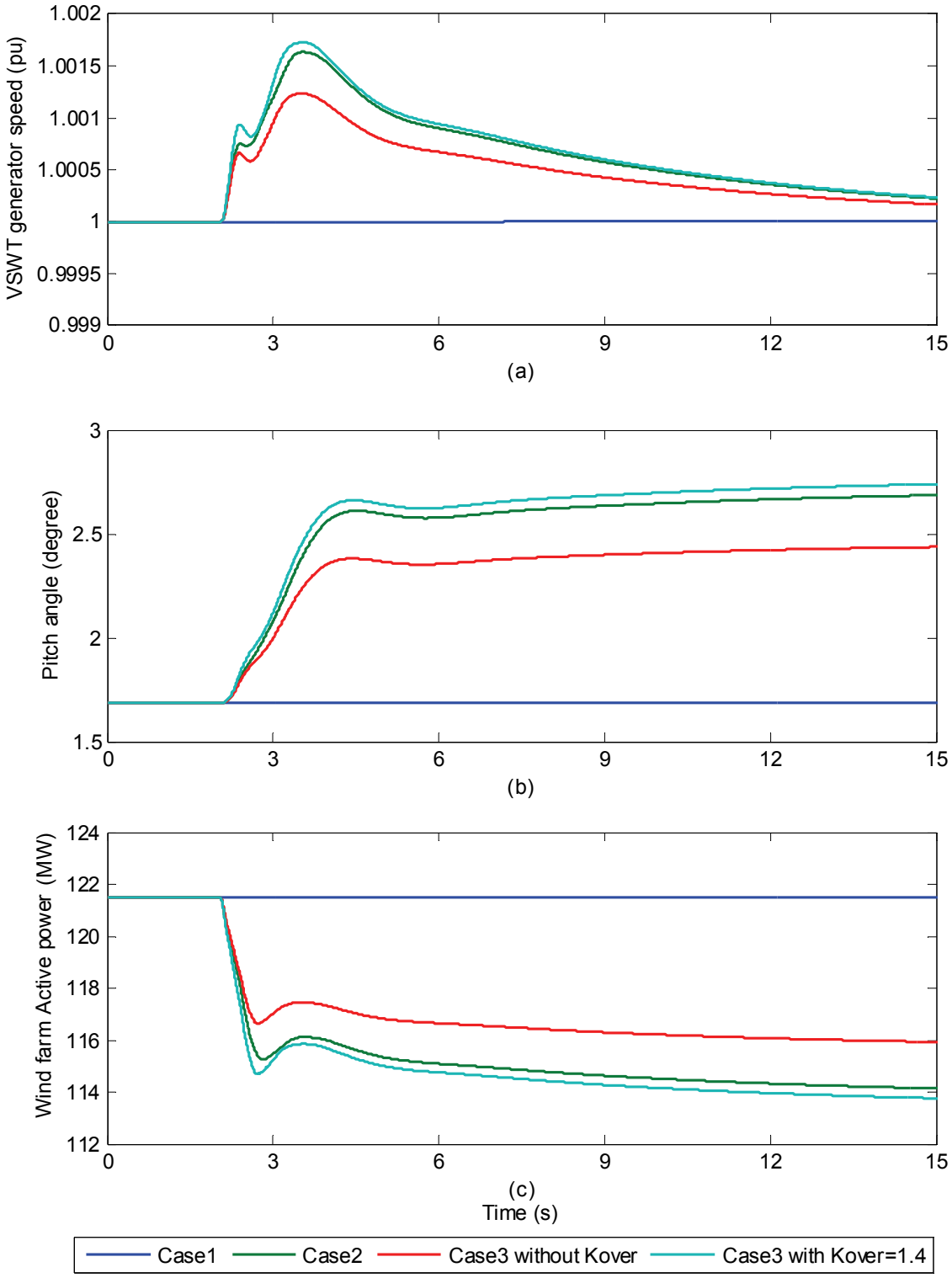

Figure 5.15 Offshore wind farm response for the load decrease: (a) FCWT generator speed; (b) Pitch angle; (c) Active power generation of offshore wind farm.

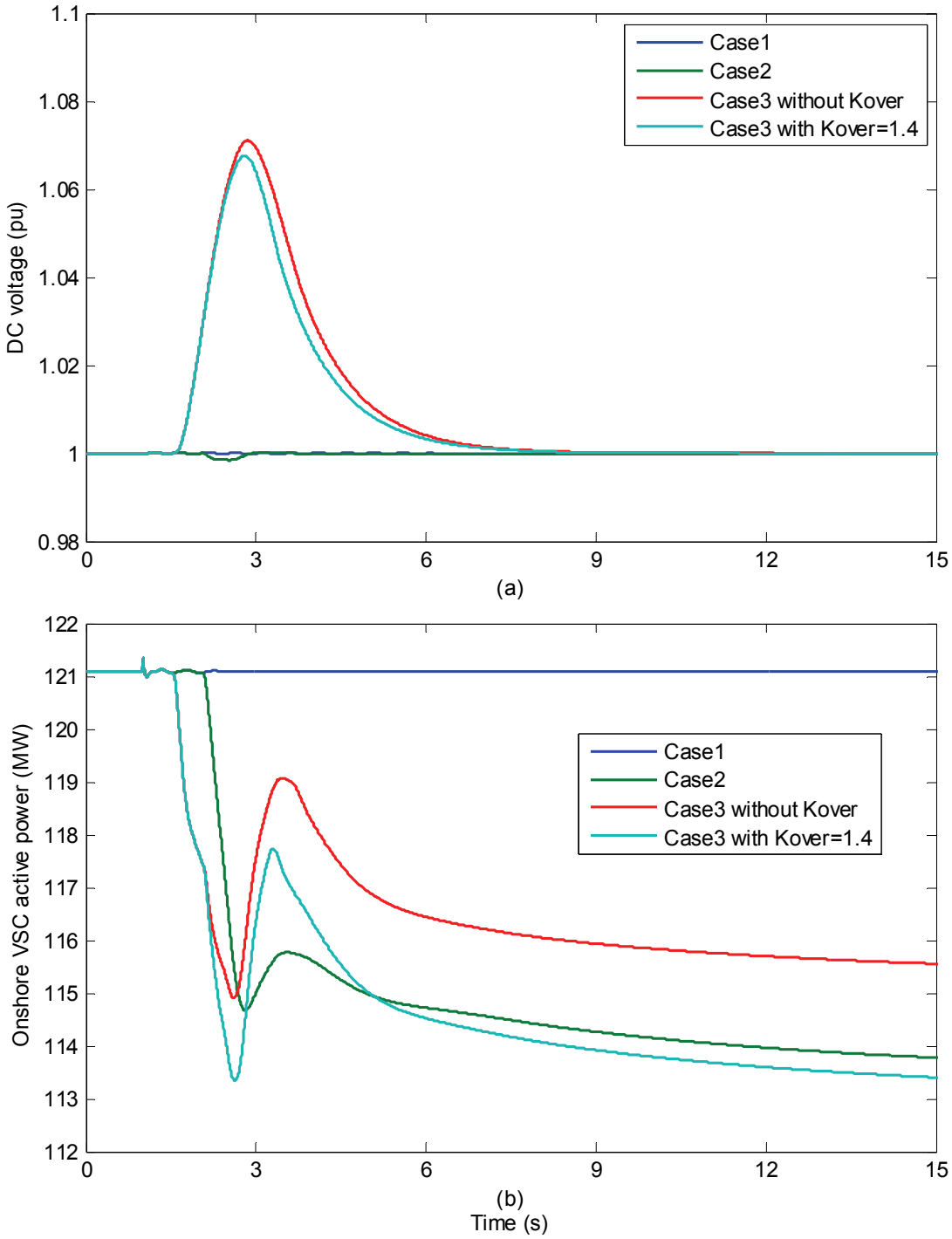

Figure 5.16 VSC-HVDC response for the load decrease: (a) DC voltage; (b) Active power output of the onshore VSC.

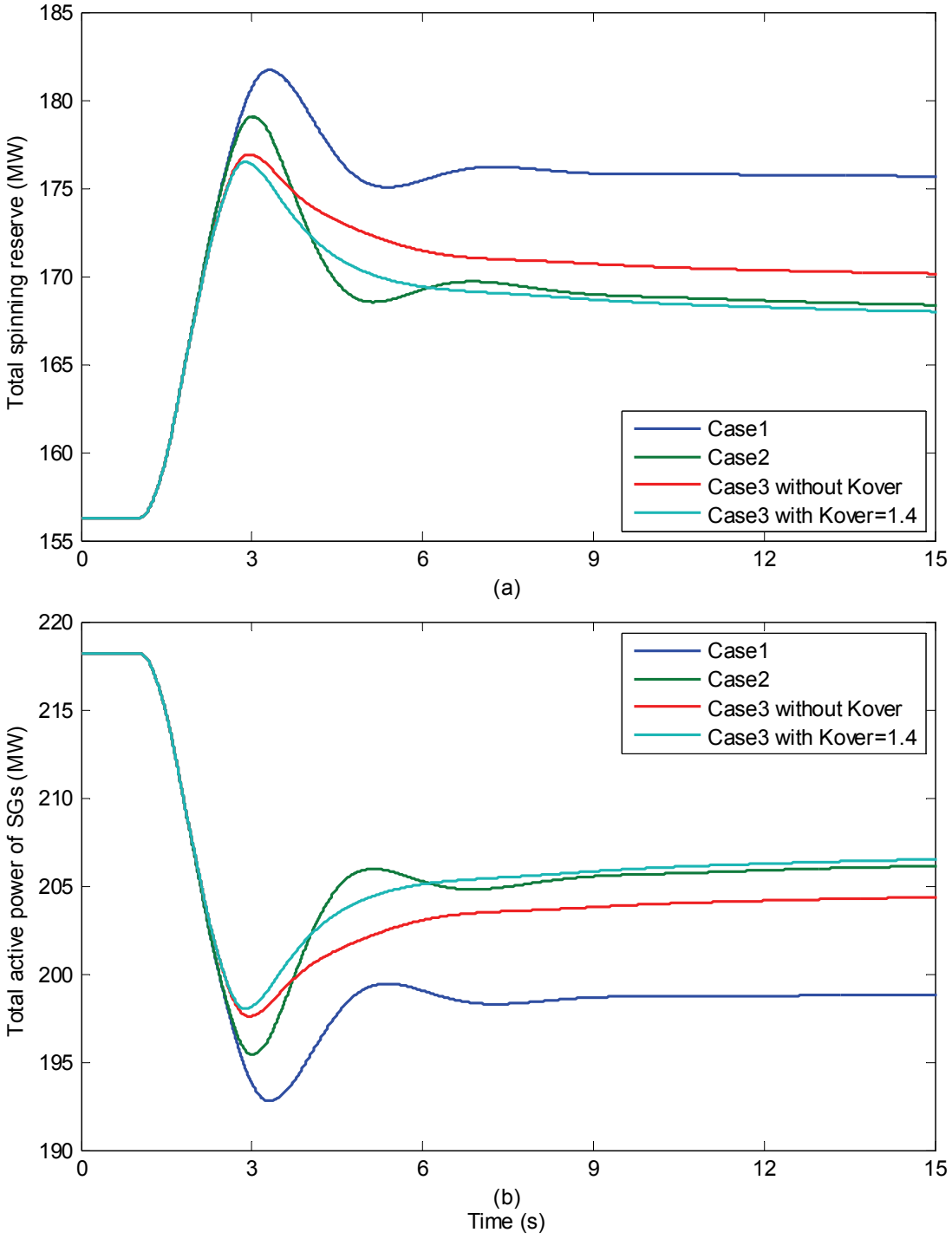

Figure 5.17 Main grid response for the load decrease: (a) Total spinning reserve; (b) Total active power generation of conventional synchronous generators.

5.2.1 Effect of delay of VSC-HVDC communication interface

The communication delay of VSC-HVDC depends on the distance between onshore and offshore VSC stations and the type of communication system. While implementing the proposed coordinated frequency control strategy for offshore wind farm and VSC-HVDC, Figure 5.18 and Figure 5.19 illustrates the effect of various delay of VSC-HVDC communication on the system frequency response, HVDC DC voltage and onshore VSC active power output for both under- and over-frequency scenarios, respectively. The studied communication delays are 10ms, 300ms and 1000ms.

From Figure 5.18a, we can see that with the increasing VSC-HVDC communication delay, the frequency falls deeper and the improvement on ROCOF is degraded. However, for the given three delays, the frequency is restored to almost the same level. From Figure 5.18b, it is observed that the slope of decline of DC voltage is smaller for a longer communication delay. Thus, the power-releasing of DC capacitance lasts longer as shown in Figure 5.18c. The slower decline of DC voltage and slower power-releasing of DC capacitance for a longer communication delay are proposed to avoid the second frequency drop when the DC capacitance has finished discharging but offshore wind farm has not increased its generation due to the communication delay.

Figure 5.19a illustrates that for a longer VSC-HVDC communication delay, the proposed frequency support strategy has a weaker suppression on the frequency ascending, but achieves better frequency restoring performance. From Figure 5.19b, it can be seen that a longer communication delay corresponds to a more moderate DC voltage change. The softer the DC voltage change, the milder and longer the energy-releasing of the DC capacitors as shown in Figure 5.19c. Therefore, by applying the proposed control strategy, the longer communication delay leads to less peak frequency regulation of the onshore VSC and then the offshore wind turbines would recognize a severer frequency deviation so as to provide stronger support for frequency regulation.

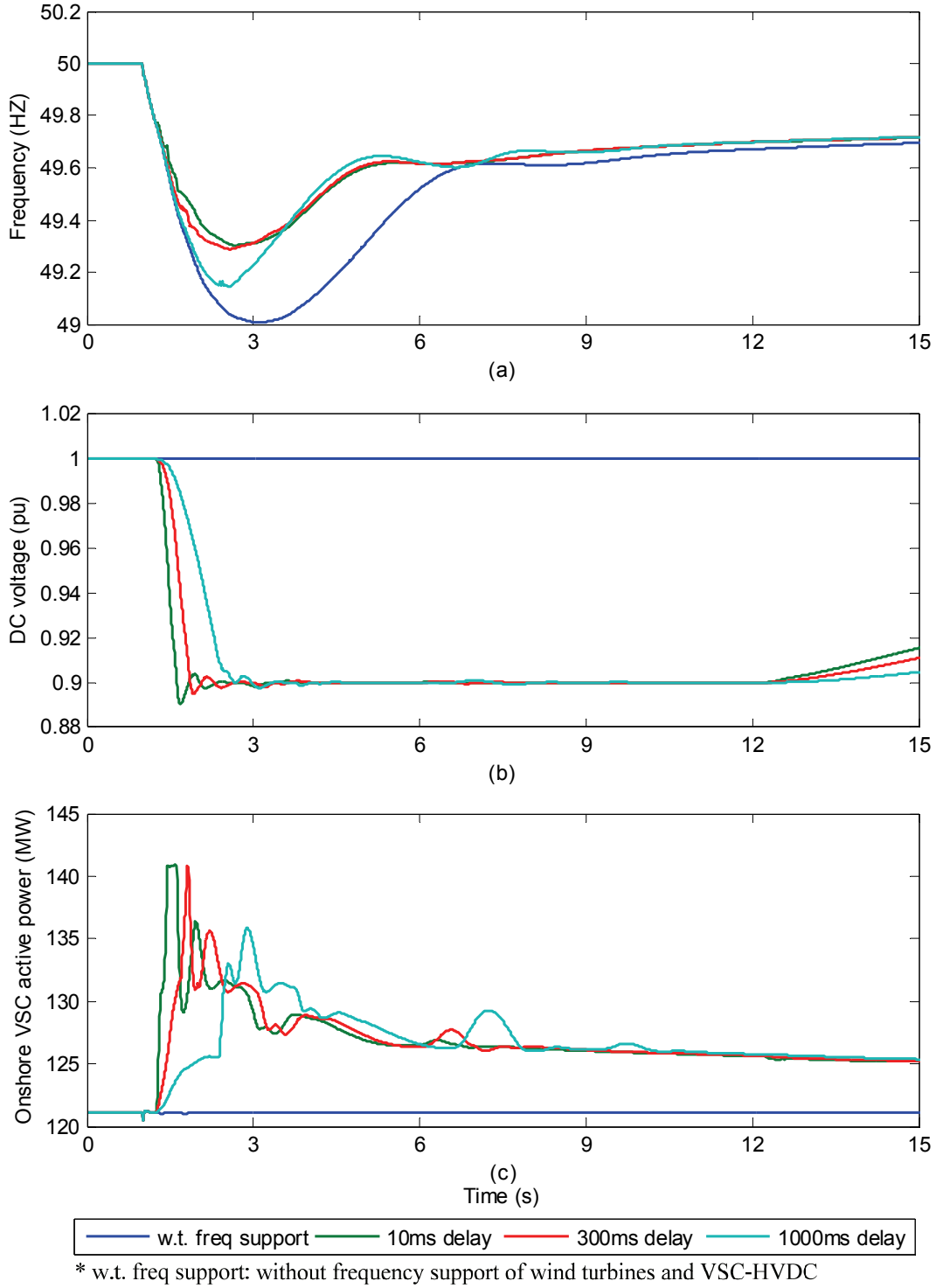

Figure 5.18 Effect of VSC-HVDC communication delay for the sudden load increase: (a) System frequency; (b) DC voltage; (c) Active power output of the onshore VSC.

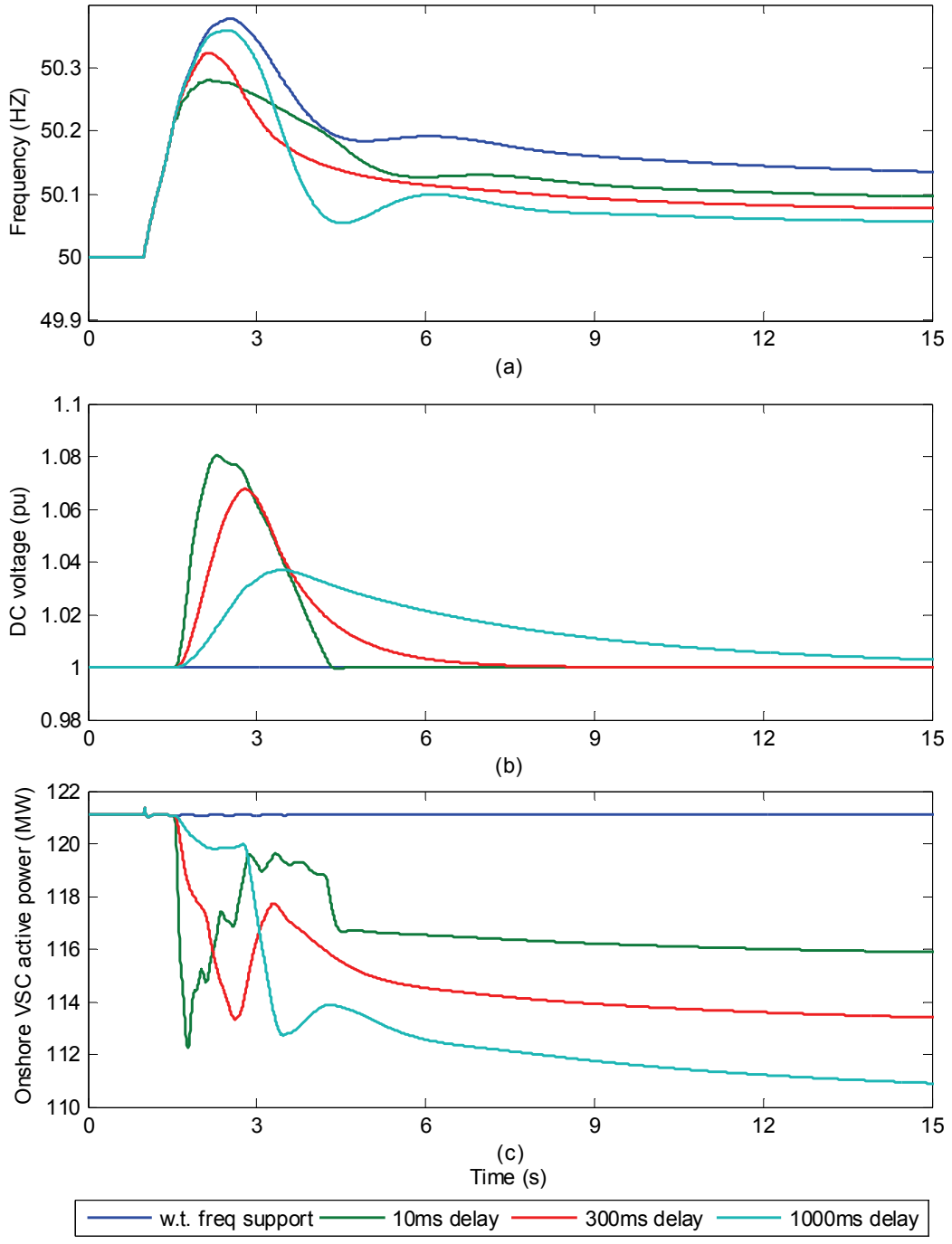

Figure 5.19 Effect of VSC-HVDC communication delay for the sudden load decrease: (a) System frequency; (b) DC voltage; (c) Active power output of the onshore VSC.

5.4 Summary

A new control strategy is developed in this study to allow the VSC-HVDC transmission to contribute to system frequency regulation without additional investment. The ancillary frequency controller added to the offshore VSC simplifies frequency signal communicating and reduces the latency of offshore wind farm responding to the onshore grid frequency deviation. The ancillary frequency controller added to the onshore VSC utilizes the DC capacitors to release / absorb energy by adjusting its voltage to fluctuate in a certain range. As a consequence, the VSC-HVDC is able to respond to system frequency excursion almost immediately and vary its active power output to support system frequency.

The implementation of the proposed control strategy is deliberately coupled with the frequency control of the variable-speed wind turbines of the offshore wind farm which is integrated into the onshore power grid by the VSC-HVDC. Through simulations and analysis, it is shown that the proposed control strategy allows the VSC-HVDC to provide effective frequency regulation without any extra investment. The coordination of the frequency control of the VSC-HVDC and wind turbines obtains a significantly enhanced frequency response for the studied power system. The collective frequency support capability is comparable to that of conventional power plants.

However, subject to the VSC-HVDC DC-link voltage and DC capacitor capacity constraints, the amount of the energy released / absorbed by the DC capacitors is limited and therefore the frequency support from VSC-HVDC is only temporary. In view of this, the frequency-responding latency of the offshore wind farm directly affects the strength of the frequency regulation from the VSC-HVDC. The larger the latency is, the weaker the frequency regulation strength of VSC-HVDC.

It is foreseeable that with the large-scale development and utilization of offshore wind power and VSC-HVDC interconnections, the participation of offshore wind farm and VSC-HVDC transmissions in system voltage and frequency regulation will play a substantial role. Hence, the significance of the method provided herein becomes more notable.

Bibliography

[1] P. Kundur, J. Paserba, V. Ajjarapu*, et al.*, "Definition and classification of power system stability IEEE/CIGRE joint task force on stability terms and definitions," *IEEE Transactions on Power Systems,* vol. 19, no. 3, pp. 1387-1401, 2004.

[2] J. Matevosyan, T. Ackermann, and S. Bolik, "Technical regulations for the interconnection of wind farms to the power systems," in *Wind Power In Power Systems*, ED: John Wiley & Sons, Ltd, pp. 115-142, 2005.

[3] G. Lalor, J. Ritchie, S. Rourke, D. Flynn, and M. J. O'Malley, "Dynamic frequency control with increasing wind generation," in *IEEE Power Engineering Society General Meeting*, vol. 2, pp. 1715-1720, June 2004.

[4] G. Lalor, A. Mullane, and M. O"Malley, "Frequency control and wind turbine technologies," *IEEE Transactions on Power Systems*, vol. 20, no. 4, pp. 1905-1913, Nov. 2005.

[5] E. Vittal, J. D. McCalley, V. Ajjarapu, and T. Harbour, "Wind penetration limited by thermal constraints and frequency stability," in *39th North American Power Symposium*, pp. 353-359, Sept.-Oct. 2007.

[6] J. Morren, S. W. H. De Haan, W. L. Kling, and J. A. Ferreira, "Wind turbines emulating inertia and supporting primary frequency control," *IEEE Transactions on Power Systems*, vol. 21, no. 1, pp. 433-434, Feb. 2006.

[7] J. F. Conroy and R. Watson, "Frequency response capability of full converter wind turbine generators in comparison to conventional generation," *IEEE Transactions on Power Systems*, vol. 23, no. 2, pp. 649-656, May 2008.

[8] S. El Itani and G. Joos, "Assessment of inertial potential of variable-speed wind turbines," in *IEEE Energy Conversion Congress and Exposition (ECCE*), pp. 851-856, 17-22 Sept. 2011.

[9] G. C. Tarnowski, P. C. Kjar, P. E. Sorensen, and J. Ostergaard, "Variable speed wind turbines capability for temporary over-production," in *IEEE Power & Energy Society General Meeting*, pp. 1-7, 26-30 July 2009.

[10] Z. S. Zhang, Y. Z. Sun, J. Lin, and G. J. Li, "Coordinated frequency regulation by doubly fed induction generator-based wind power plants," *IET Renewable Power Generation*, vol. 6, no. 1, pp. 38-47, Jan. 2012.

[11] J. M. Mauricio, A. Marano, A. Gomez-Exposito, and J. L. Martinez Ramos, "Frequency regulation contribution through variable-speed wind energy conversion systems," *IEEE Transactions on Power Systems*, vol. 24, no. 1, pp. 173-180, Feb. 2009.

[12] C. Feltes, H. Wrede, F. W. Koch, and I. Erlich, "Enhanced Fault Ride-Through Method for Wind Farms Connected to the Grid Through VSC-Based HVDC Transmission," *IEEE Transactions on Power Systems*, vol. 24, no. 3, pp. 1537-1546, Aug. 2009.

[13] X. Dawei, L. Ran, J. R. Bumby, P. J. Tavner, and S. Yang, "Coordinated control of an HVDC link and doubly fed induction generators in a large offshore wind farm," *IEEE Transactions on Power Delivery*, vol. 21, no. 1, pp. 463-471, Jan. 2006.

[14] Y. WANG, X. R. ZHU, L. XU, AND H. M. LI, "Contribution Of VSC-HVDC Connected Wind Farms To Grid Frequency Regulation And Power Damping," IN *36th Annual Conference on IEEE Industrial Electronics Society*, PP. 397-402, 2010.

[15] Y. Phulpin, "Communication-free inertia and frequency control for wind generators connected by an HVDC-link," *IEEE Transactions on Power Systems*, vol. 27, no. 2, pp. 1136-1137, May 2012.

[16] Y. Pipelzadeh, B. Chaudhuri, and T. C. Green, "Inertial response from remote offshore wind farms connected through VSC-HVDC links: A Communication-less scheme," in *IEEE Power and Energy Society General Meeting*, pp. 1,6, 22-26, July 2012.

[17] T. M. Haileselassie, R. E. Torres-Olguin, T. K. Vrana, K. Uhlen, and T. Undeland, "Main grid frequency support strategy for VSC-HVDC connected wind farms with variable speed wind turbines," in *IEEE PowerTech*, Trondheim, pp. 1,6, 19-23, June 2011.

[18] J. Zhu, C. D. Booth, G. P. Adam, and J. A. Roscoe, "Inertia emulation control of VSC-HVDC transmission system," in *International Conference on Advanced Power System Automation and Protection (APAP)*, pp. 1,6, 16-20, Oct. 2011.

[19] J. Zhu, C. D. Booth, G. P. Adam, A. J. Roscoe, and C. G. Bright, "Inertia emulation control strategy for VSC-HVDC transmission systems," *IEEE Transactions on Power Systems*, vol. 28, no. 2, pp. 1277-1287, May 2013.

[20] Grid Code: High and Extra High Voltage, E.ON Netz GmbH Tech. Rep., April 2006, Status:1.

[21] I.Erlich and M. Wilch, "Primary frequency control by wind turbines," in *IEEE Power and Energy Society General Meeting*, pp. 1-8, 2010.

[22] G. Zhang; Z. Xu; Y. Cai, "An equivalent model for simulating VSC based HVDC," in *IEEE/PES Transmission and Distribution Conference and Exposition,* vol.1, pp. 20-24, 2001.

[23] L. Xu, L. Z. Yao, and C. Sasse, "Grid Integration of Large DFIG-Based Wind Farms Using VSC Transmission," *IEEE Transactions on Power Systems*, vol. 22, no. 3, pp. 976-984, 2007.

[24] O. A. Giddani, G. P. Adam, O. Anaya-Lara, G. Burt, and K. L. Lo, "Control strategies of VSC-HVDC transmission system for wind power integration to meet GB grid code requirements," in *International Symposium on Power Electronics Electrical Drives Automation and Motion (SPEEDAM)*, pp. 385-390, 2010.

Chapter 6

Application of Battery Energy Storage System to Enhance Frequency Response of Power System with High Wind Power Penetration

Employing BESS is an effective solution to mitigate wind power fluctuation and improve the wind power integration. This chapter explores the capability of PWM converter-interfaced BESS to enhance the system frequency response in cooperation with smoothing wind power fluctuation for the power system with high wind penetration. The PWM converter size is evaluated on the requirements of wind power fluctuation mitigation and frequency regulation. A new power management strategy is also proposed to enable the BESS to fulfil the two tasks.

6.1 Introduction

Due to the intermittency of wind energy and different electromechanical characteristics of wind turbines, high penetration of wind power is prone to introduce many technical challenges that threaten the stability and reliability of power systems, especially in the case of large scale offshore wind farm integration. One of the solutions, which may meet the more and more strict wind power integration requirement, is to enable large wind farms to have the similar characteristics as conventional generation units, such as automatic frequency and voltage control. Employing energy storage devices into power systems is another solution that can alleviate the adverse effects of large wind power integration and allow higher wind power penetration [1]-[7]. In addition, energy storage devices also play a very important role in electric energy time-shift, load following, area regulation, power quality, reserve capacity and transmission congestion relief and so on [8].

To provide frequency reserve as conventional power plants, wind farms inevitably have to operate in a de-loading mode and generate less power than available as mentioned in the previous chapter. This would like to increase the system costs as other generation units have to compensate for the spilt wind energy and the participation in frequency regulation could also increase the fatigue of mechanical components of wind turbines. In addition, due to the continuous variation of wind speed, the frequency reserve of wind farms is not possible to keep a constant amount but is only a proportion of the available power. By comparison, using energy storage devices to replace

the frequency reserve of wind farms may be a good alternative.

There are many types of energy storage technologies that are available for improving wind power integration, such as compressed air energy storage (CAES), pumped hydro, super-capacitor, flywheel, super-conducting magnetic energy storage (SEMS), BESS etc. [7], [9]. Among them, as one of the most cost-effective energy storage technologies available [9], BESS has been increasingly used for mitigating the wind power fluctuation, enhancing the wind power integration and improving the power quality [8], [10]-[14]. The combination of BESS and static compensator (STATCOM) has also been developed in [15], [16] to improve the power quality and stability to fixed-speed wind turbines.

However, for applications of BESS to wind farm integration, most of the researches focused on using the BESS to complete a single task. The potential of enabling the BESS to fulfil multitask has not been addressed much. This chapter explores the capability of PWM converter-interfaced BESS to enhance the system frequency response in cooperation with smoothing the wind power fluctuation for the power system with high wind penetration. The power system is characterized by a large-scale offshore wind farm that is integrated through a VSC-HVDC transmission system. The BESS is connected at the same point as the onshore VSC of the VSC-HVDC link.

The converter rating of the BESS is based on the requirement of wind power fluctuation mitigation and the consideration that the BESS is able to supply frequency reserve and regulation at all times to a certain extent. This extent is determined, in this study, to be comparable to that provided by offshore wind farm and VSC-HVDC implemented the coordinated control strategy described in Chapter 5. Accordingly, a new power management strategy is also proposed to adjust BESS's frequency reserve based on its fulfilment of smoothing wind power fluctuation. Case studies show that the proposed method allows the BESS to achieve multitasking and improve the system frequency response.

6.2 Battery energy storage system model

A battery system is made up of a set of low-voltage/power battery modules connected in parallel and series to achieve a desired electrical characteristic [9]. Through chemical reactions, batteries are charged and discharged in a DC manner. Therefore, to interface a battery with an AC system, a power conversion unit is necessary for transforming the DC-voltage of the battery to the AC-

voltage needed for the grid and vice versa. The power conversion unit is normally based on a PWM voltage source converter. In consequence, a BESS comprises mainly of a storing part (battery modules), PWM converter and relevant control. The fundamental configuration of an equivalent BESS is shown in Figure 6.1, in which SOC represents the state of charge of the battery and P_{md} and P_{mq} represent the *d*- and *q*-axis pulse-width modulation index respectively. The control variables of PWM converter may consist of active power, voltage and frequency of the grid and the SOC of the battery.

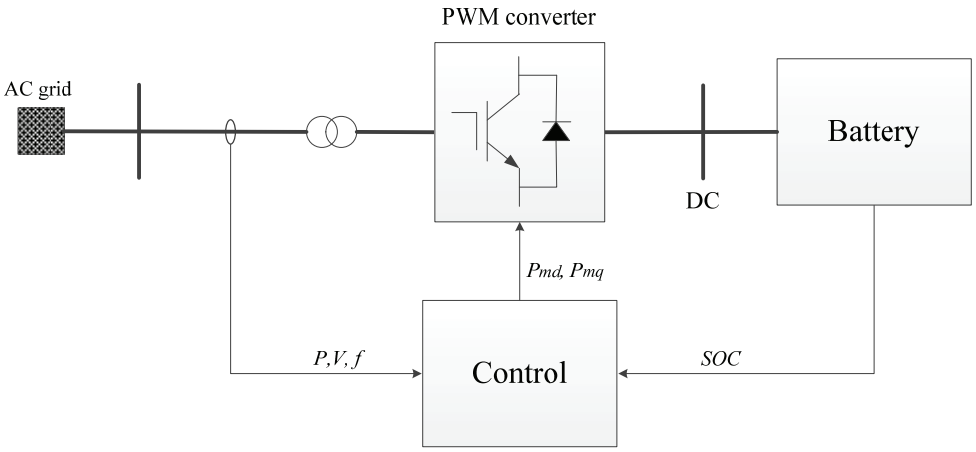

Figure 6.1 Fundamental configuration of the BESS in power system.

6.2.1 Battery model

The challenge with a BESS model largely lies in the battery modelling. To design an accurate and complete battery model is complex, time-consuming and application-dependent. In addition, the huge diversity and fast development of battery technologies make it unrealistic to have an accurate model that is valid for all batteries. Amongst all the current available battery types, the lead-acid battery is the most mature technology and has been extensively used for a majority of power system applications [6], [17], [18]. Therefore, the battery model in this study is based on the lead-acid technology.

Different approaches of simulating lead-acid batteries for power system applications have been developed in [17] – [21]. In DIgSILENT, a simplified battery model is provided and the equivalent circuit is shown in Figure 6.2, in which *R* represents the internal resistance and *E(soc)* represents the battery voltage dependent on SOC.

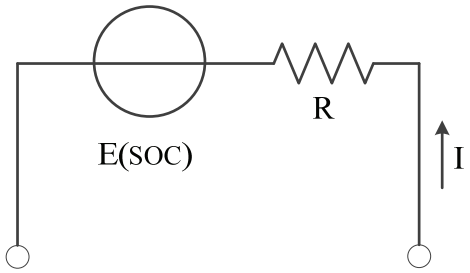

Figure 6.2 Simple battery electrical equivalent.

The SOC of the battery is determined by integrating the current in- and out-put of the battery. In sequence, the DC-voltage of a battery cell can be calculated as:

$$V_{cell} = V_{cell\,\max} \cdot SOC + V_{cell\,\min} \cdot (1 - SOC) - I_{cell} \cdot R \tag{6.1}$$

where $V_{cellmax}$ is the voltage of the fully loaded cell, $V_{cellmin}$ is the voltage of the empty cell and I_{cell} is the DC-current of the battery cell. The block diagram of the simplified battery model is presented in Figure 6.3. The cell current is calculated by dividing the battery current by the number of parallel cells. The result of the integrator divided by the capacity of the cell makes the SOC. The DC-voltage of a cell is deduced by equation (6.1). The DC terminal voltage of the battery is then the result of the cell voltage timed by the number of cells in a row.

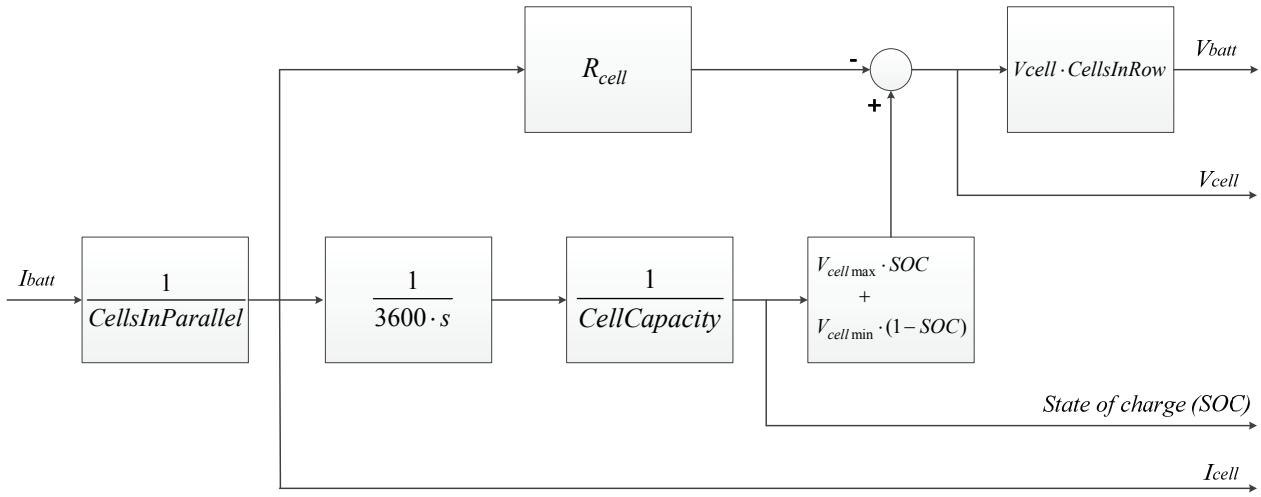

Figure 6.3 Block diagram of the simplified battery model.

6.2.2 BESS control

Figure 6.4 presents the overall control structure of the BESS applied in this study. The simplified

battery model, which is explained in the above section, controls the instantaneous value of the voltage of the DC Voltage Source that is the representation of the battery in DIgSILENT. The output current of this DC Voltage Source is, in turn, fed into the battery model as the input signal. The controller of the PWM converter consists of a power management unit, an active power-voltage (PV) controller, a charging controller and a current controller. The current controller, which generates the modulation factor, is an internal controller that is built in the PWM converter model in DIgSILENT. The other controllers are explained in detail as below.

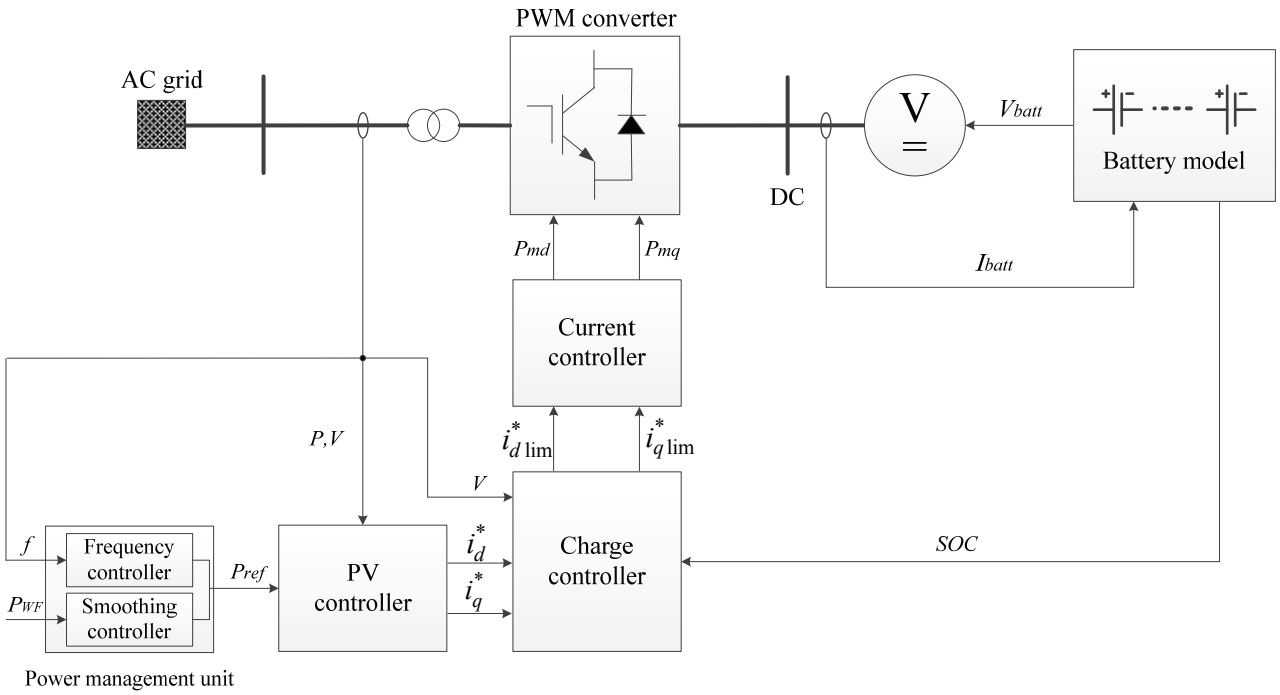

Figure 6.4 Overall control structure of the BESS.

A. Proposed power management unit

The power management unit is responsible for determining the active power reference for the BESS. In this study, it is a combination of a smoothing controller and a frequency controller.

For smoothing wind power fluctuations, various control strategies have been developed for battery energy storage systems [11]-[14], [23]-[25]. Though taking account of different limitations, for example, fluctuation restrictions and battery SOC limits, most of those strategies are based on first-order low-pass filters (FLF). The fundamental of the wind power smoothing approaches based on FLF is demonstrated in Figure 6.5. The wind farm generation P_{WF} is filtered by a FLF with a

smoothing time constant T_f, which is basically determined by fluctuation restrictions. Thus, the output of the FLF is seen as the expected wind power P_{WF_exp}. The power order P_{odr} for the BESS is then given by the difference between the actual and expected wind power. After the power regulation of BESS (absorbing/releasing), the fluctuation of the combines power P_{WFC} is finally limited to an acceptable boundary. Consequently, the grid frequency deviation caused by wind power fluctuation can also be diminished by implementing BESS with appropriate controls. An accurate wind forecast may further improve the performance of the smoothing controller and reduce the dimension of the battery [23].

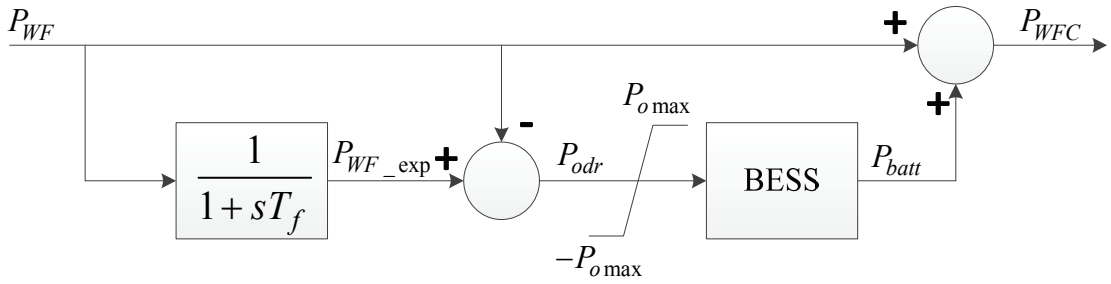

Figure 6.5 Fundamental of FLF-based strategies for wind power fluctuation smoothing.

Since the mitigation of wind power fluctuation is not the research emphasis and the focus is on the transient performance of the power system during a short time, it is assumed in this study that an ideal FLF-based smoothing controller is implemented and is capable of limiting the wind power fluctuation to a satisfactory level.

However, it is apparent that the smoothing controller is not sensitive to system frequency deviation and not effective for suppressing frequency deviations caused by grid contingencies such as synchronous generator outage and sudden load change. Therefore, in this study, a frequency controller is also employed and coordinated with the smoothing controller to equip the BESS with enhanced frequency response capability.

Similar to the speed-droop characteristic of the governor in conventional generating units, the frequency controller of the BESS is a proportional controller with a dead band and a gain *1/droop* as shown in Figure 6.6. The value of the droop determines the amount of active power output of the BESS with respect to the absolute value of the frequency deviation. Thus, this controller can take the responsibility for primary frequency control. The generated active power reference P_{fref} is limited within a certain range and also depends on the value of P_{odr}.

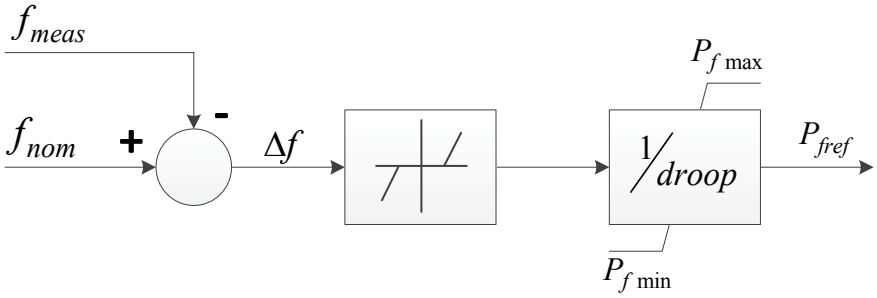

Figure 6.6 Block diagram of frequency controller of the BESS.

The power reference P_{odr} together with P_{fref} compose the total active power reference P_{ref} to the PV controller and thus determines the active power in- / out-put of the BESS. The per unit value of P_{odr} and P_{fref} satisfies the following relationship

$$P_{odr} + P_{fref} \le 1, \quad -P_{o\max} \le P_{odr} \le P_{o\max} \;\&\; P_{f\min} \le P_{fref} \le P_{f\max} \tag{6.2}$$

in which P_{omax} is the maximum value of P_{odr}, and P_{fmin} and P_{fmax} are the minimum and maximum value of P_{fref}.

To ensure a certain amount of frequency reserve at all times and enhance the system frequency response, capacity constraints are also set for fluctuation mitigation and frequency regulation in this study as

$$P_{o\max} < 1 \tag{6.3}$$

$$P_{f\max} = 1 - P_{odr} \tag{6.4}$$

B. PV controller

The PV controller is to provide active power and reactive power/voltage control in a grid voltage oriented reference frame as shown in Figure 6.7. By means of PI controllers, the *d*-axis control loop controls the amount of active power in- / output of the BESS and the *q*-axis control loop controls the voltage of the measured point to the desired level. The active power reference is generated by the power management unit as described above.

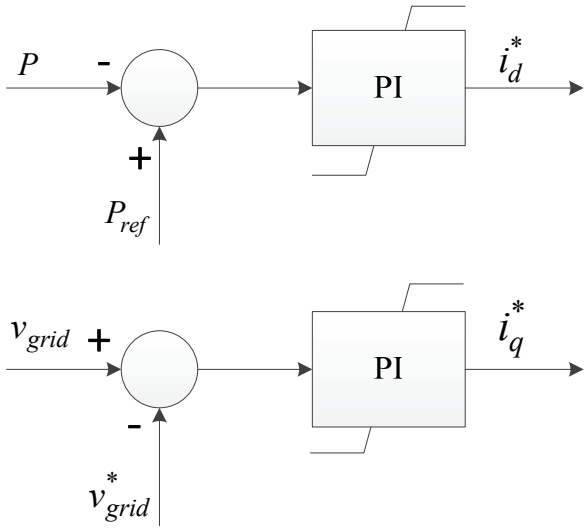

Figure 6.7 Block diagram of PV controller of the BESS.

C. Charge controller

The charge controller is used to judge whether the battery needs to be charged or not and set the active and reactive current boundary. As can be seen from Figure 6.8, the charge controller consists of two parts: a charging logic and a current limiter.

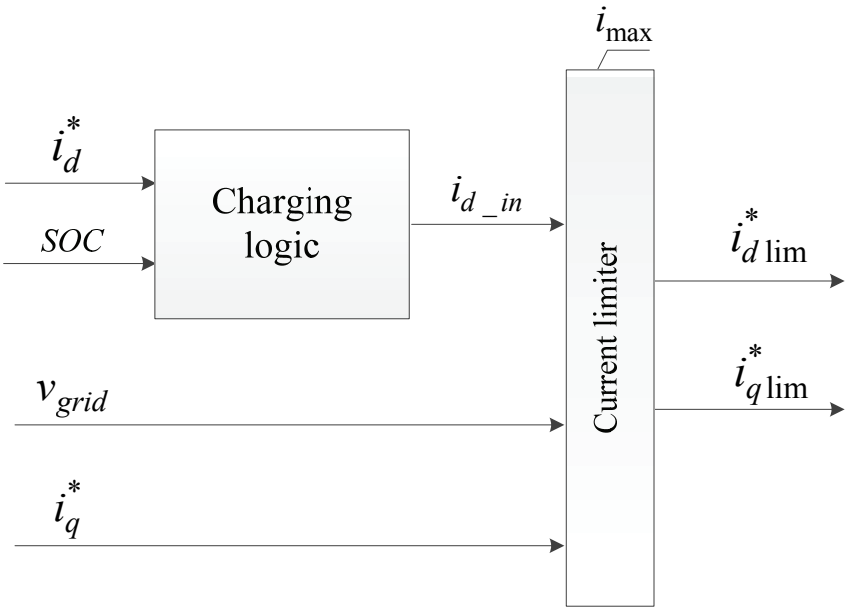

Figure 6.8 Block diagram of charge controller of the BESS.

The charging logic determines the charging / discharging of the battery based on the value of

SOC and active current. It also prevents a discharging of the battery if the SOC is below a certain value and prevents a charging of the battery if the SOC is above a certain value. The current limiter, on the one hand, limits the *d*- and *q*-axis current values according to the rated current of the PWM converter. On the other hand, it decides the current priority based on the magnitude of the measured voltage. The active current has the higher priority as long as the measured voltage is higher than 0.9 pu. Otherwise, the reactive current is preferred.

Details of the BESS model and control frames used in this study can be found in Appendix D.

6.3 Studied System

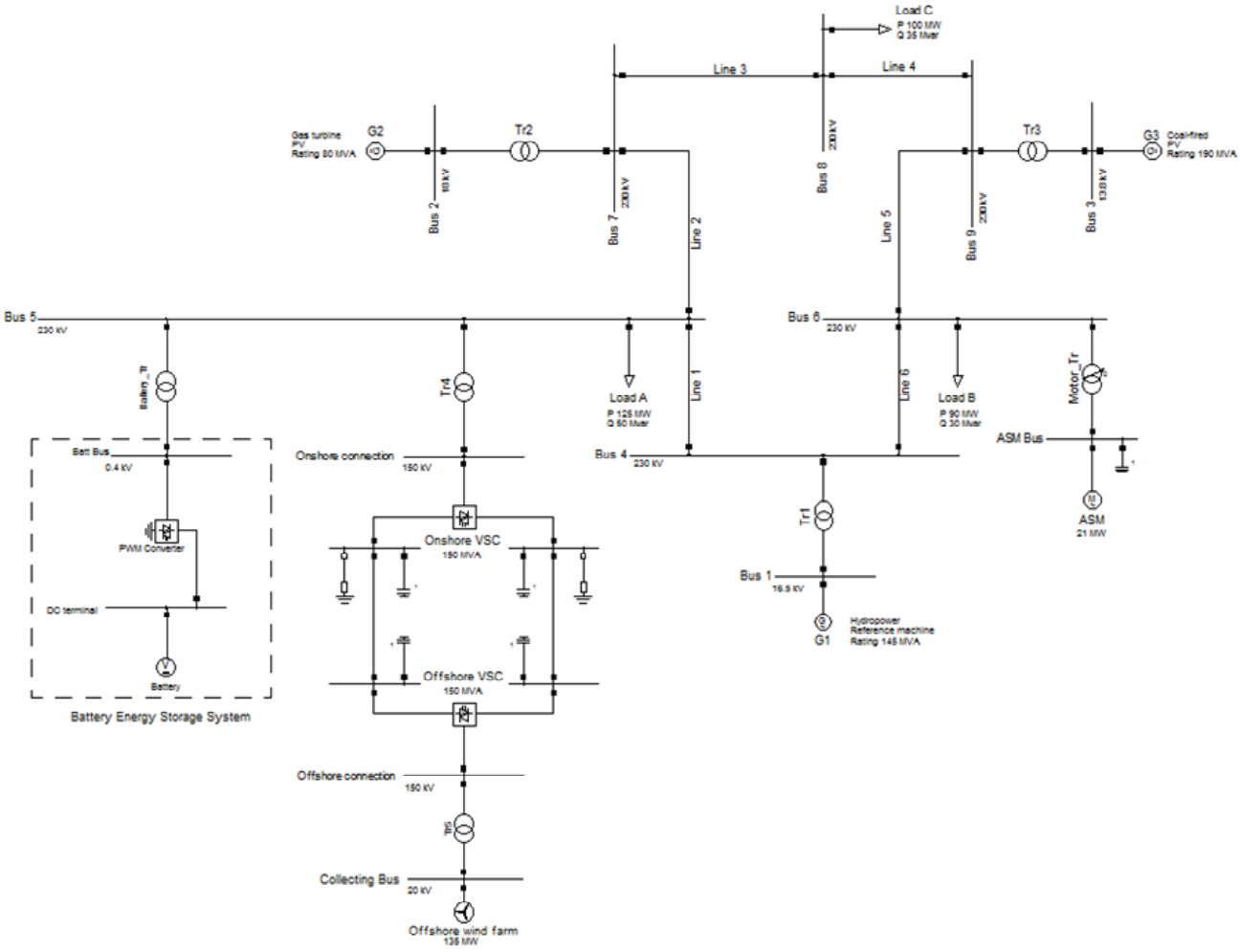

Figure 6.9 Single line diagram of power system with offshore wind farm and BESS.

The above described BESS model is implemented to the power system with high wind penetration presented in Chapter 4.4 and is connected at Bus 5 as shown in the dashed line block in

Figure 6.9. The rated capacity of the offshore wind farm and the VSC-HVDC transmission system remains the same as that in the Chapter 4. The BESS is applied not only to mitigate wind power fluctuation, but also to provide primary frequency control.

Upon time-domain simulations based on this system, a few reasonable assumptions have been made to underline the interested concerns. They are listed as follows:

1. The wind speed is considered constant during the studied short timescale.

2. It is supposed that there is no wind forecast error and the wind power fluctuation rate is controlled to be zero. Thus, the power generation of the offshore wind farm can be predicted exactly. The power order P_{odr} to the BESS can also be determined accurately.

3. Since the concerned timescale is short, the impact of BESS participating in frequency regulation on SOC of BESS is ignored in this study.

6.4 Evaluation of BESS size

The size of a BESS includes the battery MWh energy capacity and PWM converter MVA rating. With the same rating of PWM converter, a BESS of different energy capacity has different charging / discharging time [26]. However, the smoothing and frequency regulation effect of a BESS during a short time period is mainly determined by the PWM converter rating, because this short period is normally much less the charging / discharging time of the BESS . Hence, the sizing of the battery capacity is not studied as mentioned above and the detailed battery data used in this study is given in Appendix D. The rating of the PWM converter takes account of the requirements of both wind power fluctuation mitigation and frequency regulation.

For wind power smoothing applications, the dimensioning of PWM converter of a BESS is highly dependent on wind distribution data. In this study, a 20MVA converter, which is about 15% of the wind farm rated power, is supposed to be enough to suppress the wind power fluctuation to the desired level. However, during the period that the BESS uses all 20MVA to mitigate wind power fluctuation, there is no margin for the BESS to provide frequency regulation. Therefore, to provide the BESS with stable and reliable frequency regulation, a supplementary capacity is added to the PWM converter. This supplementary capacity of the converter is selected on the basis that the BESS has at least the same frequency regulation capability as that of the offshore wind farm and

VSC-HVDC, which are implemented the control strategy for frequency support as described in Chapter 5.

To find the right supplementary capacity to the BESS converter, the frequency regulation effect of a BESS with different PWM converter ratings and different droop values of its frequency controller has been studied and compared with that of offshore wind farm and VSC-HVDC. Operating at rated wind speed, the offshore wind farm employs around 10% of its available generation for frequency regulation reserve and its ancillary frequency controller has a 4% droop that is comparable to the droop setting of conventional synchronous generation units. The rating of PWM converter ranges from 5% to 10% of the rated capacity of offshore wind farm, namely from 6.75MVA to 13.5MVA. The droop value is within the range of 0.4% to 4%. The 0.4% droop corresponds to the activation of the full active power of PWM converter within 200mHz frequency deviation, whereas the 4% droop is equal to the droop setting of offshore wind farm. The frequency disturbance simulated here is caused by the generator outage of the gas turbine G2 at 1.0s by opening the switches of its main transformer. It is worth noting that while the combination of offshore wind farm and VSC-HVDC regulates the frequency deviation, the BESS is disconnected from the grid; while investigating the frequency regulation effect of the BESS, the offshore wind farm generates all its available power (without de-loading) and the frequency controllers of offshore wind farm and VSC-HVDC are not activated.

Figure 6.10 illustrates the comparison of frequency regulation effect between the BESS and the combination of offshore wind farm and VSC-HVDC. The occurring time of the nadir frequency, the nadir frequency and the post-fault steady-state frequency are presented in Figure 6.10a, b and c respectively. It can be seen from Figure 6.10 that the BESS is able to produce approximate frequency regulation effect as does the combination of offshore wind farm and VSC-HVDC, even if the rated power of its PWM converter is smaller than the power reserve of the offshore wind farm. In this scenario, the 9.45MVA converter with 0.8% droop has been enough for the BESS to provide the comparable frequency regulation capability to the combination of offshore wind farm and VSC-HVDC as shown in Figure 6.11. Figure 6.11-6.12 presents the results of system frequency, active power increase of BESS converter and onshore VSC, power generation of synchronous generators and the system spinning reserve.

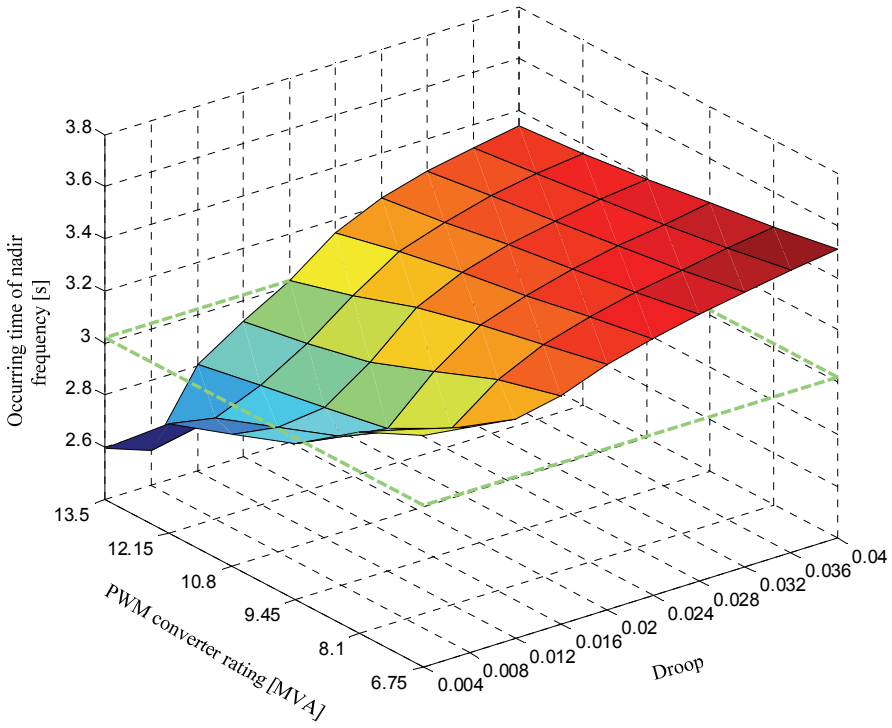

(a) Occurring time of system nadir frequency for G2 outage.

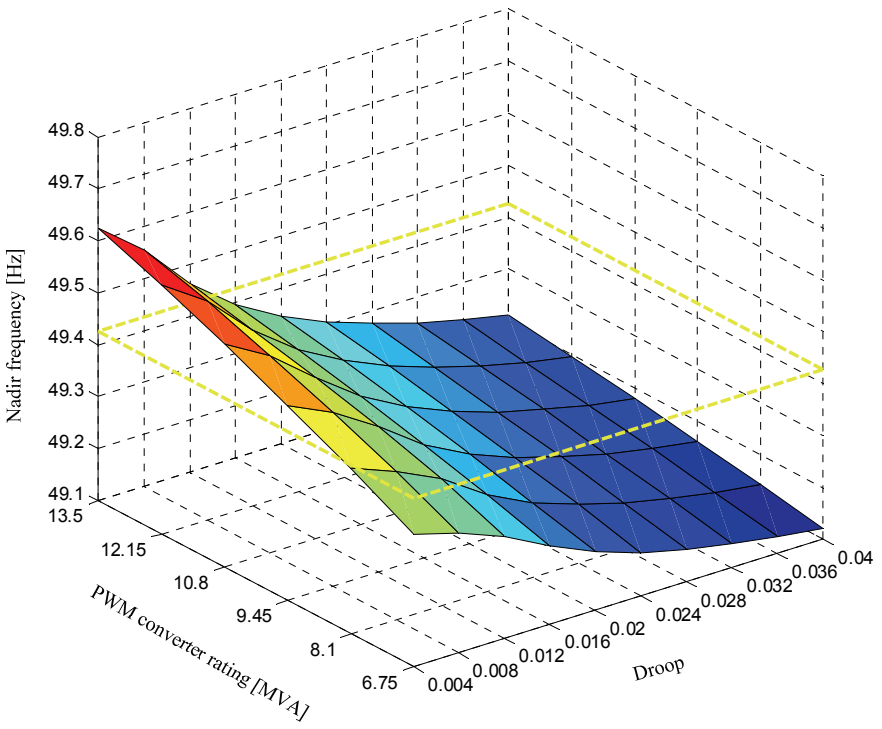

(b) System nadir frequency for G2 outage.

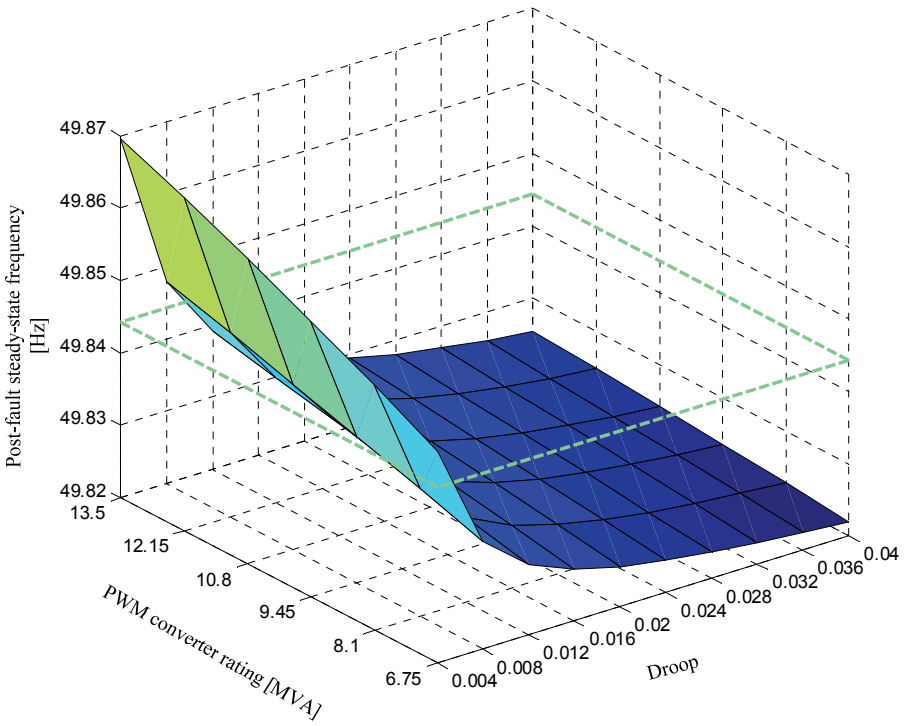

(c) System post-fault steady-state frequency for G2 outage.

Figure 6.10 Comparison of frequency regulation effect between the BESS and the combination of offshore wind farm and VSC-HVDC. The curved surfaces represent the results for the BESS with various PWM converter rating and frequency controller droop. The dashed line surfaces represent the result for the combination of offshore wind farm and VSC-HVDC.

From the view of nadir frequency and post-fault steady-state frequency, there is nearly no difference in the frequency regulation between the BESS and the combination of offshore wind farm and VSC-HVDC. However, as we can see from Figure 6.11a, the grid frequency response regulated by the BESS is smoother. Figure 6.11b compares the active power increase of onshore VSC and BESS converter to the frequency deviation caused by G2 outage. Obviously, the active power output of the BESS experiences less fluctuations. The onshore VSC injects a little bit more active power into the grid than the BESS converter during the post-fault steady-state period, but it doesn't exert much influence on the system frequency response as presented in Figure 6.11a. Additionally, using BESS to replace the primary control reserve of offshore wind farm can, on one hand, allow the offshore wind farm to operate more efficiently, and on the other hand, it also reduces the loading of conventional synchronous generating units and increases the system spinning reserve as clearly illustrated in Figure 6.12.

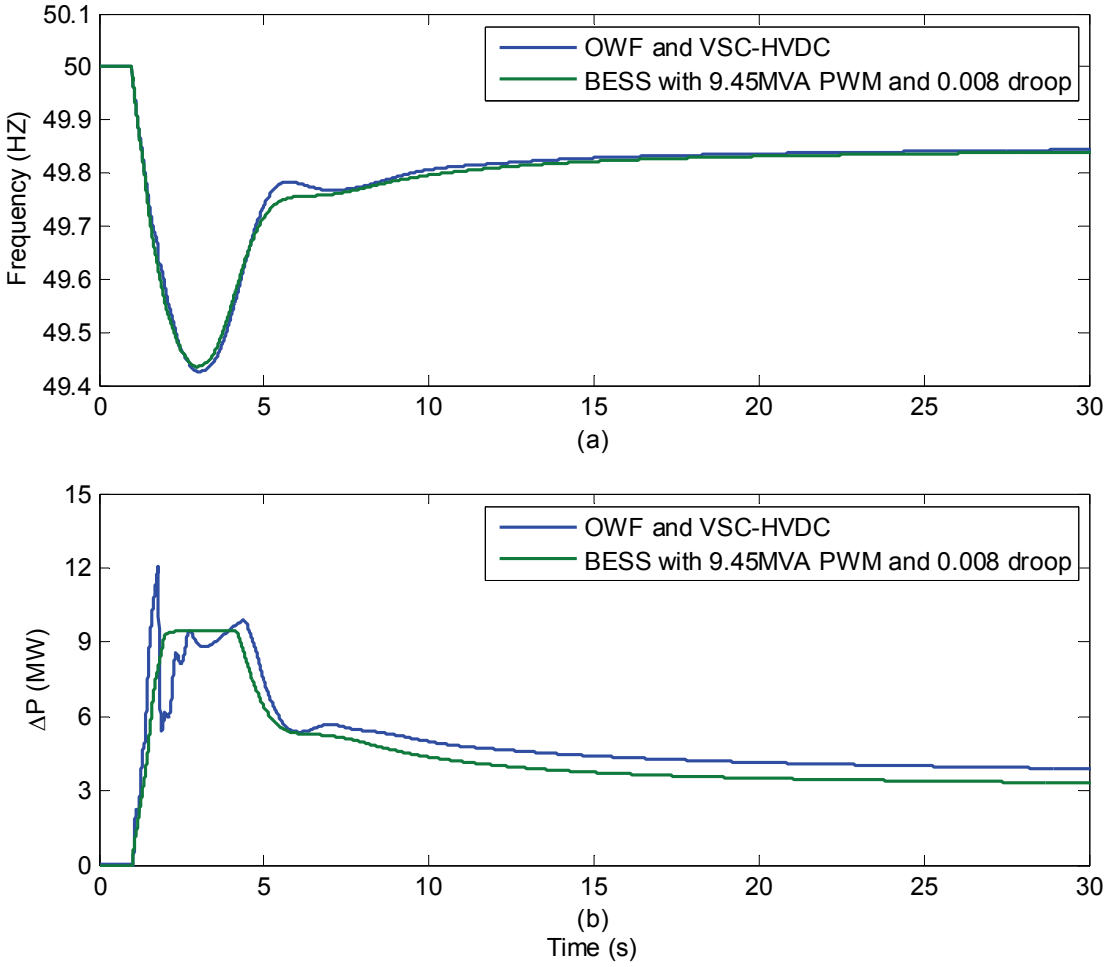

Figure 6.11 Grid frequency response and active power increase following G2 outage: (a) grid frequency response; (b) Active power increase of onshore VSC and BESS converter to the frequency deviation.

Therefore, based on the analysis above, a supplementary capacity of 9.45MVA is selected for the BESS system to fulfil frequency regulation purpose in this study, whereas the offshore wind farm is freed from de-loading operations. In other words, the total capacity of PWM converter is 29.45MVA and is used for the BESS to meet the demands for wind power fluctuation mitigation and frequency regulation. However, because of the uncertainty of frequency disturbances, the 9.45MVA of PWM converter must be spared for the frequency regulation at all times. In other words, the maximum capacity of BESS converter that is used for wind power fluctuation mitigation is 20MVA. Moreover, since the BESS is not always charging / discharging at 20MW, it is possible to use more than 9.45MVA of its converter to regulate grid frequency deviations.

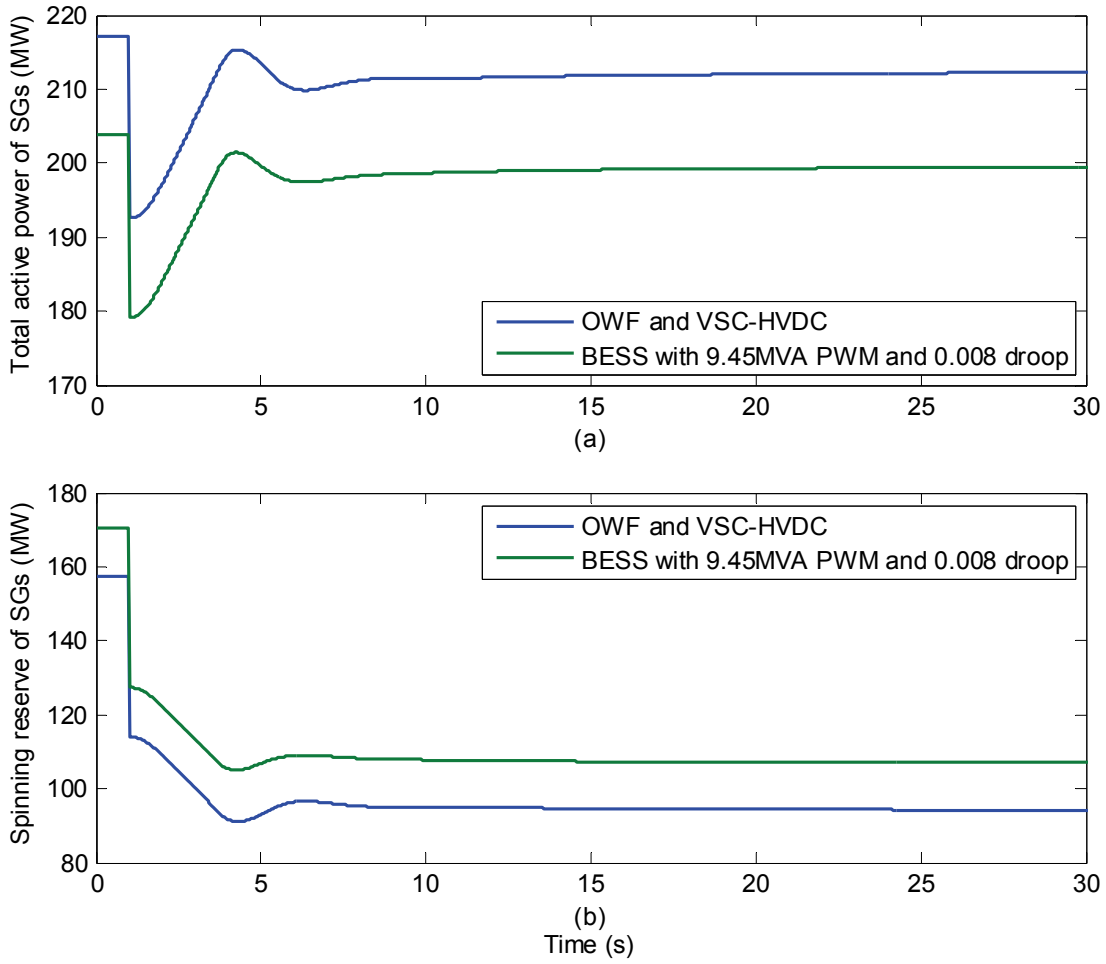

Figure 6.12 Variation of total active power and spinning reserve of conventional SGs following G2 outage: (a) Total active power of SGs; (b) Spinning reserve of SGs.

6.5 Evaluation of Frequency Response Capability of BESS

The grid performance improvement of applying BESS is evaluated regarding frequency stability support. The BESS is used to stabilize the system frequency in cooperation with smoothing wind power fluctuation, whereas the offshore wind farm and VSC-HVDC don't contribute to primary frequency control any more. The simulation studies are carried out on DIgSILENT for the cases listed in Table 6.1. During the pro-fault period, the combined active power output of BESS and offshore wind farm is controlled to be 109.5MW that is initially about 80% of the rated capacity of offshore wind farm. Therefore, the BESS is in various charging / discharging states in terms of the active power generation of offshore wind farm. As aforementioned, the wind forecast error is not taken into account. For comparison, the last case studies the scenario that the BESS is not equipped

and offshore wind farm, which operates in a 20% de-loading mode, also generates 109.5MW.

For studying the frequency behavior enhancement by BESS, the outage of the power plant with the fast gas turbine G2 is simulated at 1.0s by switching off its main transformer. That causes a sudden grid power imbalance and an under-run frequency. Figure 6.13 – 6.15 present the system response to the G2 outage with BESS of various charging / discharging states.

TABLE 6.1

Study cases

	Active power output (MW)		
	BESS (PWM 29.45MVA)	**Offshore wind farm**	**Combined**
Case1	-20 (charging)	129.5	109.5
Case2	-10 (charging)	119.5	109.5
Case3	0	109.5	109.5
Case4	10 (discharging)	99.5	109.5
Case5	20 (discharging)	89.5	109.5
Case6	N/A	109.5 (20% de-loading)	109.5

Figure 6.13 shows the grid frequency response and the combined active power output of onshore VSC and BESS, respectively. It can be seen that owing to the proposed power management approach for multi-task, the BESS is able to provide enhanced primary frequency control. The extent of the enhancement depends on the charging / discharging state of the BESS, and the converter capacity used for mitigating wind power fluctuation. By using BESS to replace the primary reserve of offshore wind farm, the system even has a stronger ability to regulate frequency deviation. Apparently, the system frequency response in Figure 6.13a is better when the BESS is in charging states compared with in discharging states. From Figure 6.13b, we can see that the increase of the BESS's charging power (or the decrease of the BESS's discharging power) improves the combined active power infeed to the system. In charging states, the BESS absorbs active power from the grid, but it stops this power absorption during the frequency under-run. In other words, the BESS in charging states not only provides power reserve, but decreases the power consumption of the grid that also improves the frequency response.

Figure 6.14 presents the active power output of the BESS and the amount of its variation for the given contingency. In the case (Case5) that the BESS is discharging 20MW for smoothing wind power generation before the contingency, the maximum primary frequency reserve is only 9.45MW. However, with the decrease of the discharging power, the BESS then has more potential power reserve left for frequency regulation. Table 6.2 lists the potential primary frequency reserve of the BESS for the given five cases.

With the same droop setting (0.8%), it is clear that the larger the discharging power of BESS (from Case1 to Case5), the less the power reserve of BESS for primary frequency control. In other words, the BESS is able to provide more frequency reserve if it is in charging states. The more primary frequency reserve that the BESS is able to provide, of course, also means that the less that the conventional power plants need to supply as shown in Figure 6.15.

TABLE 6.2

Primary control reserve of BESS in different charging/discharging states

	BESS with 29.45MVA converter	
	Smoothing power (MW)	**Potential primary control reserve (MW)**
Case1	-20 (charging)	49.45
Case2	-10 (charging)	39.45
Case3	0	29.45
Case4	10 (discharging)	19.45
Case5	20 (discharging)	9.45

6.6 Summary

To a power system with high wind penetration, the control of system frequency and mitigation of power fluctuation become increasingly important. Forcing wind turbines to operate in a de-loading way and applying energy storage systems are both technically feasible to increase the system frequency reserve and enhance the system frequency response.

In this chapter, a PWM converter-interfaced BESS is applied to the power system with a VSC-HVDC connected large offshore wind farm. The BESS is used to provide primary frequency control

in cooperation with wind power fluctuation mitigation.

The converter rating of the BESS is based on the requirement of wind power fluctuation mitigation and the consideration that the BESS is able to supply frequency reserve and regulation at all times to a certain extent. This extent is determined, in this study, to be comparable to that provided by offshore wind farm and VSC-HVDC implemented the coordinated control strategy described in Chapter 5. Accordingly, a new power management strategy is also proposed to adjust BESS's frequency reserve based on its fulfilment of smoothing wind power fluctuation.

The simulation studies are conducted with respect to various charging and discharging state of the BESS. The results show that the BESS with the suggested MW capacity and with the proposed control has great potential to enhance the system frequency response on the basis of wind power fluctuation mitigation.

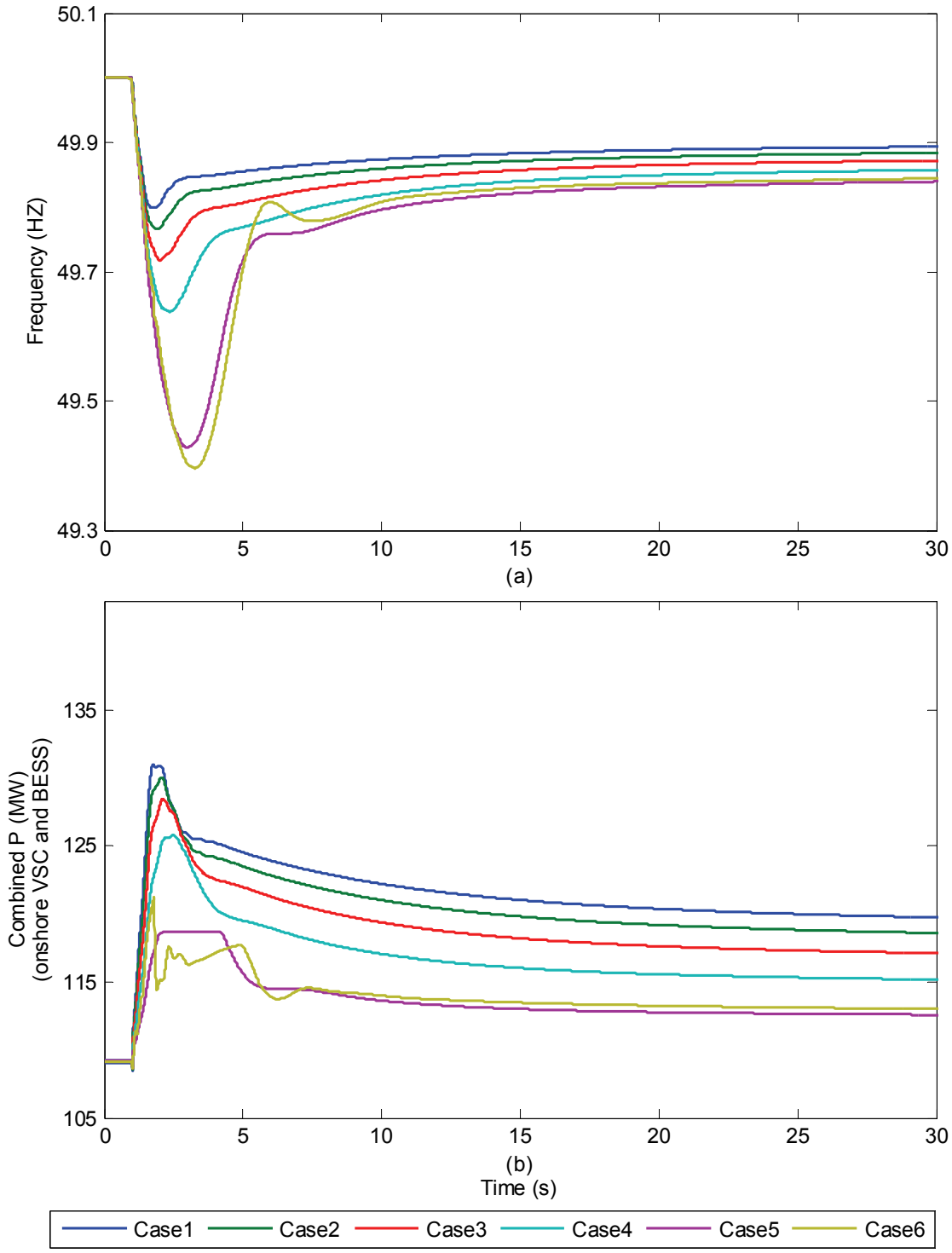

Figure 6.13 System frequency response and the combined active power output of onshore VSC and BESS during the frequency under-run: (a) Frequency response; (b) Combined active power output of onshore VSC and BESS

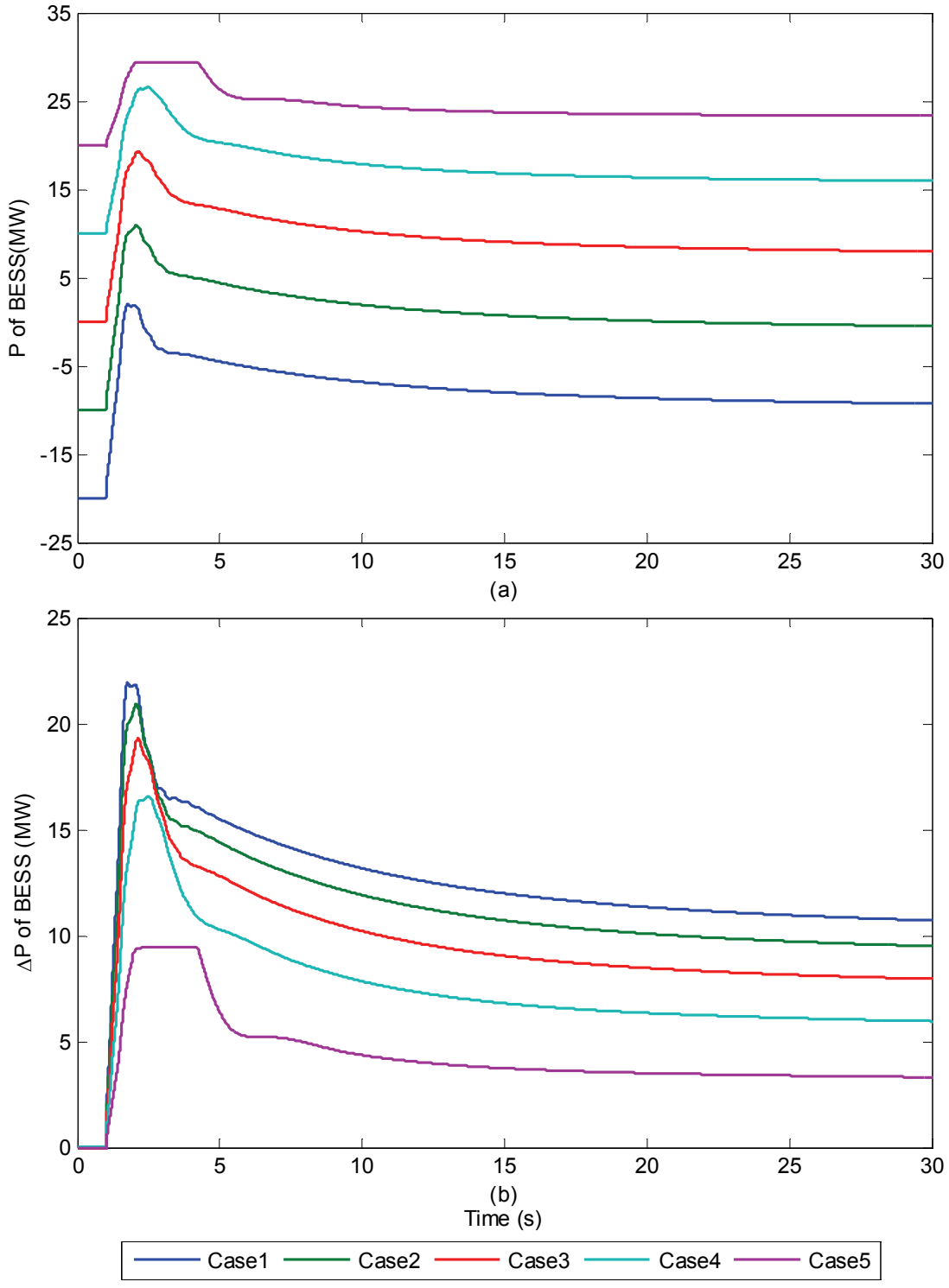

Figure 6.14 Active power response of BESS to the G2 outage: (a) Active power output; (b) Active power increment.

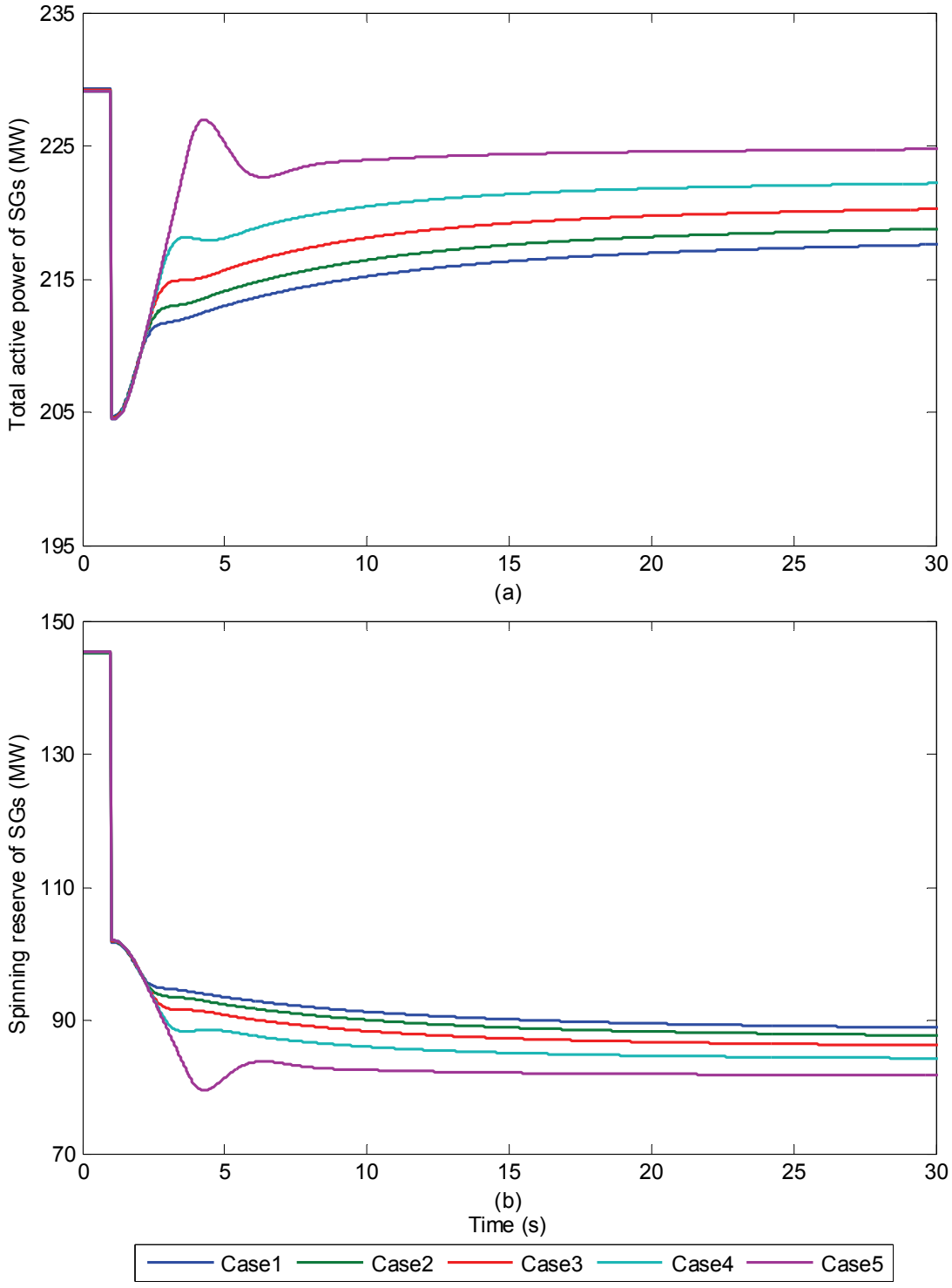

Figure 6.15 Comparison of total active power and spinning reserve of conventional SGs for the given cases: (a) Total active power of SGs; (b) Spinning reserve of SGs.

Bibliography

[1] M. Swierczynski, R. Teodorescu, C. N. Rasmussen, P. Rodriguez, and H. Vikelgaard, "Overview of the energy storage systems for wind power integration enhancement," in *IEEE International Symposium on Industrial Electronics (ISIE),* pp. 3749-3756, July 2010.

[2] M. Ghofrani, A. Arabali, M. Etezadi-Amoli, and M. S. Fadali, "Energy Storage Application for Performance Enhancement of Wind Integration," *IEEE Transactions on Power Systems,* vol. 28, no. 4, pp. 4803-4811, 2013.

[3] T. Hennessy and M. Kuntz, "The multiple benefits of integrating electricity storage with wind energy," in *IEEE Power Engineering Society General Meeting,* vol. 2, pp. 1952-1954, June 2005.

[4] C. N. Rasmussen, "Improving wind power quality with energy storage," in *IEEE PES/IAS Conference on Sustainable Alternative Energy (SAE)*, pp. 1-7, Sept. 2009.

[5] J. V. Paatero and P. D. Lund, "Effect of energy storage on variations in wind power," *Wind Energy,* vol. 8, no. 4, pp. 421-441, 2005.

[6] K. C. Divya and J. Østergaard, "Battery energy storage technology for power systems - An overview," *Electric Power Systems Research,* vol. 79, no. 4, pp. 511-520, 2009.

[7] J. P. Barton and D. G. Infield, "Energy storage and its use with intermittent renewable energy," *IEEE Transactions on Energy Conversion,* vol. 19, no. 2, pp. 441-448, 2004.

[8] J. Eyer and G. Corey, "Energy storage for the electricity grid: benefits and market potentials assessment guide", Sandia National Labs, SAND2010-0815, Feb. 2010. [Online]. Available: http://www.sandia.gov/ess/publications/SAND2010-0815.pdf

[9] P. F. Ribeiro, B. K. Johnson, M. L. Crow, A. Arsoy, and Y. Liu, "Energy storage systems for advanced power applications," *Proceedings of the IEEE,* vol. 89, no. 12, pp. 1744-1756, 2001.

[10] J. Zeng, B. Zhang, C. Mao, and Y. Wang, "Use of Battery Energy Storage System to Improve the Power Quality and Stability of Wind Farms," in *International Conference on*

Power System Technology, pp. 1-6, Oct. 2006.

[11] Q. Jiang, Y. Gong, and H. Wang, "A Battery Energy Storage System Dual-Layer Control Strategy for Mitigating Wind Farm Fluctuations," *IEEE Transactions on Power Systems,* vol. 28, no. 3, pp. 3263-3273, 2013.

[12] S. Teleke, M. E. Baran, S. Bhattacharya, and A. Q. Huang, "Optimal Control of Battery Energy Storage for Wind Farm Dispatching," *IEEE Transactions on Energy Conversion,* vol. 25, no. 3, pp. 787-794, 2010.

[13] S. Dutta and T. J. Overbye, "Optimal storage scheduling for minimizing schedule deviations considering variability of generated wind power," in *IEEE Power Systems Conference and Exposition (PSCE),* pp. 1-7, March 2011.

[14] T. Tanabe, T. Sato, R. Tanikawa, I. Aoki, T. Funabashi, and R. Yokoyama, "Generation scheduling for wind power generation by storage battery system and meteorological forecast," in *IEEE Power and Energy Society General Meeting - Conversion and Delivery of Electrical Energy in the 21st Century,* pp. 1-7, July 2008.

[15] S. W. Mohod and M. V. Aware, "A STATCOM-Control Scheme for Grid Connected Wind Energy System for Power Quality Improvement," *IEEE Systems Journal,* vol. 4, no. 3, pp. 346-352, 2010.

[16] A. Arulampalam, M. Barnes, N. Jenkins, and J. B. Ekanayake, "Power quality and stability improvement of a wind farm using STATCOM supported with hybrid battery energy storage," *IEE Proceedings-Generation, Transmission and Distribution,* vol. 153, no. 6, pp. 701-710, 2006.

[17] Z. M. Salameh, M. A. Casacca, and W. A. Lynch, "A mathematical model for lead-acid batteries," *IEEE Transactions on Energy Conversion,* vol. 7, no. 1, pp. 93-98, 1992.

[18] M. Ceraolo, "New dynamical models of lead-acid batteries," *IEEE Transactions on Power Systems,* vol. 15, no. 4, pp. 1184-1190, 2000.

[19] N. K. Medora and A. Kusko, "Dynamic Battery Modeling of Lead-Acid Batteries using Manufacturers' Data," in *Twenty-Seventh International Telecommunications Conference,* pp. 227-232, Sept. 2005.

[20] M. A. Casacca and Z. M. Salameh, "Determination of lead-acid battery capacity via mathematical modeling techniques," *IEEE Transactions on Energy Conversion,* vol. 7, no. 3, pp. 442-446, 1992.

[21] S. Barsali and M. Ceraolo, "Dynamical Models of Lead-Acid Batteries: Implementation Issues," *IEEE Power Engineering Review,* vol. 22, no. 2, pp. 63-63, 2002.

[22] Application Manual: Battery Energy Storing Systems in PowerFactory, DIgSILENT GmbH, Nov. 2010.

[23] Q. Jiang and H. Wang, "Two-Time-Scale Coordination Control for a Battery Energy Storage System to Mitigate Wind Power Fluctuations," *IEEE Transactions on Energy Conversion,* vol. 28, no. 1, pp. 52-61, 2013.

[24] K. Yoshimoto, T. Nanahara, and G. Koshimizu, "New Control Method for Regulating State-of- Charge of a Battery in Hybrid Wind Power/Battery Energy Storage System," in *IEEE Power Systems Conference and Exposition,* pp. 1244-1251, Nov. 2006.

[25] X. Li, D. Hui, L. Wu, and X. Lai, "Control strategy of battery state of charge for wind/battery hybrid power system," in *IEEE International Symposium on Industrial Electronics (ISIE)*, pp. 2723-2726, July 2010.

[26] C.F. Lu, C.C. Liu, and C.J. Wu, "Effect of battery energy storage system on load frequency control considering governor deadband and generation rate constraint," *IEEE Transactions on Energy Conversion,* vol. 10, no. 3 pp. 555-561, 1995.

Chapter 7

Conclusions and Future Work

7.1 Conclusions

With the increasing demand for renewable energy, offshore wind power has been paid significant attention in recent years owing to its relatively stable wind condition, broad installation space, and plenty of reserve and so on. The development of offshore wind farms has been on the agenda of many European countries, especially. The capacity of offshore wind farms could be up to hundreds of MWs. Together with the fast growing wind power penetration level, the integration of large-scale offshore wind farms would seriously influence the operation and stability of the power grid and thus bring technical challenges in many aspects.

This dissertation, as a consequence, has addressed some of the key technical issues with grid integration of large-scale offshore wind farms based on VSC-HVDC transmission system, with regarding mainly to voltage-reactive power regulation and frequency-active power regulation. The impact on power system stability of integrating large-scale offshore wind farms via VSC-HVDC transmission has been firstly investigated in consideration of the voltage support capability of VSC-HVDC. An up-scaling method for VSC-HVDC based on trajectory sensitivity analysis is then proposed for enhancing the system voltage stability. For improving system frequency response, a coordinated control strategy is then proposed to enable both offshore wind farm and VSC-HVDC to contribute to frequency regulation. Finally, the application of BESS to power systems with high wind penetration is investigated and a control approach is developed to allow the BESS to fulfil multitask.

The impact study of VSC-HVDC based offshore wind integration has been carried out on a transmission grid focusing on voltage stability and transient stability of the grid with different wind penetration levels. The impact on the grid steady-state voltage stability is explored based on the analysis of P-V curves that are drawn under two wind power injection conditions: unity power factor wind power supply and rated PCC voltage wind power supply. It can be deduced from the P-V curves that the grid voltages experience a decrease with an increase in wind power in general. However, with the rated-PCC-voltage wind power supply, the wind power penetration limit can be

greatly enhanced compared to that with unity power factor wind power supply for the given power grid. It proves that the VSC-HVDC plays a very important role in wind power transfer owing to its reactive power support capability. The dynamic voltage study demonstrates that the bus voltage is higher with higher wind penetration during grid disturbances. The main reason is that the implemented control strategy of the onshore VSC and the fact that higher wind injection brings higher rating converters that can provide more reactive power support. For the studied transmission grid, the transient angle stability generally becomes worsen with higher wind penetration due to the change of power flow. However, owing to the control strategy of VSC-HVDC during grid faults, the VSC-HVDC is able to limit its active power output and, at the same time, enhance its reactive current output when it detects grid voltage faults. Therefore, an improvement in transient angle stability has actually been achieved when the given fault occurs at the line close to PCC.

Owing to the independent active and reactive power control of the VSC, VSC-HVDC is able to provide reactive power / voltage support during grid voltage disturbances. The voltage support capability of VSC-HVDC depends on both its VSC capacity and the corresponding control schemes. TSA is a technique that can effectively complement time domain simulation and provide valuable insights into the behavior of the dynamic system in accordance with the changes in parameters and operating conditions. With respect to the studied voltage support strategies of VSC-HVDC, a TSA-based two-stage design method is developed to identify the minimum onshore VSC capacity with which VSC-HVDC can provide enough support for stabilizing the grid voltage following a grid disturbance. By using the proposed TSA-based two-stage method, the design is accomplished by numerical calculations based on only a few time domain simulations. The two-stage approximation strategy also improves the accuracy of the TSA-based linear approximation. Both reactive power-based and voltage-based trajectory sensitivities are applied to the design procedures. And the effectiveness of the proposed method is finally verified by results based on time-domain simulations.

Besides the voltage support capability, VSC-HVDC also has the potential to contribute to system frequency regulation. A coordinated frequency control scheme is developed not only to reduce the responding latency of offshore wind farms effectively but also to allow VSC-HVDC to contribute to system frequency regulation by adjusting its DC-link voltage. The adaptive control of the DC-link voltage enables the DC capacitors of VSC-HVDC to release/absorb energy to regulate the frequency deviation. To further enhance the system frequency response, the frequency support from VSC-HVDC is also finely coordinated with that from offshore wind farm according to the latency of

offshore wind farm responding to onshore grid frequency excursion. Through simulations and analysis, it is shown that the proposed control strategy allows the VSC-HVDC to provide effective inertial response without any extra investment. The coordination of the frequency control of the VSC-HVDC and wind turbines obtains a significantly enhanced frequency response for the studied power system.

To improve the stability of power systems with high wind penetration, one of the effective solutions is the application of energy storage devices. Therefore, a PWM converter-interfaced BESS is applied to the power system integrated with a large offshore wind farm via VSC-HVDC link. The BESS is used to provide primary frequency control in cooperation with wind power fluctuation mitigation. A new converter rating evaluation approach as well as a new power management strategy is proposed to enable the BESS to enhance the system frequency response on the basis of wind power fluctuation mitigation. The simulation studies are conducted with respect to various charging and discharging state of the BESS. The results show that the BESS with the suggested MW capacity and with the proposed control has great potential to enhance the system frequency response on the basis of wind power fluctuation mitigation.

7.2 Main contributions

The major contributions of this thesis are as follows.

- An impact study of grid integration of large-scale offshore wind farm via VSC-HVDC has been carried out. Though the impact greatly depends on the inherent characteristics of the studied power system, the study shows that owing to the voltage support capability, the application of VSC-HVDC link can benefit offshore wind farm integration by improving the penetration level, enhancing dynamic voltage stability and transient angle stability.

- A TSA-based two-stage design method is developed to identify the minimum onshore VSC capacity with which VSC-HVDC can provide enough support for stabilizing the PCC voltage following a grid disturbance for the applied control strategies. The proposed approach improves the accuracy of the TSA-based linear approximation and avoids large number of time domain simulations.

- A coordinated control strategy has been proposed to enable VSC-HVDC to provide

short-term frequency regulation by partially charging / discharging of its DC capacitors and consequently to enhance the system frequency response together with the regulation of offshore wind turbines.

- A new converter rating evaluation approach as well as a new power management strategy is proposed to enable the BESS to enhance the system frequency response on the basis of wind power fluctuation mitigation.

7.3 Future work

Grid integration of offshore wind farms involves many challenges in both the technical area and the economic area. Based on the achievement and findings of this thesis work, there are several future research directions suggested in the area of offshore wind power integration as follows.

- The impact study could be further investigated considering the variability of wind power and load based on probabilistic assessment.

- The application of STATCOM is another effective measure to improve the system voltage stability. The optimal sizing and placing of STATCOM devices could be studied using the proposed TSA-based technique.

- When the grid frequency restores to the normal state, offshore wind turbines and VSC-HVDC should stop providing frequency regulation. Therefore, the withdrawal of the frequency control of offshore wind turbines and VSC-HVDC needs to be further studied to avoid the second frequency deviation caused by this withdrawal.

- The VSC-interfaced BESS has the potential to provide reactive power compensation during grid disturbances. The coordination of voltage support between VSC-HVDC and BESS is attractive for further study.

- Performing multitask means more frequent charging/discharging process to the BESS. The impact on BESS SOC and lifetime needs to be investigated.

Appendix A

Control frames of VSC-HVDC and FCWT

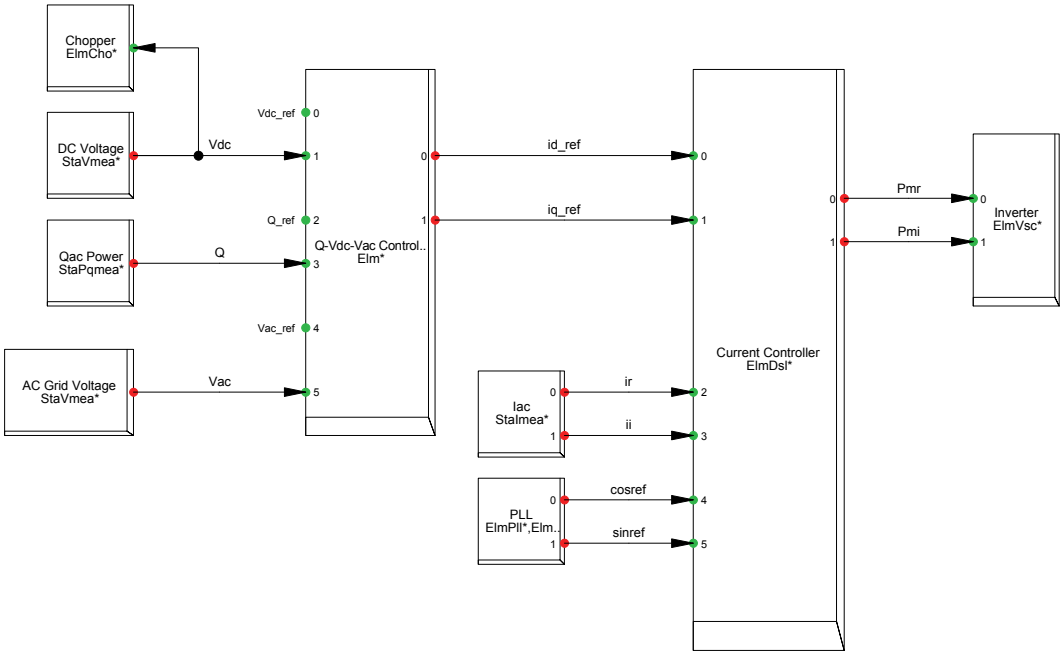

Figure A.1 Control frame of VSC-HVDC inverter

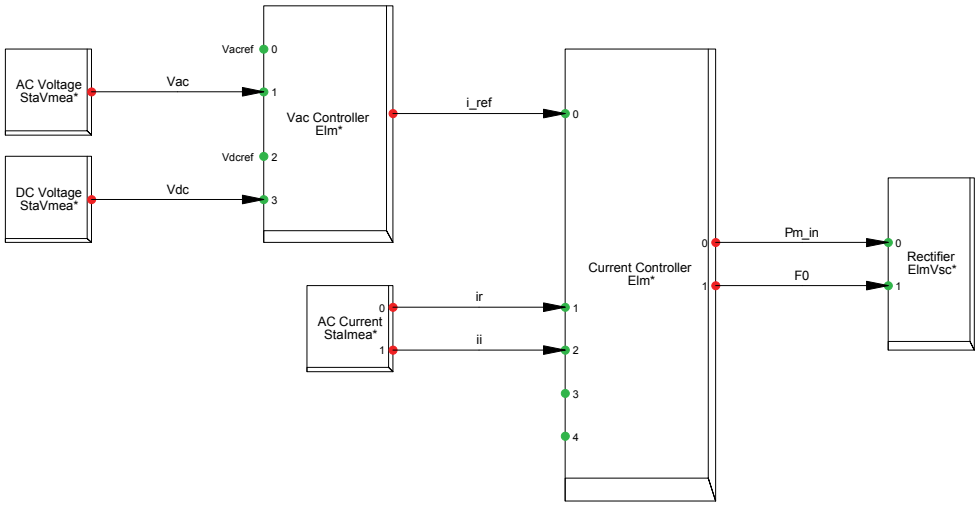

Figure A.2 Control frame of VSC-HVDC rectifier

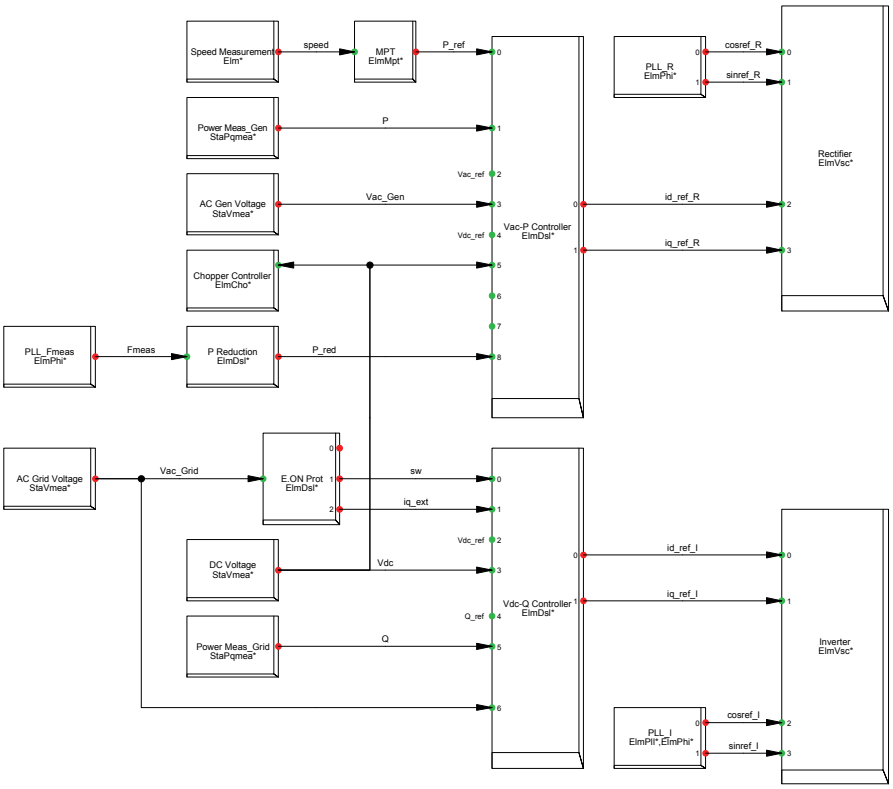

Figure A.3 FCWT Converter control frame

Appendix B

Relevant data of the transmission grid applied in Chapter 3

TABLE B.1

Synchronous generator dynamic parameters

Gen No.	H (s)	$x_l(pu)$	$x_d(pu)$	$x_q(pu)$	$x'_d\,(pu)$	$x'_q\,(pu)$	$x''_d\,(pu)$	$x''_q(pu)$	$T'_{d0}(s)$	$T'_{q0}(s)$
G1	999	0.15	2	2	0.3	0.7	0.2	0.2	6.6	2.5
G2	5	0.15	2.43	2.33	0.307	0.6	0.2	0.2	7.5	2.5
G3	5	0.15	2.1	2	0.365	0.7	0.2	0.2	7.4	2.5
G4	5	0.15	2.09	2.04	0.254	0.39	0.2	0.2	6.6	1.3

TABLE B.2

Synchronous generator load flow settings

Gen No.	S (MVA)	Load Flow	
		P (MW)	Voltage (pu)
G1	2500	Slack bus	1.02
G2	750	650	1.03
G3	1400	650	1.025
G4	1500	1250	1.03

TABLE B.3

Load settings

Load No.	Bus No.	Load Flow	
		P (MW)	Q (Mvar)
Load1	7	100	-50
Load2	10	330	300
Load3	9	2750	1700
Load4	9	-100	0
Load5	8	650	100

TABLE B.4

Parameters of AVRs

	AVR1	AVR2	AVR3	AVR4
Tf (s)	0.0235	0.04	0.04	0.04
K (pu)	150	40	140	110
T1 (s)	5.6	4	12.09	8
T2 (s)	2.7	1.2	1.37	2
T3 (s)	0.06	0.02	0.02	0.02
T4 (s)	0.19	0.1	0.0565	0.05
Vmin (pu)	-3.3	-6.1	-4.75	0
Vmax (pu)	4.125	6.1	5.25	0
Efdmin (pu)	-3.3	-4.1	-4.75	5
Efdmax (pu)	4.125	5.3	5.25	5

TABLE B.5

Parameters of GAST governors

	GOV1	GOV2	GOV3	GOV4
R (pu)	0.04	0.06	0.047	0.055
T1 (s)	0.4	0.4	0.4	0.4
T2 (s)	0.1	0.1	0.1	0.1
T3 (s)	3	3	3	3
AT (pu)	1	1	1	1
Kt (pu)	2	2	2	2
Dturb (pu)	0.001	0.001	0.001	0.001
Vmin (pu)	0	0	0	0
Vmax (pu)	1	1	1	1

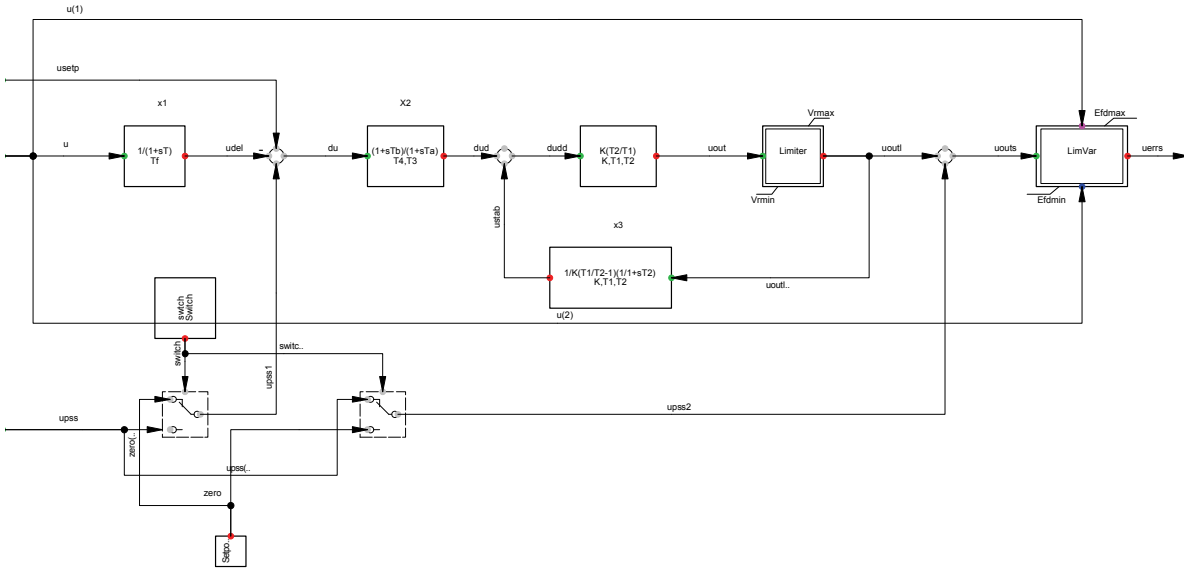

Figure B.1 Generic BBSEX1 AVR model

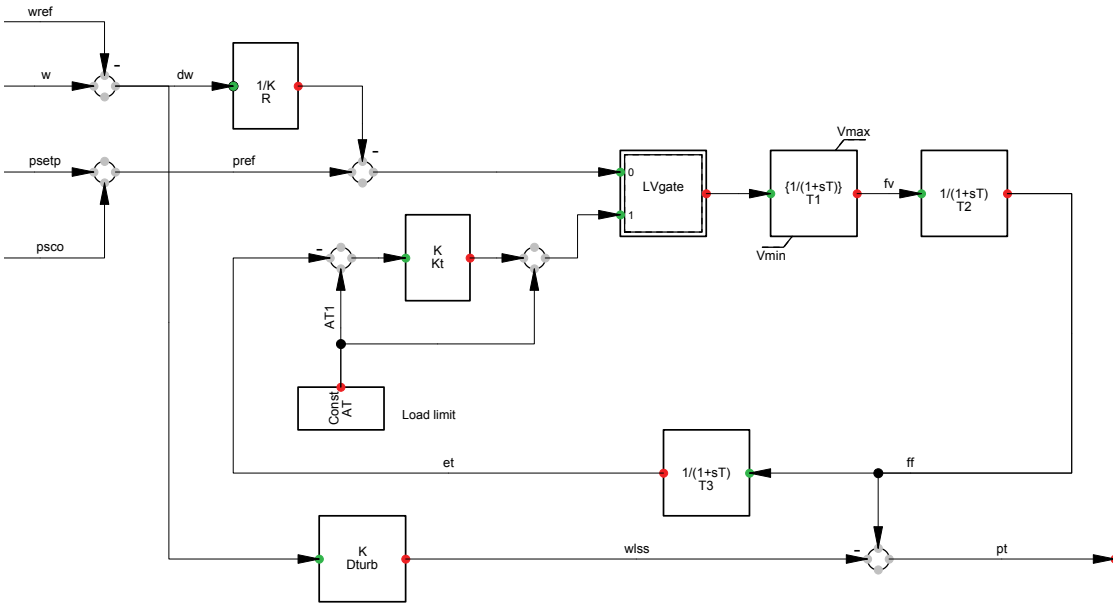

Figure B.2 Generic GAST governor model

Appendix C

Relevant data of the transmission grid applied in Chapter 4, 5 and 6

TABLE C.1

Synchronous generator dynamic parameters

Gen No.	$H\ (s)$	$x_l(pu)$	$x_d(pu)$	$x_q(pu)$	$x'_d\ (pu)$	$x'_q\ (pu)$	$x''_d\ (pu)$	$x''_q(pu)$	$T'_d(s)$	$T'_q(s)$
G1	9.55	0.0309	0.36	0.24	0.15	-	0.1	0.1	3.73	-
G2	4.165	0.0103	1.72	1.66	0.23	0.378	0.2	0.2	0.8	0.12
G3	2.765	0.13477	1.68	1.61	0.23	0.32	0.2	0.2	0.806	0.12

TABLE C.2

Synchronous generator load flow settings

Gen No.	S (MVA)	Load Flow (Chapter 4 & 5 / Chapter 6)	
		P (MW)	Voltage (pu)
G1	145	Slack bus	1.025 / 1.025
G2	80	55 / 24.6	1.025 / 1.025
G3	190	140 / 109.6	1.025 / 1.025

TABLE C.3

Load settings

Load No.	Bus No.	Load Flow	
		P (MW)	Q (Mvar)
Load A	5	125	50
Load B	6	90	30
Load C	8	100	35

	Rotor	S (KVA)	Power factor	*Rated Speed (rpm)*	*H (s)*	$x_s(pu)$	$x_m(pu)$
ASM	Double Cage	3×9063	0.91	1492	2.252	0.01	0.01

TABLE C.4

Parameters of AVRs

EXAC1 (G1)		IEEET1 (G2 & G3)	
Tr (s)	0.025	Tr (s)	0.028
Tb (s)	1	Ka (pu)	175
Tc (s)	1	Ta (s)	0.03
Ka (pu)	200	Ke (pu)	1
Ta (s)	0.02	Te (s)	0.266
Te (s)	0.35	Kf (pu)	0.0025
Kf (pu)	0.0069	Tf (s)	1.5
Tf (s)	1	E1 (pu)	4.5
Kc (pu)	1	Se1 (pu)	1.5
Kd (pu)	0.2	E2 (pu)	6
E1 (pu)	3.13	Se2 (pu)	2.46
Se1 (pu)	1.73	Vmin (pu)	-12
E2 (pu)	4.18	Vmax (pu)	12
Se2 (pu)	4		
Ke (pu)	1		
Vmin (pu)	-36.3		
Vmax (pu)	41.7		

TABLE C.5

Parameters of governors

HYGOV (G1)		GAST (G2)		IEEEG1 (G3)	
r (pu)	0.5	R (pu)	0.047	K (pu)	25
Tr (s)	8.408	T1 (s)	0.4	T1 (s)	0.25
Tf (s)	0.05	T2 (s)	0.1	T2 (s)	0
Tg (s)	0.5	T3 (s)	3	T3 (s)	0.1
Tw (s)	0.496	AT (pu)	1	K1 (pu)	0.3
At (pu)	1.15	Kt (pu)	2	K2 (pu)	0
Pturb (pu)	0	Pturb (pu)	0	T5 (s)	10
Dturb (pu)	0	Dturb (pu)	0	K3 (pu)	0.4
qnl (pu)	0.08	Vmin (pu)	0	K4 (pu)	0
R (pu)	0.04	Vmax (pu)	1	T6 (s)	0.4
Gmin (pu)	0			K5 (pu)	0.3
Velm (pu)	0.2			K6 (pu)	0

Gmax (pu)	1			T4 (s)	0.3
				T7 (s)	0
				K7 (pu)	0
				K8 (pu)	0
				Uc (pu/s)	-0.1
				Pmin (pu)	0.3
				Uo (pu/s)	0.1
				Pmax (pu)	1

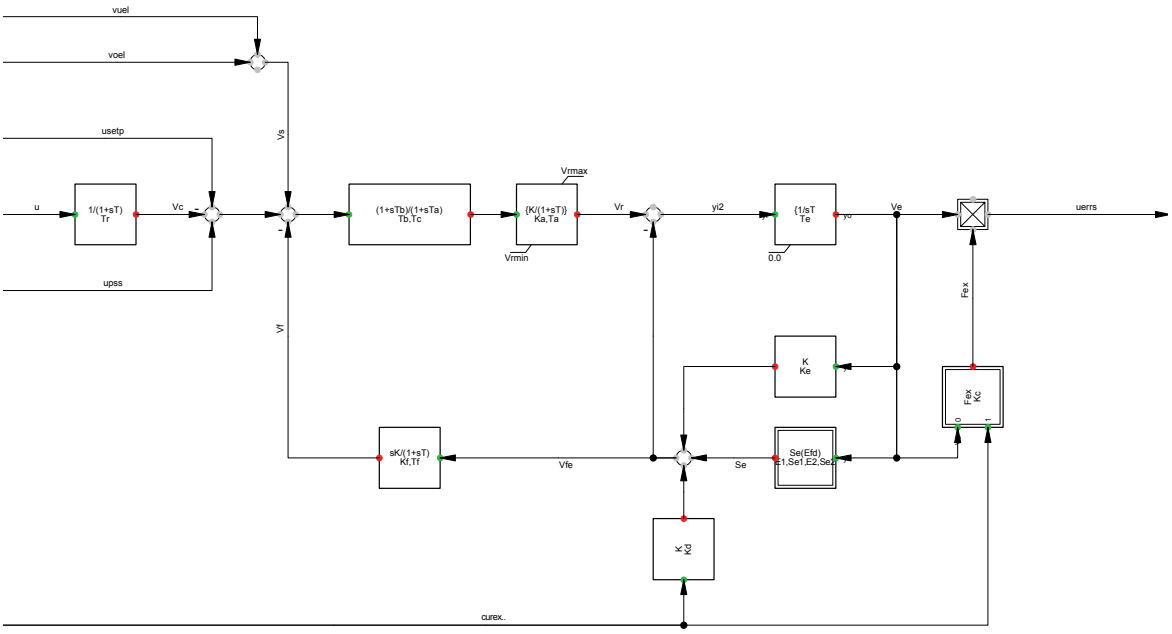

Figure C.1 Generic EEAC1 AVR model

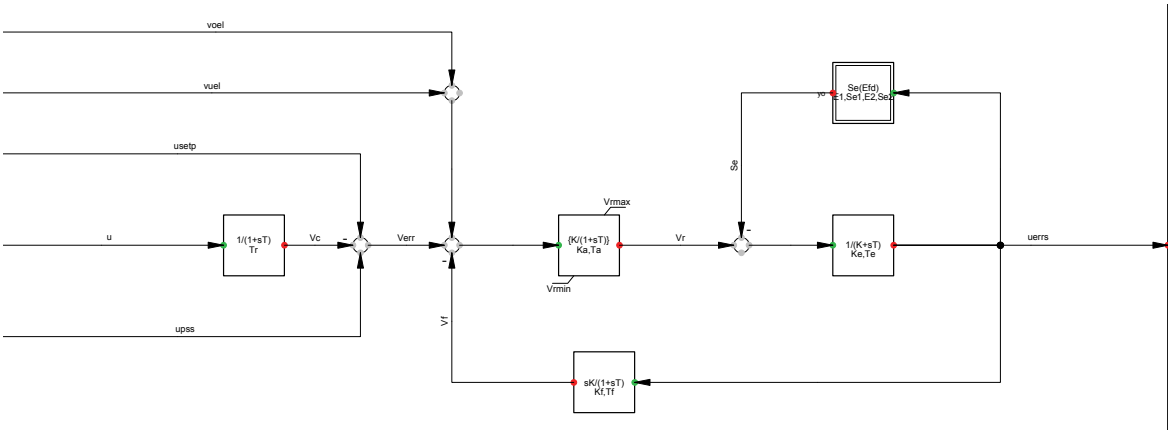

Figure C.2 Generic IEEET1 AVR model

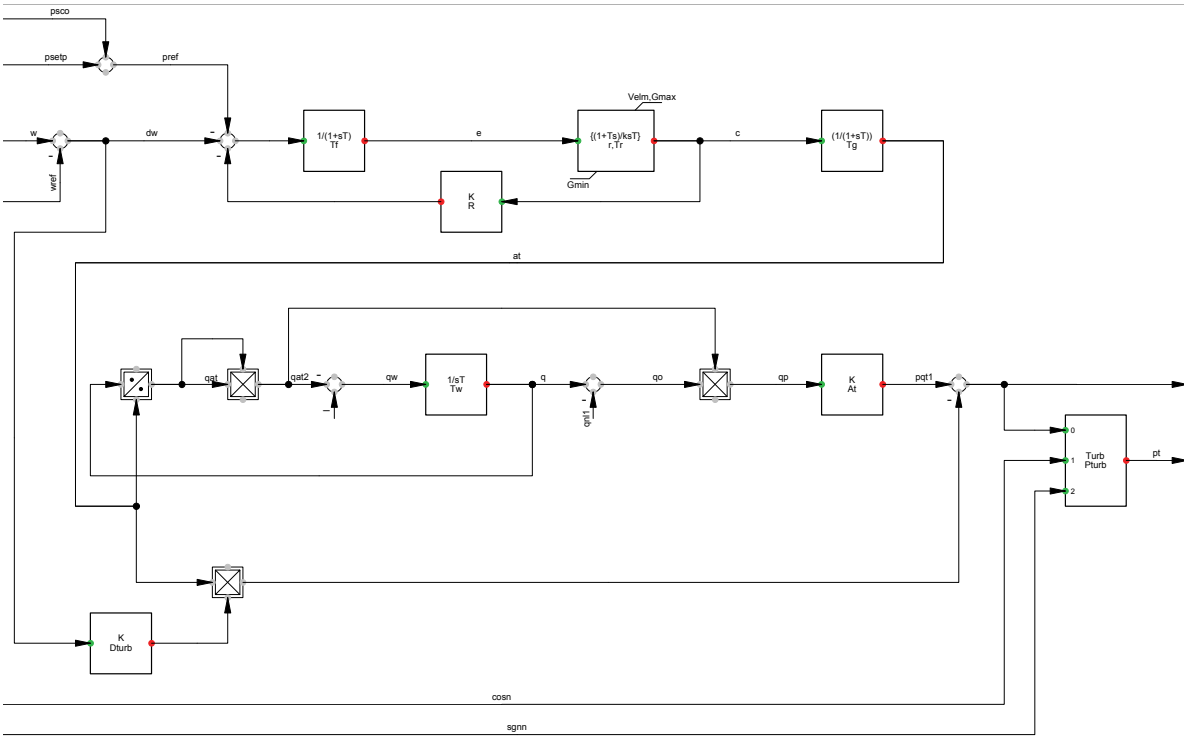

Figure C.3 Generic HYGOV governor model

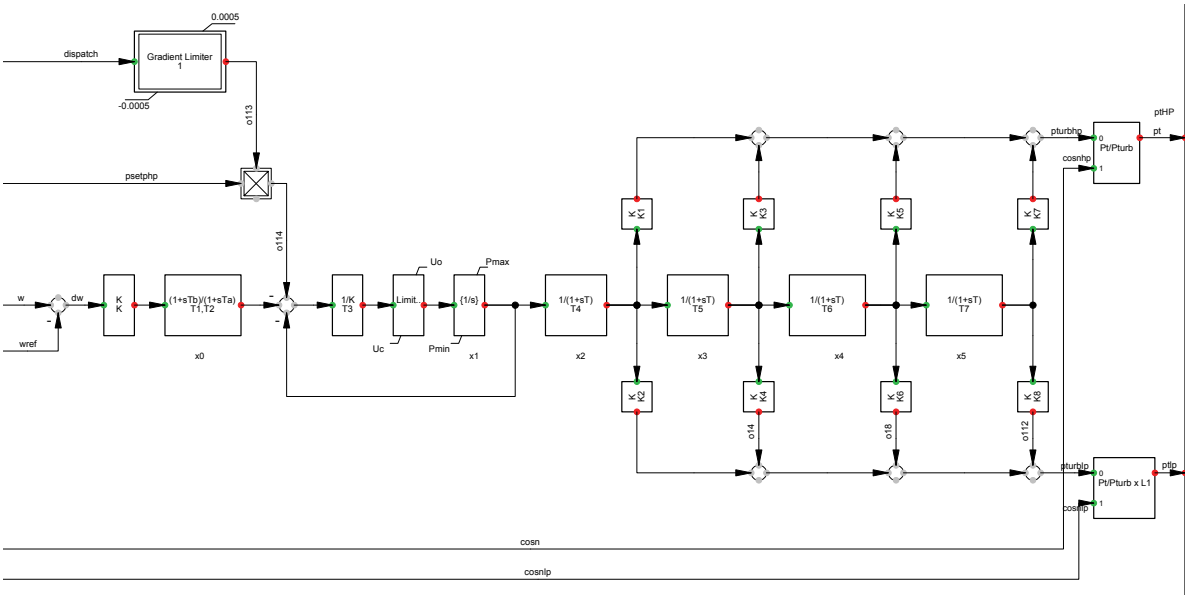

Figure C.4 Generic IEEEG1 governor model

Appendix D

Relevant data and illustration of BESS

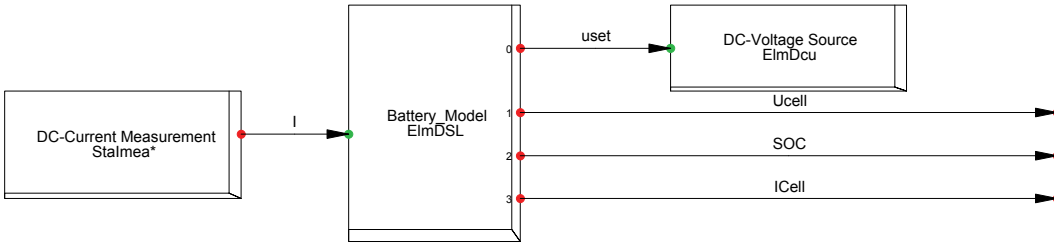

Figure D.1 Battery frame

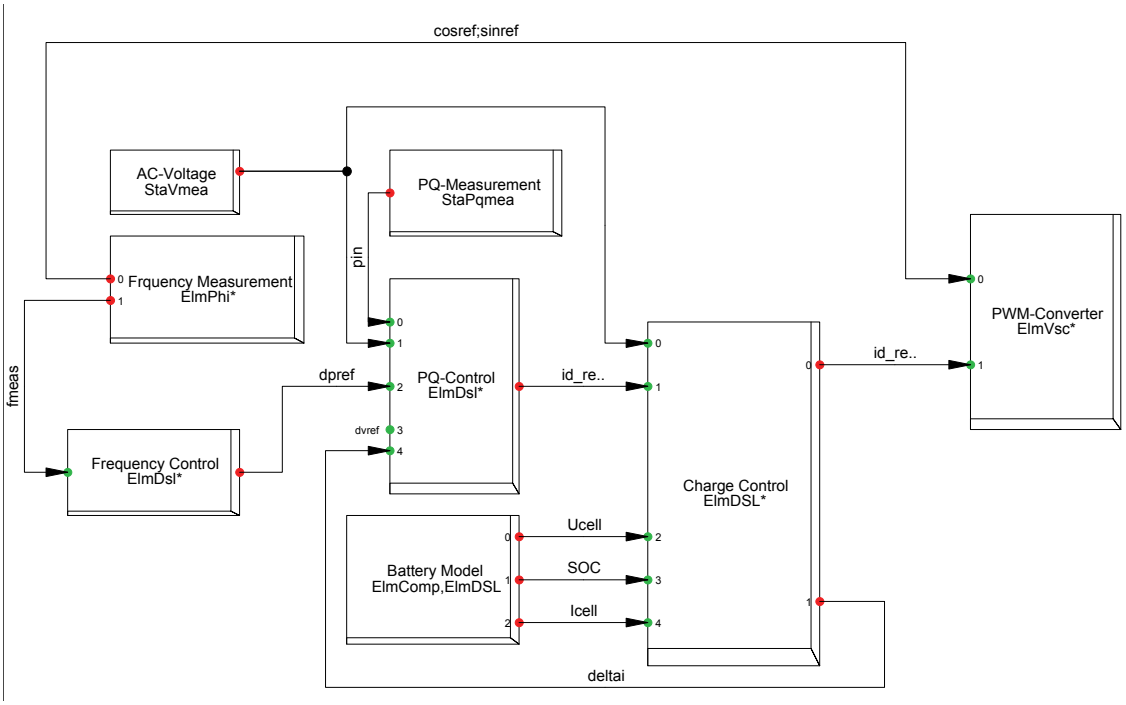

Figure D.2 Battery control frame

TABLE D.1

Parameters of the simplified battery model

	Description	Value
CellCapcity (Ah)	Capacity per cell	80
Vcellmin (V)	Voltage of empty cell	12
Vcellmax (V)	Voltage of full cell	13.85
CellsInParallel	Amount of parallel cells	60
CellsInRow	Amount of cells in a row	65
Rcell (ohm)	Intern resistance per cell	0.001
Vcell (kV)	Nominal voltage of source	0.9
SOC0	State of charge at initialization	0.8